

**Role of DNA methyltransferase 3A (DNMT3A) in
intestinal epithelial cells during homeostasis and
inflammation**

Dissertation
zur Erlangung des Doktorgrades
der Mathematisch-Naturwissenschaftlichen Fakultät der
Christian-Albrechts-Universität zu Kiel

vorgelegt von

Antonella Fazio

Kiel, 2019

First referee (supervisor): Prof. Dr. Philip Rosenstiel
Second referee: Prof. Dr. Thomas Roeder
Examiner: Prof. Dr. Andre Franke
Chairperson: Prof. Dr. Matthias Leippe

Date of the oral examination: 05 July 2019
Approved for publication on: 05 July 2019

Table of Contents

List of Figures	5
List of Tables.....	6
1 Introduction	7
1.1 Inflammatory bowel disease.....	7
1.2 DNA methylation.....	8
1.3 The <i>de novo</i> methyltransferases DNMT3A	10
1.4 DNA methylation signatures in inflammatory bowel disease.....	12
1.5 Features of the intestinal barrier	13
1.5.1 Cellular composition of the intestinal barrier.....	13
1.5.2 Intestinal intracellular junctions.....	14
1.5.3 Intestinal barrier in inflammatory bowel disease.....	15
1.6 Aims of the thesis.....	17
2 Material and Methods.....	18
2.1 Cell biological methods.....	18
2.1.1 Cell lines.....	18
2.1.2 Transfection of siRNA	18
2.1.3 Transient transfection of plasmid DNA.....	19
2.1.4 Promoter-Mediated Luciferase Reporter Assay	19
2.1.5 Generation of DNMT3A KO cell via Crispr/Cas9 genome editing.....	20
2.1.6 Generation of stable expression of DNMT3A1 and DNMT3A2 in DNMT3A KO cell line	22
2.1.7 Generation of murine colonic organoids.....	22
2.2 Molecular biological methods.....	23
2.2.1 Total RNA isolation	23
2.2.2 cDNA synthesis	23
2.2.3 Quantitative real-time polymerase chain reaction.....	23
2.2.4 Plasmid preparation	24
2.2.5 Sanger sequencing.....	24
2.3 Protein biochemical methods.....	24
2.3.1 Total protein lysate isolation	24
2.3.2 Protein quantification.....	25
2.3.3 Gel electrophoresis of proteins	25
2.3.4 Immobilization of proteins by immunoblot.....	26
2.3.5 Immunodetection of proteins	26
2.3.6 Enzyme Linked Immunosorbent Assay (ELISA)	27
2.4 Functional assays methods	27
2.4.1 Wound healing assay.....	27
2.4.2 Permeability assay.....	27
2.4.3 Transepithelial electric resistance (TEER).....	28
2.4.4 Spheroids culture.....	28
2.5 Imaging	28
2.5.1 Immunofluorescence.....	28
2.5.2 Immunohistochemistry.....	29
2.5.3 Transmission electron microscopy	29
2.6 NGS technology methods	29
2.6.1 Transcriptome analysis.....	29
2.6.2 Methylome analysis.....	30
2.7 Generation, Handling and Treatment of Mice.....	30
2.7.1 Generation of Dnmt3a conditional knockout mice (<i>Dnmt3a</i> ^{ΔIEC}).....	30
2.7.2 Animal housing and animal care.....	31

2.7.3	Genotyping	31
2.7.4	Induction of chronic colitis	32
2.7.5	Disease activity index (DAI)	32
2.8	Statistical analysis	32
3	Results	33
3.1	Protein expression analysis of DNMT3A in human and murine cell lines	33
3.2	Generation of DNMT3A knock-out cells and reconstitution with single DNMT3A isoforms	34
3.3	Downstream targets affected by short-term silencing of DNMT3A/B/L	36
3.4	Genomic deletion of <i>DNMT3A</i> alters transcriptome and methylome profiles in Caco-2 cells	39
3.5	Identification of target genes rescued by re-expression of DNMT3A isoforms	41
3.6	Gene expression analysis of DNMTs	45
3.7	Characterization of DNMT3A KO spheroids morphology	46
3.8	Role of DNMT3A in intestinal permeability	48
3.9	Role of DNMT3A in epithelial wound healing	50
3.10	DNMT3A modulates NF- κ B signaling in intestinal epithelial cells	52
3.11	DNMT3A gene expression is downregulated during intestinal inflammation	53
3.12	Characterization of <i>Dnmt3a</i> ^{ΔIEC} mice	54
3.12.1	Basal phenotype of <i>Dnmt3a</i> ^{ΔIEC} mice	54
3.12.2	<i>Dnmt3a</i> ^{ΔIEC} mice are more susceptible to chronic DSS-induced colitis	57
3.12.3	Role of DNMT3A in cell-cell junction architecture	59
4	Discussion	61
4.1	DNMT3A is expressed in intestinal epithelial cell lines	61
4.2	Deletion of DNMT3A induces a complex dysregulation of the transcriptional signatures of IECs	62
4.3	DNMT3A isoforms exhibit overlapping functions	63
4.4	DNMT3A modulates intestinal barrier homeostasis <i>in vitro</i>	65
4.5	The role of DNMT3A during intestinal homeostasis and inflammation	68
4.5.1	Deletion of <i>Dnmt3a</i> alters crypt homeostasis	69
4.5.2	Mice lacking <i>Dnmt3a</i> in the intestine are more susceptible to chronic chemically-induced colitis	70
5	Conclusions and future perspectives	71
6	Summary	73
7	Zusammenfassung	75
8	References	77
9	Supplement	87
9.1	List of Abbreviations	87
9.2	Buffers and Solutions	90
9.3	Media	91
9.4	Chemicals	91
9.5	Enzymes	92
9.6	Kits	92
9.7	Plasmids and oligonucleotides	93
9.8	Antibodies	94
9.9	Devices & Consumables	94
9.10	Acknowledgments	98
9.11	Curriculum Vitae	99
9.12	Eidesstattliche Erklärung	101

List of Figures

Figure 1.1: Conserved domain structure of DNA methyltransferase enzymes.	9
Figure 1.2: Similarity of domains composition of DNMT3A isoforms.	11
Figure 1.3: General overview of intestinal barrier layers.	15
Figure 2.1: Targeting strategy for the generation of conditional Dnmt3a knockout allele.	31
Figure 3.1: Human and murine intestinal epithelial cells express different levels of DNMT3A protein.	33
Figure 3.2: Characterization of DNMT3A KO, DNMT3A1 and DNMT3A2 cell lines.	35
Figure 3.3: Short-term silencing of DNMT3s causes transcriptional changes without modifying global DNA methylation.	38
Figure 3.4: Genomic deletion of <i>DNMT3A</i> causes transcriptional changes with global DNA hypomethylation.	41
Figure 3.5: Transcriptome analysis of rescued genes.	42
Figure 3.6: Re-expression of DNMT3A isoforms restores promoter DNA methylation and gene expression.	44
Figure 3.7: Reciprocal transcriptional regulation of DNMT3 family.	45
Figure 3.8: DNMT3A KO spheroids have an abnormal structural organization.	47
Figure 3.9: Loss of DNMT3A results in defective paracellular permeability.	49
Figure 3.10: Loss of DNMT3A impairs epithelial wound healing <i>in vitro</i> and it is rescued by re-expression of DNMT3A single isoforms.	51
Figure 3.11: Loss of DNMT3A impairs NF- κ B activity.	52
Figure 3.12: DNMT3A is dysregulated under inflammatory conditions in patient biopsies and in a murine chemical colitis model.	53
Figure 3.13: mRNA and protein levels of Dnmt3a in <i>Dnmt3a</i> ^{ΔIEC} mice and control mice.	55
Figure 3.14: Basal phenotype of <i>Dnmt3a</i> ^{ΔIEC} mice.	56
Figure 3.15: Small intestinal architecture of <i>Dnmt3a</i> ^{ΔIEC} mice.	57
Figure 3.16: Conditional Dnmt3a deficiency increases susceptibility to chronic DSS-induced colitis.	58
Figure 3.18: DNMT3A alters intestinal epithelial cell-cell junction.	60

List of Tables

Table 1: Overview of applied cell lines.....	18
Table 2: Overview of formats and volumes of siRNA transfections.....	19
Table 3: Overview of formats and volumes of plasmid DNA transfections.....	19
Table 4: Annealing reagent list.....	20
Table 5: Ligation reagent list.....	21
Table 6: List of components for cDNA synthesis.....	23
Table 7:List of reagents for SDS-Polyacrylamide Gel Electrophoresis.....	26
Table 8: License number for approved animal research.....	31
Table 9:PCR components and thermocycler program for genotyping.....	32
Table 10:Overview of expected amplicon lengths after genotyping PCR.....	32
Table 11:Scoring criteria for the determination of the disease activity index.....	32
Table 12: List of applied buffers and solutions.....	90
Table 13: List of applied media.....	91
Table 14: List of applied chemicals.....	91
Table 15: List of applied enzymes.....	92
Table 16: List of applied kits.....	92
Table 17: List of plasmids used in this study.....	93
Table 18: List of applied oligonucleotides with their sequences.....	93
Table 19: Overview of applied TaqMan probes.....	93
Table 20:Primary antibodies used in this study.....	94
Table 21: Secondary antibodies used in this study.....	94
Table 22: Devices used in this study.....	94
Table 23: List of consumables used in this study.....	95
Table 24: List of top 100 upregulated genes rescued by DNMT3A1 and DNMT3A2.....	96
Table 25: List of top 100 downregulated genes rescued by DNMT3A1 and DNMT3A2.....	97

1 Introduction

1.1 Inflammatory bowel disease

Inflammatory bowel disease (IBD) is characterized by an impaired immune response leading to chronic relapsing inflammation of the gastrointestinal tract. Crohn's disease (CD) and ulcerative colitis (UC) are the two major types of IBD [1]. They differ in their distribution and inflammatory features along the gastrointestinal tract. Crohn's disease can affect segments of the entire gastrointestinal tract; the inflammation is transmural, and it may influence all layers of the intestine. Differently, UC is limited to the colon and it is characterized by sparse mucosal inflammation with ulceration of the mucosa and submucosa layers [2, 3]. Clinical symptoms of both IBD subtypes include persistent and chronically relapsing diarrhea, abdominal pain, fever and loss of appetite. Blood in the stool, rectal bleeding and body weight loss may also occur [4, 5]. Furthermore, IBD patients with severe and long-term active disease have an increased risk for colon cancer [6]. Currently no cure is available for IBD [7, 8]. Many therapeutic approaches are based on immunosuppressive therapies such as anti-TNF monoclonal antibodies, with the aim to alleviate symptoms of inflammation [9]. The worldwide incidence rate has dramatically increased with time [10]. The highest prevalence of IBD was reported in Canada and Europe [11]. In addition, even in the low-risk populations like Asian countries, the incidence is increasing. These changes suggest that environmental factors, such as the "westernization" phenomenon play an important role in disease development [12].

IBD is a complex disorder and is known to be strongly influenced by the interaction between genetic background and environmental factors [13]. In 1996, a linkage mapping study discovered the first CD susceptibility locus on chromosome 16 also called IBD1 [14]. Later on, it was identified that the IBD1 risk locus encodes for the nucleotide-binding oligomerization domain-containing protein 2 (NOD2), characterized by a single nucleotide polymorphisms (SNPs) in the NOD2 gene that results in an impaired function of the protein [15]. With the onset of high-throughput technologies, more genes have been associated to IBD pathogenesis. A large genome-wide association study (GWAS) identified 168 loci associated with IBD and 70% of these loci are shared with other immune-mediated disorders [16]. The majority of IBD risk alleles are associated with both CD and UC, such as *IL23R* which encodes the receptor for interleukin 23 [17]. However, some loci are specifically linked to CD only, such as *NOD2* and *ATG16L1* (*autophagy related 16 like 1*) gene, that encodes a protein involved in the autophagy pathway [18], or others related to UC only like the *IL2/IL21* locus [19].

While the identification of numerous IBD risk genes has significantly contributed to our understanding of disease pathogenesis, environmental risk factors have been increasingly implicated in the growing incidence

of IBD. Lifestyle behaviours, exposure to environmental microbial components, and nutrition have been discussed to contribute at least in part to the development and manifestation of IBD [20]. High intakes of total fats, total polyunsaturated fatty acids, omega-6 fatty acids and meat increase the risk of IBD, whereas the consumption of fibre, fruit and vegetables decreases the risk of IBD [21]. The question how such transient exposures precipitate into a life-long disease state is currently not resolved.

1.2 DNA methylation

Epigenetic alterations have been associated with IBD [22]. Exploring epigenetic modifications might provide an insight into the complex gene–environment interactions in disease pathogenesis. By definition, epigenetic events are heritable and potentially reversible modifications of DNA function without altering the DNA sequence [23, 24]. All chemical modifications form a complex regulatory network that modulates chromatin structure and genome function. The epigenome refers to the complete description of these potentially heritable changes across the genome [25]. DNA methylation is the most studied epigenetic modification in mammals, and it occurs when a methyl group is transferred to the fifth position of the pyrimidine ring of cytosines in dinucleotide CpG sequences [26]. CpG sites (CpGs) represent DNA regions enriched in cytosine followed by guanine nucleotides in a linear sequence of bases along its 5' → 3' direction. CpG sites occur with high frequency in genomic regions called CpG islands. The methylation of CpG can regulate gene expression through its effect on chromatin state, as well as interfere with accessibility to transcription factor binding sites [27]. It is thought that hypermethylation of CpGs, especially when located within the promoter region or close to transcription starting sites, is associated with gene silencing, whereas hypomethylation has the opposite effect [28]. Nevertheless, more recent studies have underlined that the simplistic “gene transcription on/off” model might not be generalizable, but in fact more complex influences of methylation patterns on gene regulatory activity can be found. These include methylation in non-CpG context as well as higher order methylation variations e.g. partially methylated domains (PMDs) [29, 30].

DNA methylation patterns are established during embryonic development through a complex process that involves demethylation and *de novo* methylation, and it can be maintained during cell division through the action of maintenance methyltransferase activity [31, 32]. Generally, the mammalian genome is globally methylated, with the exception of unmethylated domains enriched in the 5' regions of genes, promoters, CpG Islands (CGIs) and first exons [33]. Most CGIs remain unmethylated throughout development, while a minority of them become methylated, and this correlates with transcriptional silencing of associated genes [34]. Recently developed DNA methyltransferase inhibitors can restore the expression of genes that are silenced by aberrant DNA methylation. Some of them have shown promising results in myelodysplastic syndrome (MDS), a preleukemic disorder. Hence, epigenetic therapies are becoming a potential alternative treatment [35].

The enzymes involved in these processes are DNA methyltransferases (DNMTs) enzymes, which are responsible for the establishment and maintenance of DNA methylation pattern. In mammals, there are five DNMTs: DNMT1, DNMT2, DNMT3A, DNMT3B and DNMT3L (Figure 1.1). All five DNMTs use a similar catalytic activity characterized by the transfer of a methyl group from the universal methyl donor, S-adenosyl-methionine (SAM), to carbon-5 (C5) of cytosine. DNMTs are usually organized into an N-terminal regulatory domain and a C-terminal catalytic domain. DNMT1 is the largest enzyme, existing in different isoforms generated by an alternative promoter. The N-terminal domain of DNMT1 contains four conserved subdomains that regulate molecular interactions [36]. DNMT2 is a small enzyme, that consists entirely of the catalytic domain, and it has a CTF motif within its catalytic domain. DNMT3A, DNMT3B and DNMT3L share/show high sequence similarity. The N-terminal parts are composed of two domains; the ATRX-DNMT3-DNMT3L (ADD) mediates the interaction with the unmethylated histone H3 tail at the lysine K4. Moreover, this domain also regulates the activity of DNMT3A through an autoinhibitory mechanism [37]. The second domain, present only in DNMT3A and DNMT3B enzymes, is a Pro-Trp-Trp-Pro (PWWP) that mediates the binding of DNMT3A and DNMT3B to histone H3 trimethylated at lysine 36. DNMT3A and DNMT3B share 81% of sequence similarity of their C-terminal domain. Although DNMT3L shares homology with DNMT3A/B, it is unable to bind SAM and does not possess any catalytic activity [38, 39].

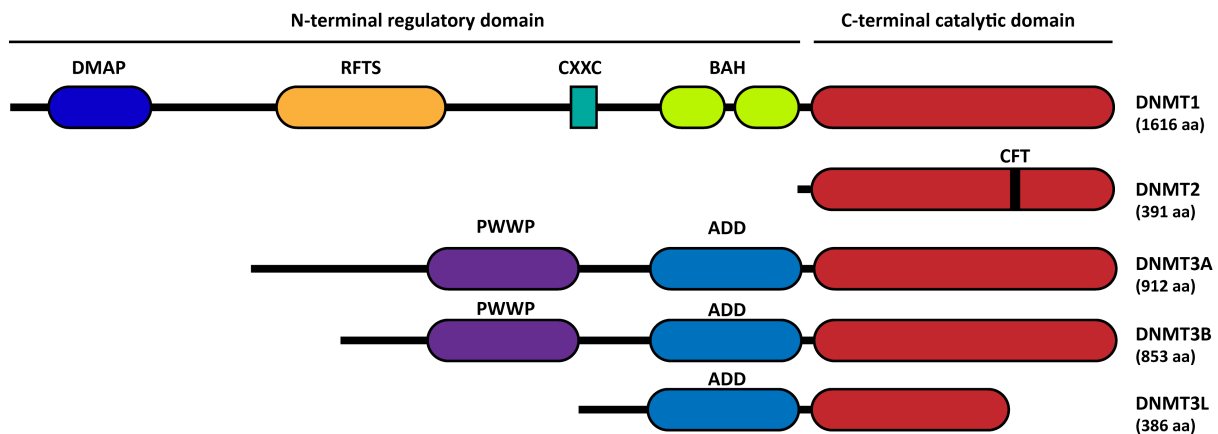


Figure 1.1: Conserved domain structure of DNA methyltransferase enzymes.

Conserved domains of DNA methyltransferase (DNMT) family members are shown in different colours. The catalytic domain (shown in red) is conserved in all DNMTs. The CTF motif within the catalytic domain of DNMT2 differentiates it from the other DNMTs. DNMT3L is a catalytically inactive DNMT3 variant that lacks the N-terminal part of the regulatory domain (including the Pro-Trp-Trp-Pro (PWWP) domain) and the C-terminal part of the catalytic domain. The number of amino acid (aa) residues is indicated below the corresponding DNMT.

DNMT1 is responsible for the maintenance of genomic DNA methylation patterns; it requires a hemimethylated DNA sequence to propagate existing methylation patterns from the old strand to the newly synthesized strand [36]. DNMT2 is a tRNA methyltransferase that methylates cytosine 38 in the anticodon loop [40]. DNMT3s are *de novo* methyltransferases enzymes. DNMT3A and DNMT3B are catalytically active

enzymes and are responsible for the establishment of *de novo* DNA methylation patterns. Differently, DNMT3L lacks the catalytic domain, acting as a regulatory factor. To elucidate the interaction between DNMT3s and the DNA, a model on how the *de novo* methylation machinery is recruited on the DNA was proposed. According to this model, DNMT3L has two functions: the C-terminal domain of DNMT3L interacts with the catalytic domain of DNMT3A, forming a dimeric structure. This structure undergoes further dimerization through a DNMT3A-DNMT3A interaction, forming a tetrameric complex. DNMT3L binds the unmethylated lysine 4 of histone H3 and it recruits the methyltransferases to specific DNA regions [41, 42]. Several studies have suggested a role of DNMT enzymes in transcriptional silencing, mostly through their ability to methylate promoters and change chromatin state [43]. These findings were supported by a CRISPR-Cas9–DNMT3A fusion protein that targets specific CpG at the promoters and induces gene silencing [44].

Interestingly, GWAS studies have unveiled a direct involvement of the DNA methylation machinery in disease onset. In a study conducted by Franke et al. the *de novo* methyltransferase enzyme DNMT3A has been identified as a risk gene for CD [45]. Similarly, Jostins et al. identified DNMT3B as a risk gene for both UC and CD [17]. The functional consequences of the identified genetic variants have not been investigated. Nevertheless, the identification of two independent loci encoding the *de novo* methyltransferase enzymes suggests a fundamental mechanism that might involve impaired DNA methylation and gene regulation.

1.3 The *de novo* methyltransferases DNMT3A

DNMT3A is essential for mammalian development, since loss of *Dnmt3a* in mice results in lethality 4 weeks after birth [46]. Along with its role in development, DNMT3A has been implicated in tumorigenesis. It has been shown that deletion of *Dnmt3a* inhibits the earliest stage of intestinal tumor development in a mouse model for colorectal cancer. Indeed, loss of *Dnmt3a* caused regional loss of DNA methylation with promoter demethylation and increased expression of tumor-suppressor genes [47]. DNMT3A is frequently mutated in acute myeloid leukemia, resulting in a reduced methyltransferase activity. Strikingly, mice with this mutation developed acute myeloid leukemia, suggesting a role of DNMT3A as tumor inducer [48].

The *DNMT3A* gene (human: 4395 base pairs (bp), RefSeq. NM_175629; mouse: 9735 bp, RefSeq. NM_007872) is located on chromosome 2 on position 23.3. The resulting protein, DNMT3A, is composed of 912 amino acids (aa) with a molecular weight of 130 kilo-Dalton (kDa). The human DNMT3A shares 98 % of amino acid sequence identity with the corresponding murine protein [49]. In both human and mouse, *DNMT3A* gene gives multiple alternative transcripts encoding various catalytically active and inactive DNMT3A isoforms. Chen et al. identified an isoform produced from a downstream alternative promoter, located in the sixth intron of the *DNMT3A* gene, resulting in a protein of 100 kDa band named DNMT3A2.

Unlike the full-length protein DNMT3A1, the shorter isoform lacks the N-terminal 219 amino acids (Figure 1.2).

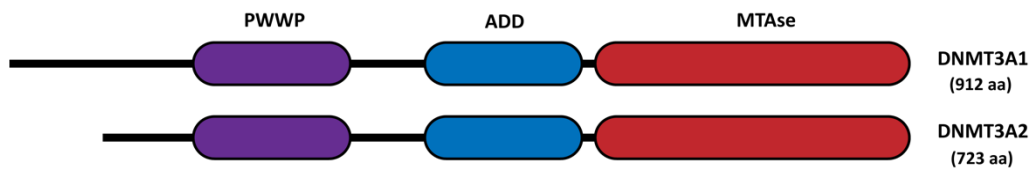


Figure 1.2: Similarity of domains composition of DNMT3A isoforms.

DNMT3A isoforms DNMT3A1 and DNMT3A2 are shown. Similarity between domain composition are shown in different colours. The PWWP depicted in purple and the ATRX-DNMT3-DNMT3L (ADD) depicted in blue form the N-terminal regulatory region, while the domains form the C-terminal catalytical region is shown in red. The number of amino acid (aa) residues is indicated below the corresponding DNMT3A isoform.

Although DNMT3A2 displays similar cytosine methyltransferase activity as DNMT3A *in vitro*, DNMT3A1 and DNMT3A2 exhibit different subcellular localization patterns. Fluorescence microscopy analysis identified nuclear localization of DNMT3A1, resulting in heterochromatin association. In contrast, DNMT3A2 shows a diffused pattern excluding nucleoli and heterochromatin, resulting in association with euchromatin [50]. The different subcellular distribution was further investigated by immunoblotting of endogenous DNMT3A in subcellular fraction parts. As a result, DNMT3A1 and DNMT3A2 fractionate mainly with chromatin (77–85%), and small proportions (8–18%) of these proteins also associate with the nuclear matrix. Whereas DNMT3A1 was exclusively nuclear, a significant proportion (15%) of DNMT3A2 was present in the cytoplasmic fraction, consistent with the imaging results [50]. ChIP-seq analysis showed a preferential localization of the longer isoform DNMT3A1 to CpG islands, that are marked by both H3K4me3 and H3K27me3 in mouse embryonic stem cells. This preference coincides with the promoters of several transcription factors. DNMT3A binding does not completely overlap with the H3K27me3 signal over the CGIs, but it is restricted to the methylated regions outside of the island known as CpG island shores [51]. The isoform-specific targeting of DNMT3A1 coincides with elevated hydroxymethylcytosine (5-hmC) deposition, suggesting an involvement of this isoform in mediating turnover of DNA methylation at these sites. Re-expression of DNMT3A1, but not DNMT3A2, in *Dnmt1/3A/3B* triple KO embryonic stem cells (ESCs) preferentially re-targets DNA methylation to bivalent CpG island shores and results in increased production of 5-hmC. These results demonstrate that the DNMT3A1 isoform is responsible for sustaining methylcytosine turnover at bivalent CpG islands, whereas the shorter version, DNMT3A2, has a more global DNA binding and methyltransferase activity throughout the genome [52].

1.4 DNA methylation signatures in inflammatory bowel disease

In addition to genetic predisposition and environmental risk factors, epigenetics may be relevant to understand the complexity of the etiopathogenesis of Crohn's disease and ulcerative colitis. In this context, *de novo* DNA methylation has been shown to play a role in IBD pathogenesis [53]. Furthermore, the reported genetic association of the main methyltransferase enzymes, DNMT3A and DNMT3B, suggest a relevant role for this arm of epigenetic modification in IBD.

The link between altered DNA methylation and IBD pathogenesis has received increasing attention. The first study that linked epigenetics and IBD was carried out by Gloria et al. in 1996. The authors reported that the rectal mucosa of UC patients shows global DNA hypomethylation [54]. Later on, with the advantage of high-throughput technologies, epigenome-wide methylation association studies (EWAS) have been widely used to analyse the methylation profile of IBD patients, and the potential role of epigenetic regulatory events on IBD pathogenesis. Nimmo et al. analysed peripheral blood of CD individuals, and they identified 50 genes showing a differential methylation signature compared to the healthy group. Indeed, gene ontology analysis identified several pathways associated with IBD, including "immune response" and "host response to bacteria" [55]. Häslér et al. performed a functional EWAS study using intestinal biopsy samples from 20 monozygotic twins discordant for ulcerative colitis. This study identified 61 differential methylated loci, including several loci responsible for regulation of immune responses [57]. Additional studies provided new insights into the DNA methylation profiles in IBD, employing samples of different nature such as peripheral blood, whole biopsy tissue or isolated intestinal epithelial cells, and using different techniques [58-62]. Noteworthy, the large cohort study by Ventham et al. used an integrative approach to identify over 400 differentially methylated positions (DMPs) and 5 differentially methylated regions (DMRs). To consolidate their findings, the authors used different methodological approaches and an independent cohort. This detailed methylome data reveal a link between altered DNA methylation and gene expression, and highlight the importance of the cell-type specificity DNA methylation analysis [62].

Given the important role of intestinal epithelial cells (IECs) in the pathogenesis of IBD [63], understanding the epigenetic signature, and what follows from them, is highly interesting. DNA methylation plays a critical role during intestinal development and homeostasis. Indeed, loss of DNA methylation causes transcriptional dysregulation and delayed cell differentiation [64]. Genome-wide DNA methylation analysis from human fetal gut and pediatric isolated IECs reveals a distinct methylation profile between the developmental status (fetal versus pediatric) and the gut segments (large versus small intestine). Furthermore, differentially methylated regions revealed a strong association with genes involved in gastrointestinal development, immune function and intestinal disease [65]. The DNA methylation profile is not only associated with gut-segments and developmental stages, but it differs also between healthy and diseased individuals. In fact, in

children diagnosed with IBD, genome-wide DNA methylation profiling is able to clearly distinguish between healthy individuals and IBD groups [66]. These findings suggest that impaired DNA methylation during intestinal development could predispose and favour disease development.

Epigenetic modifications seem to be the missing link between genetic susceptibility and environmental exposure to predisposition and manifestation of the disease. However, epigenetic information alone cannot provide an elusive diagnostic tool. On the contrary, integration of transcriptome and methylome data will enhance the capacity to develop new diagnostic and therapeutic strategies, raising the possibility to translate these signatures into functional approaches.

1.5 Features of the intestinal barrier

The intestinal barrier is a complex structure that physically separates the intestinal lumen from the underlying tissues. The intestinal barrier consists of the intestinal epithelium, which forms a single layer, followed by the mucus layer and the commensal microbiota towards the intestinal lumen (Figure 1.3). The gut barrier prevents loss of water and nutrients and the entry of microorganisms and antigens from the lumen side. At the same time, it enables the absorption of nutrients from the diet and the exchange of molecules between the host and the environment. Furthermore, the intestinal barrier performs two similar but opposite functions. While it allows a co-existence with the symbionts of the intestinal flora without triggering chronic inflammation, it provides a controlled inflammatory and defensive response against pathogens [67, 68].

1.5.1 Cellular composition of the intestinal barrier

The key elements of the gastrointestinal barrier are shown in Figure 1.3. The single cell monolayer, composed by intestinal epithelial cells, divides the immune compartment (lamina propria (LP)) from the luminal content of the host. The intestinal epithelium is characterized by a crypt-villus organization. At the bottom of the crypts, pluripotent intestinal epithelial stem cells (IESCs) are located. These give rise to all intestinal epithelial cell types and allow the continuous renewal of the epithelial layer. Differentiated intestinal epithelial cells, with the exception for Paneth cells, migrate up the crypt-villus axis until they are shed from the epithelium layer [69]. The intestinal epithelium is composed of several cell subtypes, which have different functions. Most cells lining the intestinal lumen are absorptive enterocytes, which have mainly metabolic and digestive functions. Enteroendocrine cells, goblet cells and Paneth cells are secretory IECs specialized in maintaining epithelium homeostasis. Enteroendocrine cells produce gastrointestinal hormones or peptides in response to various stimuli. They can diffuse into the bloodstream, functioning as local messengers or transmitting to

the enteric nervous system [70]. Goblet cells synthesize mucin glycoproteins (MUC2) and bioactive molecules, such as trefoil factor peptides (TFF) or epithelial membrane-bound mucins (MUC1, MUC3, MUC17). The mucin glycoproteins form the mucus layer, which consist of a gel formed by two types of mucin molecules. The major gel-forming mucin is Mucin2. It gets heavily glycosylated and polymerized, together with other mucins, forming a large net-like structure. The second group is composed by transmembrane mucins that cover the apical surface of the enterocytes. The mucus layer represents the first innate host defence, it plays an important role in keeping the microbes distance from the epithelial surface, thereby inhibiting inflammation and infection [71] [72].

Paneth cells are found only in the small intestine. Unlike the other epithelial cell types, Paneth cells migrate bottom ward from the stem cell area and locate adjacent to it. They secrete antimicrobial peptides (AMPs), which are key mediators of host-microbe interactions, and have an important role in sustaining and modulating the epithelial stem cells niche [73]. In addition, Paneth cell dysfunction is implicated in pathogenesis of chronic inflammatory bowel disease [74, 75].

1.5.2 Intestinal intracellular junctions

A crucial function of IECs is the maintenance of barrier integrity. The intestinal epithelium is tightened by intracellular junctional complexes, known as tight, adherens and desmosome junctions [76]. They are determinant for intestinal epithelial barrier properties and its functions. The junctional complexes prevent the direct diffusion of small molecules derived from the intestinal lumen, into the interstitial underlying tissues and finally the bloodstream [77].

The tight junctions (TJ) are the most apical junctional complex and are responsible for the paracellular space between two adjacent cells. These junctions regulate the flux of small molecules and water ions. The major types of tight-junctions proteins are claudins, a large family that includes over 24 members [78], and occludins. The actin cytoskeleton of adjacent cells is linked via the interaction between claudins, occludins and the cytoplasmic plaque proteins known as Zonula occludens (ZO-1, ZO-2 and ZO-3) [79].

The adherence junctions (AJ) are protein complexes localized to the basal side of TJ on the lateral membrane. They are formed by interactions of transmembrane proteins, adaptor proteins and the cytoskeleton. AJs are formed mainly by cadherin-catenin interactions. The cell-cell adhesion is promoted by the homotypic interactions between the extracellular domains of E(epithelial)-cadherins. The E-cadherin intracellular domain contains a catenin-binding domain. Catenin links the formed adherence junctions to the cytoskeleton via the binding with the F-actin domain or indirectly with other adaptors proteins [80]. Adherence junctions are not only important for cell-cell adhesion but also are involved in other processes such as cell polarity, cell migration and the formation of desmosomes [81].

Desmosomes are transmembrane protein complex that are tightly associated with the cytoskeleton. They provide mechanical stability and are essential for tissue integrity. Three main group of proteins are forming the desmosomes complex: cadherins, armadillo proteins and plakins [82].

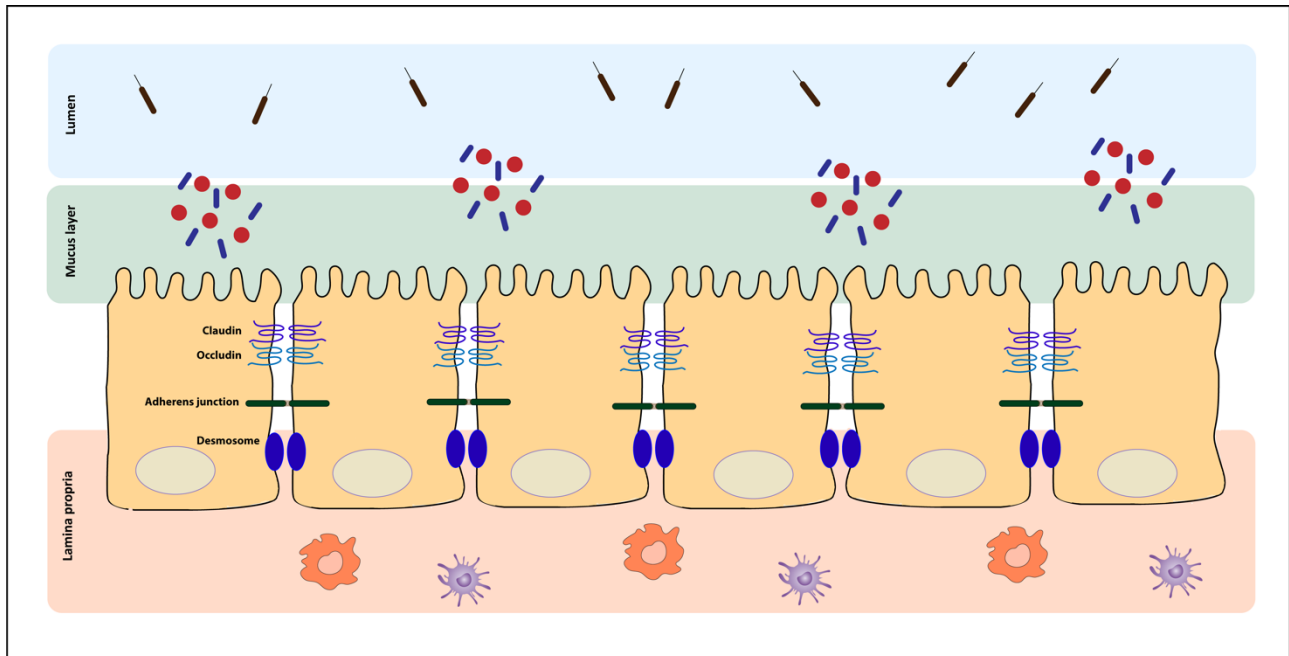


Figure 1.3: General overview of intestinal barrier layers.

The intestinal barrier is composed of several layers providing a separation between the intestinal lumen and the tissues below. Amongst others, the intestinal lumen contains food content/particles, commensal bacteria, (opportunistic) pathogens, and anti-microbial peptides (AMPs) secreted by Paneth cells. A mucus layer protects the underlying epithelial cell layer. The latter consists of a single layer of epithelial cells. Apical and basolateral compartments are depicted. They are characterized by tight junction proteins, such as occludin and claudin, adherens junctions and desmosomes, respectively. The lamina propria is populated with cells of the innate and adaptive immune system.

1.5.3 Intestinal barrier in inflammatory bowel disease

Inflammatory bowel disease is characterized by barrier dysfunction, leading to impaired intestinal permeability, thin mucus layer and bacterial invasion [83-85]. A leaky gut barrier may be an initial event of the pathogenesis of IBD, allowing bacteria-derived molecules into the mucosa and initiate an uncontrolled inflammatory response. Intestinal permeability can be compromised by many factors, such as the gut microbiota, an altered mucus structure and a damaged epithelial layer. High-fat diet induces increased circulating LPS, possibly due to increased gut permeability [86]. Although the link between the intestinal barrier and disease is extensively studied, there is a limited knowledge on the causes and mechanisms triggering intestinal barrier dysfunction. Several studies revealed that in both active and inactive CD, small intestinal permeability is increased [87]. Interestingly, an increased intestinal permeability (up to 10%) has been observed in relatives of CD patients, suggesting that impaired permeability may be an etiologic factor in IBD [88]. Intestinal barrier dysfunction is often associated with defects in epithelial tight junctions in IBD.

More specifically, it has been found an upregulation of claudin 2 protein and a downregulation and redistribution of claudins 5 and 8 proteins, leading to altered tight junctional complexes with a pronounced barrier dysfunction [89]. Some genetic studies have revealed a potential link between mutations in TJ-associated proteins, such as myosin IXB (MYO9B), partitioning defect protein (PARD3), PDZ containing protein 2 gene (MAGI2), and the development of IBD [90, 91]. In addition, truncated forms of E-cadherin (encoded by CDH1) have been associated with Crohn's disease [92].

Aside from impaired barrier permeability, IBD is characterised by mucosal damage with extensive areas of ulceration. Damage and impairment of the epithelial barrier may result in increased penetration of microbial products into the body, leading to increased inflammation, uncontrolled immune response and altered host homeostasis. Therefore, a rapid reestablishment of the gastrointestinal barrier is essential to preserve the normal homeostasis [93]. Epithelial regeneration is a tightly controlled and complex process that involves epithelial cell migration and proliferation, and it is regulated by a variety of growth factors [94]. After epithelial injury, IECs surrounding the wounded area lose their polarity and immediately migrate to the damaged area to initiate tissue repair. This process is called epithelial restitution, and it is a crucial step during healing [95]. Increased epithelial proliferation and differentiation are the next steps after epithelial restitution [96]. Cell proliferation is important to restore the number of IECs in the damaged area, which is needed for re-epithelialization. This process is regulated by numerous signals, including growth factors and cytokines [97]. Several studies have shown the involvement of toll like receptors (TLRs) and TLRs induced molecules (i.e. TFF3) in epithelial regeneration [98]. Indeed, TLRs ligands such as Lipopolysaccharides (LPS) can trigger cell death, but is also involved in mucosal wound healing. Activation of TLRs by commensal bacteria is critical for the protection from injuries and maintenance of epithelial homeostasis [99]. In addition, TLR4 signaling through MyD88 in the intestine is important to trigger repair of the intestinal epithelium [100, 101].

The elucidation of the role of diseases in barrier integrity and the underlying regulatory mechanisms can improve our understanding of the intestinal barrier to allow the development of novel therapeutic approaches.

1.6 Aims of the thesis

DNA methylation is one of the epigenetic events involved in regulation of gene expression. Several studies have reported an association between aberrant DNA methylation and inflammatory bowel disease (IBD) pathogenesis. DNMT3A is one of the three members of *de novo* DNA methyltransferases family. Notably, genetic variants in the human *DNMT3A* gene have been associated with an increased risk of IBD. However, little is known about the contribution of DNMT3A on intestinal homeostasis and inflammatory responses. The aim of the present study was to investigate the role of DNMT3A in intestinal epithelial cells. *DNMT3A*-deficient *in vitro* and *in vivo* models were used to shed light on the following aspects:

1. Effect of deletion of DNMT3A on gene expression and DNA methylation of intestinal epithelial cells:
In order to determine DNMT3A target genes, the current study identified short and long-term consequences of deletion of DNMT3A in intestinal epithelial cells, with a focus on transcriptional regulation driven by methylation.
2. Role of DNMT3A in maintaining intestinal barrier homeostasis:
To assess the functional role of DNMT3A *in vitro*, intestinal barrier properties were investigated using intestinal epithelial cells carrying genomic ablation of *DNMT3A*.
3. Role of DNMT3A in intestinal inflammation *in vivo*:
To investigate the role of *Dnmt3a in vivo*, the impact of DNMT3A-deficiency on the intestinal homeostasis and regeneration was assessed using a conditional mouse model lacking *Dnmt3a* in intestinal epithelial cells under baseline and inflammatory conditions.

2 Material and Methods

2.1 Cell biological methods

2.1.1 Cell lines

Cell lines used for in vitro experiments were purchased from the Leibniz-Institute DSMZ-German collection of Microorganisms and Cell Cultures or from the American Type Culture Collection (ATCC). All applied cell lines were cultured at 37°C and 5% (v/v) carbon dioxide in their appropriate nutrition media (Gibco/Life Technologies, Darmstadt, Germany) (Table 1).

Table 1: Overview of applied cell lines.

cell line	Company	product nr.	species	tissue	nutrition medium
HT-29	DSMZ	ACC-299	human	colon	DMEM, 10 % (v/v) FCS
Caco-2	DSMZ	ACC-169	human	colon	MEM, 20 % (v/v) FCS
Model K			murine	colon	DMEM, 10 % (v/v) FCS

The cell lines were passaged twice per week for maintenance. Cells were washed with PBS and treated with a trypsin/EDTA solution (Life Technologies, Darmstadt, Germany) for 5 min at 37 °C. The resulting cell suspension was centrifuged at 300 g for 5 min. The cell pellet was resuspended in 5 ml fresh nutrition medium. A dilution of cells was transferred into new culture flasks for maintaining cultured cells or seeded with a defined cell number for experiments. All steps were performed under sterile conditions using a laminar flow workbench (Thermo Scientific, Bremen, Germany).

2.1.2 Transfection of siRNA

Transfection of small interfering RNA (siRNA) into cultured eukaryotic cells was performed by using Viromer® BLUE transfection reagent (Lipocalyx GmbH, Halle, Germany). Viromers® technology emulate the key mechanism of viral nucleic acid delivery to the cell. The viromer particles, containing the siRNA, are undergoing endocytosis and accumulate near the nucleus, ongoing acidification. The low pH causes the endosome uncharged and hydrophobic and enables the release of the siRNA in the cell. For the transfection of siRNA, the appropriate volume of Viromer® BLUE was placed into the wall of a 1.5 ml reaction tube and diluted with Buffer BLUE (Table 2). Target-specific siRNA was diluted to 2.8 µM using Buffer BLUE. The solutions of both tubes were combined and incubated for 15 min at room temperature. After incubation, the solution was added dropwise to the cells and distributed in the well by gently shaking the plate horizontally. Cells were placed back into the incubator for 72 h. All steps were performed under sterile conditions.

Table 2: Overview of formats and volumes of siRNA transfections.

Reagents	12-well plate	6-well plate
siRNA (2,8µM)	-	-
Buffer BLUE	45	1
Viromer® BLUE	5	90
Diluted siRNA	5	10
Diluted Viromer® BLUE	45	90

2.1.3 Transient transfection of plasmid DNA

Transient transfection of plasmid DNA was performed by using Lipofectamin® 3000 reagent kit (ThermoFisher Scientific). The lipid nanoparticle technology employed by the Lipofectamin® 3000 results in a higher transfection efficiency with an improved cell viability especially for difficult-to-transfect cells such as Caco-2 cells. The appropriated amount of Lipofectamine™3000 reagent was diluted in Opti-MEM™ (Life Technologies, Darmstadt, Germany) (Table 3). Plasmid DNA was diluted in Opti-MEM™ and P3000™ reagent. Diluted plasmid DNA and diluted Lipofectamine™3000 reagent were combined and incubated for 10 min at room temperature. After incubation, the solution was added dropwise to the cells and distributed in the well by gently shaking the plate horizontally. Cells were placed back into the incubator for 24 h. All steps were performed under sterile conditions.

Table 3: Overview of formats and volumes of plasmid DNA transfections.

Reagents	96-well plate	6-well plate	10 cm dish
Opti-MEM™ (µL)	5	125	500
Lipofectamine™3000 reagent (µL)	0,3	3,75	7,5
Opti-MEM™(µL)	5	250	500
DNA (µg)	-	-	-
P3000™ reagent (2µL/µg DNA)	-	-	-
Diluted DNA (µL)	5	125	500
Diluted Lipofectamine™3000 (µL)	5	125	500

2.1.4 Promoter-Mediated Luciferase Reporter Assay

To measure the NF-κB promoter activation, NF-κB–dependent firefly luciferase (pNF-κB-Luc; Clontech) and a Renilla luciferase driven by thymidine kinase promoter (pRLTK; Clontech) was used. For Wnt/b-catenin transcriptional activation, M50 Super 8x TOPFlash reporter assay was used. The reporter contains eight copies of TCF/LEF binding sites upstream of luciferase. M50 Super 8x TOPFlash was a gift from Randall Moon (Addgene plasmid #12456; <http://n2t.net/addgene:12456>; RRID:Addgene_12456) [102]. Bioluminescence from the *Renilla* luciferase was used as internal control for transfection efficiency and cell viability. Caco-2 cells were seeded into a 96-well plate at a density of 2×10^4 cells per well. After 24h, cells were transfected with 90ng plasmid DNA of M50 Super 8x TOPFlash or 25ng of pNF-κB-Luc and 3ng of pRLTK. Cells were

subjected to dual-luciferase assay 24 h after stimulation with IL1 β (100 ng/ml) or unstimulated. For cell lysis, 25 μ l of passive lysis buffer was used and cells were subjected to a freeze-thaw cycle. Cell lysates were analysed on a 96-well microplate reader (Tecan, Männedorf, Switzerland) and dual-luciferase activity was expressed as relative light units (RLU).

2.1.5 Generation of DNMT3A KO cell via Crispr/Cas9 genome editing

To generate a stable cell line lacking DNMT3A, Caco-2 cells were transfected with a plasmid encoding the non-coding guide RNA and the nuclease Cas9. The short guide RNA targets the nuclease Cas9 to a specific genomic locus. To generate the Crispr/Cas9 construct, GeneArt[®] CRISPR Nuclease Vector Kits (Life Technologies) was used according to the manufacture's protocol. The vector used was supplied of CD4 reporter. Two single-stranded oligonucleotides, forward 5'-GAGGACCGAAAGGTGAGCAGGTTTT-3' and reverse 5'-CTGCTCACCTTTCGGTCCTCCGGTG-3', targeting the shared sequence of all three DNMT3A isoforms were designed by following the protocol's guidelines.

2.1.5.1 Annealing procedure

Single-stranded oligonucleotides were annealed to generate a double-stranded oligonucleotide. The following reagents were added to a 1.5 ml reaction tube with a total volume of 20 μ L in a final concentration of 90 μ M (Table 4). The annealing mixture was placed in a thermocycler using the following conditions: 95°C for 4 min and 25°C for 10min.

Table 4: Annealing reagent list.

Forward strand oligonucleotide (100 μ M)	5 μ L
Reverse strand oligonucleotide (100 μ M)	5 μ L
10x Oligonucleotide Annealing buffer	2 μ L

2.1.5.2 Ligation reaction

After the double-stranded oligonucleotide was generated, 5nM working solution was prepared and cloned into the GeneArt[®] CRISPR Nuclease Vector. A twenty μ L ligation reaction was set up at room temperature using the reagents in table 5. The mix reaction was incubated for 1 hour at room temperature and afterwards placed on ice.

Table 5: Ligation reagent list.

5x Ligation buffer	2 μ L
Linearized GeneArt® CRISPR Nuclease Vector	1 μ L
Ds oligonucleotide (5 μ M)	1 μ L
RNase-Free water	5,5 μ L
T4 DNA ligase	0,5 μ L

2.1.5.3 Transformation of competent *E.coli* cells

One Shot® TOP10 chemically competent *E. coli* was (Life Technologies, Darmstadt, Germany) used for the cloning of CRISPR nuclease construct. These cells are ideal for high-efficiency cloning, allowing a stable replication of high-copy number plasmids. After thawing the cells on ice, 0.2 μ L of the ligation reaction was added into a vial of One Shot® TOP10 chemically competent *E. coli* and mixed gently the tube. After 20 min incubation on ice, the cells were heat-shocked for 30 sec at 42°C in a water bath and immediately transferred to ice for 2 min. Successively 250 μ L of room temperature S.O.C. medium was added to the tube and it was shaken horizontally at 350 rpm, 37°C for 45 min. 150 μ L of the transformation reaction was spread in a pre-warmed LB agar plate containing 100 μ g/mL ampicillin. The plate was incubated overnight at 37°C.

2.1.5.4 Analysis of transformants

Four ampicillin-resistant colonies were culture overnight in LB medium containing 100 μ g/mL ampicillin at 37°C. Plasmid DNA was isolated (as described in 2.2.4) and verified by Sanger sequencing using the U6 Forward primer (as described in 2.2.5).

2.1.5.5 Transfection of Caco-2 cells

The Lipofectamine®3000 kit was used for the transfection of the CRISPR plasmid. Caco-2 cells were seeded in a 10 cm dish. After 24h, the transfection was performed using 3 μ g of CRISPR/Cas9 expression vector (as described in 2.1.3).

2.1.5.6 Enrichment of CRISPR nuclease expressing cells

Cells transfected with GeneArt® CRISPR Nuclease Vector with CD4 reporter can be enriched using Dynabeads®CD4 magnetic beads kit (ThermoFisher scientific). Twenty-four hours after transfection, cells were harvested, centrifuged at 1500RPM for 2 min and resuspended in 2 mL of Buffer I (sterile PBS with 0.1% BSA and 2 mM EDTA). After two washing steps with Buffer I, the cell were resuspended in 500 μ L of Buffer I. Ten μ L of Dynabeads®CD4 magnetic beads were washed and resuspended in 25 μ L of Buffer I. In a 1.5 mL reaction tube, the cells were mixed with the Dynabeads®CD4 magnetic beads and filled up to a final volume of 1 mL with Buffer I. After 30 min of incubation at 4 °C on a mixer, the tube was placed on a magnet and the supernatant was collected in a new 1.5 mL reaction tube. The cells bound to the beads were washed 5 times with Buffer I and resuspended in 100 μ L of Buffer II (sterile MEM with 2% FCS). Ten μ L of DETACHaBEAD®CD4 was added to the cells and the beads and incubated on a mixer at room temperature for 45 min. During this

step the cells will detach from the beads. Afterwards the tube was placed on a magnet and the supernatant, containing the CD4⁺ cells, were transferred to a new 1.5 mL tube. In order to collect all CD4⁺ cells, this step was repeated for 3 times. The cells were centrifuged at 400g for 6 min and resuspended in MEM +20%FCS with a cell density of 5 cells/mL.

2.1.5.7 Screening of CRISPR clones

Monoclonal population of DNMT3A KO cells were obtained by single seeding of CD4⁺ cells in 96 well plates. After 10 days, the cells were harvested and plated in a 24 well plate. Once the cells were ≥ 90 confluent, they were harvested and plated in duplicate in 12 well plate. One well was used for western blot analysis and the duplicate as backup. After confirmation of the successful deletion of DNMT3A by Western blot, the monoclonal cell population was expanded in a T75 flask for further investigation.

2.1.6 Generation of stable expression of DNMT3A1 and DNMT3A2 in DNMT3A KO cell line

Expression vectors encoding DNMT3A1 and DNMT3A2 isoforms were transfected into DNMT3A KO cells, as described in as described in 2.1.3. Briefly, DNMT3A KO cells were seeded on 10cm dish at a density of 2×10^6 cells per dish. After 24h, cells were transfected with 3 μ g of p-Piggy-GFP2a-puro-TY1-DNMT3A1 or p-Piggy-GFP2a-puro-TY1-DNMT3A2 and 1 μ g of pTransposase. After 24h, transfected cells were selected with in puromycin-containing medium for 7 days. Puromycin-resistant monoclonal cell line population were obtained and examined for protein expression.

2.1.7 Generation of murine colonic organoids

Colonic organoids are originated from intestinal crypts, and they have a cyst structure-like with an inner lumen flanked by a polarized epithelial layer. The basal side of the epithelial cells is oriented towards the outside, whereas the apical side is oriented towards the lumen [103]. Crypts were isolated from mouse small intestine by EDTA-based Ca²⁺/Mg²⁺ chelation and intestinal organoids were cultivated as described by Sato et al [104]. In brief, colon was removed and cut longitudinally. The washed colon was laterally cut into pieces of 0.5 cm. Intestinal pieces were incubated in cold PBS supplemented with 2.5 mM EDTA for 40 min at 4°C. EDTA was removed and fresh PBS was added. Crypts dissociation was made by pipetting for 10 times. Supernatant containing crypts was collected. This procedure was repeated 3 times. The resulting crypt suspension was passed through a 100 μ m strainer and centrifuged at 1200 rpm at 4 °C. Supernatant was removed and epithelial crypts were resuspended in Matrigel (5-10 crypts/1 μ l Matrigel) (BD Bioscience/Heidelberg, Germany). Matrigel provides 3D laminin- and collagen-rich matrix resembling the basal lamina. Crypts were embedded in 24-well plates and cultivated in 50% L-WNR conditioned medium and 50% 2x basal medium supplemented with 30% FCS. L-WRN conditioned media was generated as

previously described using the L-WRN cell line [105]. Medium was changed twice per week and organoids were stimulated after 5 days of cultivation.

2.2 Molecular biological methods

2.2.1 Total RNA isolation

Cell line samples were washed with PBS and lysed in 350 μ L of RLT buffer (Qiagen, Hilden, Germany) containing 1% 2-mercaptoethanol. Murine tissue samples were ground using mortar and pestle in liquid nitrogen to prevent RNA degradation. The grounded samples were lysed in 700 μ L RLT buffer (Qiagen, Hilden, Germany) containing 1% 2-mercaptoethanol. Resulting sample lysates were applied to QIAshredder columns for homogenization. RNeasy Mini Kit (Qiagen, Hilden, Germany) was used for RNA extraction according to the manufacturer's protocol. To avoid contaminations by genomic DNA, an incorporated on-column DNase step was carried out. The purified RNA was eluted in 50 μ L RNase-free water and the RNA concentration was determined using the NanoDrop ND-1000 spectrophotometer (PeqLab Biotechnologie GmbH, Erlangen, Germany). RNA samples were stored at -80 °C.

2.2.2 cDNA synthesis

500 ng to 1 μ g of total RNA was reverse transcribed by using Maxima H Minus First Strand cDNA Synthesis Kit (ThermoFisher Scientific, Bremen, Germany) according to the manufacturer's protocol. RNA was incubated with Oligo(dt)18 oligonucleotide, dNTP mix and water at 65 °C for 5 min. Subsequently, 5X RT buffer and Maxima H Minus reverse transcriptase (RT) was added to the mixture and incubated as indicated (Table 6). The synthesized cDNA was diluted 1:10 with nuclease-free water and stored at -20 °C until further usage.

Table 6: List of components for cDNA synthesis.

step	component	amount	temperature	time
1	RNA Oligo (dt)18 oligonucleotide dNTP mix (10 Mm each) nuclease-free water	100-1000ng 0.125 μ l 0.5 μ l to 7.5 μ l	65 °C	5 min
2	5x RT bufffer Maxima H Minus RT	2 μ l 0.5 μ l	25°C 50°C 85°C	10 min 15 min 5 min

2.2.3 Quantitative real-time polymerase chain reaction

Quantitative real-time PCRs (qPCRs) enabled the quantification of mRNA levels using target-specific oligonucleotides. The qPCR method is based on the PCR technique with an additional DNA quantification step at the end of each amplification cycle. Predesigned TaqMan probes were applied, which were obtained from Applied Biosystems (Carlsbad, USA). The employed TaqMan probes and their order numbers are listed in the

supplementary information (Table 19). 5 µl of sample cDNA was mixed with 5 µl TaqMan PCR Master Mix. The reaction was carried out on 384-well plates using the 7900 HT Fast Real-Time PCR System (Applied Biosystems, Carlsbad, USA). All results were normalized to their respective GAPDH or ACTIN housekeeper mRNA level and shown as foldchange relative to a reference.

2.2.4 Plasmid preparation

Plasmid mini preparations were performed to identify positive clones after generation of expression constructs. Four clones per transformation were picked using sterile pipette tips and cultured overnight in 2 ml LB medium at 37 °C in a shaker. The medium was supplemented with 2 µl of 100 mg/ml ampicillin. Plasmid DNA was isolated using the GeneJET Plasmid Miniprep Kit (Thermo Scientific, Bremen, Germany) according to the manufacturer's protocol. The sequence of the isolated plasmid DNA was identified using Sanger sequencing (as described in 2.2.5). For larger DNA quantities, 100 ml LB medium was inoculated and cultured overnight in a shaker at 37 °C. Plasmid DNA was isolated using the PureLink® HiPure Plasmid Filter Midiprep Kit (Life Technologies, Darmstadt, Germany) according to the manufacturer's protocol. The DNA concentration was determined using the NanoDrop ND-1000 spectrophotometer (PeqLab Biotechnologie GmbH, Erlangen, Germany). Plasmid DNA was stored at -20 °C for further usage.

2.2.5 Sanger sequencing

The precise order of nucleotides in all generated plasmids was determined by Sanger sequencing (166) using the BigDye Terminator v1.1 cycle sequencing Kit (Life Technologies, Darmstadt, Germany). 200 ng of plasmid DNA was mixed with 10 µM of a template-specific oligonucleotide, 1.5 µl of BigDye, 1.5 µl of 5X sequencing buffer and 4 µl PCR-grade water. During the following PCR, the fluorescent labeled ddNTPs were incorporated into the PCR products. The PCR program contained an initial denaturation step at 95 °C for 1 min, followed by cycling 35 times through a denaturation step at 95 °C for 10 sec, annealing phase at 50 °C for 5 sec and an elongation phase at 60 °C for 4 min. A laser of the 3730xl DNA Analyzer (Applied Biosystems, Carlsbad, USA) detected the fluorescence of the incorporated ddNTPs while passing through thin capillaries filled with a gel matrix for separation. DNA sequences were analysed using the Sequencher 5.0 software (Gene Codes Corporation, Ann Arbor, USA).

2.3 Protein biochemical methods

2.3.1 Total protein lysate isolation

Total protein lysates were extracted to analyse the protein content of cells by applying the gel electrophoresis technique. Adhered cells were washed once with ice-cold PBS and lysed using 50-100µl cold RIPA buffer,

containing 1X Halt™ combined protease and phosphatase inhibitor (Thermo Scientific, Bremen, Germany). Lysates were stored on ice for 30 min to ensure complete cell lysis. Afterwards, lysates were centrifuged at 16000 g for 15 min at 4 °C to remove cell debris and genomic DNA. Supernatant was transferred to new 1.5 ml reaction tubes. Protein lysates were stored short-term at -20 °C or at -80 °C for several months.

2.3.2 Protein quantification

Protein quantification was determined using the colorimetric assay Bio-Rad DC (detergent compatible) protein assay (Bio-Rad, Munich, Germany). The assay is similar to the Lowry method [106] where copper ions react with peptide bonds under alkaline conditions, leading to subsequent reduction of the folin reagent by the copper-treated proteins. This results in the development of blue colour with a maximum absorbance at 750 nm. Five µl of protein lysate were diluted with 5µl of dist. water and mixed with the assay reagents. After 15 min in the darkness, absorbance of protein samples were determined and correlated with protein concentrations using a bovine serum albumin (BSA) standard curve.

2.3.3 Gel electrophoresis of proteins

The separation of proteins by their molecular weight was performed using sodium dodecyl sulfate polyacrylamide gel electrophoresis (SDS-PAGE). According to the Laemmli standard protocol [107] for SDS-PAGE, proteins were treated with the reducing agent dithiothreitol (DTT) to dissociate disulfide bonds. Additionally, the anionic detergent SDS denaturizes proteins and masked their intrinsic charges by negatively charged sulfate groups. Applying an electric field to the polyacrylamide gel matrix causes the separation of proteins by their molecular weight. The discontinuous gel for SDS-PAGE was composed of a stacking and a separating gel (Table 7). Ammonium persulfate (APS) and tetramethylethylenediamine (TEMED) were added for the polymerization of the polyacrylamide matrix in the gels. Electrophoresis was performed in two steps using Tris-glycine-SDS (TGS) buffer. During the first step, proteins concentrate at the interface of stacking and separation gel by applying a constant current of 15 mA and a maximum voltage of 300 V per gel for 30 min. In the second step, proteins were fractionated by their molecular weight in the separating gel at a constant current of 30 mA and a maximum voltage of 300 V per gel. Protein lysates were mixed with 5X DTT and heated at 95 °C for 5 min. An equal protein amount was loaded into the wells of the gels. The molecular weight of the proteins was estimated by the prestained PageRuler plus protein ladder 10-250K (Thermo Scientific, Bremen, Germany).

Table 7: List of reagents for SDS-Polyacrylamide Gel Electrophoresis.

Protein size (kDa)		50-200	30-120	20-100
Separation gel	% Acrylamide	7.5%	10%	12%
	A.bidest (ml)	5	4.15	3.5
	4xSeparation Buffer (ml)	2.5	2.5	2.5
	(Bis)Acrylamide (ml)	2.5	3.35	4
	TEMED (μ l)	10	10	10
	10% APS (μ l)	100	100	100
Stacking gel	% Acrylamide	3%		
	A.bidest (ml)	1.95		
	4xStacking Buffer (ml)	0.75		
	(Bis)Acrylamide (ml)	0.3		
	TEMED (μ l)	3		
	10% APS (μ l)	30		

2.3.4 Immobilization of proteins by immunoblot

The immunoblot technique allows electrophoretic transfer of separated proteins from polyacrylamide gels to polyvinylidene difluoride (PVDF) membranes [108]. Using this method, the proteins can be detected by specific antibodies. PVDF membranes (Bio-Rad, Munich, Germany) were activated with methanol for 10 sec, washed in dist. water and incubated in anode buffer 1 for 5 min. One blot paper (Bio-Methods 32 Rad, Munich, Germany) each was equilibrated in either anode buffer 1, anode buffer 2 or cathode buffer. After protein separation by gel electrophoresis, the blotting sandwich was assembled in the following way: thick blot paper soaked with cathode buffer, gel, PVDF membrane, thick blot paper soaked with anode buffer 1 and thin blot paper soaked with anode buffer 2. The electrophoretic transfer of the proteins was carried out using the Trans-Blot® Turbo™ Transfer System (Bio-Rad, Munich, Germany) at a constant current of 0.1 A and a maximum voltage of 25 V for 60 min.

2.3.5 Immunodetection of proteins

The visualization of transferred proteins of interest was achieved by immunodetection with specific primary antibodies and horseradish peroxidase (HRP)-conjugated secondary antibodies. The HRP enzyme activity is detectable by incubating the membrane with an enhanced chemiluminescent (ECL) substrate (GE Healthcare, Freiburg, Germany). To prevent unspecific interactions of the PVDF membrane and the antibody, the PVDF membrane was blocked with either 5 % (w/v) non-fat dry milk or 5 % (w/v) BSA for 1 h. The membrane was incubated with a specific primary antibody at room temperature for one hour. Afterward, the membrane was washed with TTBS three times for 10 min. The secondary antibody was incubated with the membrane for 1h at room temperature. The secondary antibody was removed and the membrane was washed with TTBS three times for 15 min at room temperature. For detection, the membrane was treated with ECL

substrate for 1 min, exposed to chemiluminescence hyperfilm and developed using an automated developer machine (Agfa, Mortsel, Belgium). For analyzing different proteins on one membrane, primary and secondary antibodies were removed by stripping. Therefore, membranes were incubated with stripping buffer at 55 °C for 20 min and washed with TTBS three times for 10 min. Membranes were incubated with new primary antibodies after blocking with either 5 % (w/v) non-fat dry milk or 5% (w/v) BSA for 1 h.

2.3.6 Enzyme Linked Immunosorbent Assay (ELISA)

Detection of human IL8 chemokine levels in cell culture supernatants was achieved with enzyme linked immunosorbent assays (ELISA), performed according to the manufacturer's protocol (Life Technology). Absorbance was measured using the microplate reader Infinite M200 Pro (Tecan, Männedorf, Switzerland) and the associated software i-control™ 1.9 (Tecan, Männedorf, Switzerland).

2.4 Functional assays methods

2.4.1 Wound healing assay

Wound healing assay is an *in vitro* technique used to study cell migration. In this assay, a wound is made on a confluent cellular monolayer by physical exclusion or via mechanical damage. The cell-free area induces the cells to migrate into the gap. For performing a wound healing assay, we used Ibidi culture-insert 4 well (©ibidi GmbH, Martinsried, Germany). Caco-2 cells were seeded in a concentration of 6×10^5 cells/ml. 110 μ L of cell suspension was added in the culture-insert. After 24h the insert was removed and the cells were washed twice with PBS. Images of the gap were taken at time 0, immediately after removing the insert, and at time 24h using an inverted microscope (Zeiss Axio Vert.A1).

2.4.2 Permeability assay

Two different assays were used to assess paracellular permeability. For the first assay, permeability of Caco-2 cells monolayers was determined by measuring the apical-to basolateral passage of the fluorescent dye, Lucifer yellow (LY). Caco-2 cells were seeded in a transwell cell culture insert. After 10-14 days, cells were washed twice with Hank's balanced solution (HBSS). 1 ml of HBSS was added to the recipient basolateral compartment and 500 μ L of LY with a final concentration of 100 μ g/ml to the donor apical compartment. Immediately after LY addition, 50 μ L of aliquots were taken from the apical compartment (F_{c0}) and from the basolateral compartment at time 0, 1h, 2h, 3h, and 4h. LY fluorescence was measured λ_{exc} : 485 nm; λ_{em} : 530 nm. Percentage of LY passage was calculated from the formula: % LY pass= $F_{test} / (F_{c0} - F_{blank})$. Being F_{test} , fluorescence of the sample; F_{c0} , the fluorescence of LY in the apical compartment at time 0; and F_{blank} , the fluorescence of HBSS. As a second assay, Caco-2 spheroids were used. Briefly, Caco-2 spheroids were

incubated with 4kDa fluorescein isothiocyanate-dextran (FITC-4D) with a final concentration of 1mg/ml overnight. Fluorescence intensity was measured using the confocal laser scanning microscope TCS SP5 (Leica, Wetzlar, Germany) and the appropriate software Leica Application Suite Advanced Fluorescence (Leica, Wetzlar, Germany). Spheroids permeability was assessed by measuring the FITC-4D fluorescence ratio between luminal (L) and basolateral (LB) side. Imaging analysis was performed using Fiji software [109].

2.4.3 Transepithelial electric resistance (TEER)

Transepithelial electrical resistance (TEER) is the measurement of electrical resistance across a cellular monolayer and is a very sensitive and reliable method to confirm the integrity and permeability of the monolayer. TEER of Caco-2 WT and DNMT3A KO monolayers were checked by using the Millicell[®]-ERS system (Millipore Corporation, Bedford, MA). The resistance was calculated as following: $R_{\text{cell monolayer}} = (R_{\text{sample}} - R_{\text{blank}}) \times \text{area cm}^2$.

2.4.4 Spheroids culture

A spheroid is a 3D (three-dimensional) structure with a lumen enclosed by a single layer of polarized cells. This 3D organization partially represents the *in vivo* structural organization of intestinal epithelial cells, providing a good *in vitro* model system to study the property of intestinal barrier. Caco-2 cells 2×10^3 cells/well were resuspended in MEM +20%FCS, mixed with 60% Matrigel and plated on 8well chamber slide. After solidification of the Matrigel, growth medium was added and spheroids were allowed to form at 37°C for 7-10 days. Formed spheroids were used for further experiments.

2.5 Imaging

2.5.1 Immunofluorescence

Caco-2 spheroids in respective chamber slides, after two washing steps with PBS, were fixed with 4% (w/v) paraformaldehyde in PBS for 30 min at room temperature. Spheroids were washed one time with PBS for 5 min and permeabilized with 0.5 % (v/v) Triton X-100 in PBS for 10 min. Unspecific binding sites were blocked with 5% (v/v) BSA in PBS for 30 min at room temperature. Incubation with primary antibody was performed overnight at 4°C (see table with details). Following three washing steps with PBS for 5 min, incubation with secondary antibody conjugated with Alexa Fluor-488 together with phalloidin and DRAQ5 was performed for 2h at room temperature. Cells were washed for three times for 5 min with PBS. Stainings were analysed using the confocal laser scanning microscope TCS SP5 (Leica, Wetzlar, Germany) and the appropriate software Leica Application Suite Advanced Fluorescence (Leica, Wetzlar, Germany).

2.5.2 Immunohistochemistry

2.5.2.1 Tissue Processing

Murine tissue was removed and immediately fixed in 10 % (w/v) formalin for 24 h at 4 °C. For complete dehydration, tissue was immersed in a series of ethanol solutions of increasing concentrations until 100%. In a next step, the ethanol was gradually replaced with xylene, which is then replaced by paraffin. The paraffin embedded tissue was dissected into 3.5 - 4.5µm sections using the RM2255 microtome (Leica, Wetzlar, Germany).

2.5.2.2 Hematoxylin and Eosin (H&E) Staining

Samples were rehydrated in decreasing xylene and ethanol solutions followed by washing steps with distilled water. Slides were stained for 2 - 5 min in hematoxylin. Haematoxylin in complex with aluminium salts is positively charged and reacts with negatively charged, basophilic cell components including nucleic acids which are stained blue. Counterstaining of the cytoplasm was achieved with 1 % (v/v) eosin solution for 2 min. Eosin is negatively charged and therefore reacts with positively charged, acidophilic components such as amino groups in proteins in the cytoplasm, which are stained pink. Slides were dehydrated and embedded in Roti-Histo-Kit mounting medium (Roth, Karlsruhe, Germany). Slides were examined with a Zeiss AxioImager.Z1 apotome fluorescence microscope and the AxioVision Rel 4.9 software (ZEISS, Oberkochen, Germany).

2.5.3 Transmission electron microscopy

0.5 cm long pieces of the ileum and Caco-2 cells growing on transwell support were fixed in 3 % glutaraldehyde in PBS at 4°C overnight. Transmission electron microscopy of semi thin ileal sections and Caco-2 cells were performed at Institute of Anatomy (AG Lucius) as described previously [110].

2.6 NGS technology methods

2.6.1 Transcriptome analysis

Total RNA was isolated according to chapter 2.1.2. Samples were sequenced on HiSeq3000 (Illumina, San Diego, United States) using Illumina total RNA stranded TruSeq protocol. An average of ~40 million 75-nt paired-end reads was sequenced for each sample. Raw reads were pre-processed using cutadapt [96] to remove adapter and low quality sequences. RNAseq reads were aligned to the human genome (GrCh38) reference genome with TopHat2 [111]. Gene expression values of the transcripts were computed by HTSeq [112]. Differential gene expression levels were analysed and visualized by the Bioconductor package DESeq2 [113]. Venn diagrams were drawn using VennDiagram package in R [114]. Gene Ontology (GO) terms were obtained within the category of biological processes using GO package in R [115].

Differential expression of genes between each treatment type versus control samples was determined using Wald tests to calculate the significance of differential expression for each gene in a pair-wise comparison between treatment types versus control.

2.6.2 Methylome analysis

Methylation profiling was performed by using Infinium®MethylationEPIC BeadChip (Illumina). Isolation of genomic DNA was performed using DNeasy Blood & Tissue Kit (Qiagen, Hilden, Germany) according to the manufacturer's protocol. Total DNA was treated with sodium bisulphite using EZ DNA methylation kit (Zymo Research, CA, USA). Samples were run on an Illumina iScan System (Illumina, Ca, USA). Row IDAT files were processed using RnBeads package [116].

2.7 Generation, Handling and Treatment of Mice

2.7.1 Generation of Dnmt3a conditional knockout mice (*Dnmt3a*^{ΔIEC})

In this study, *Dnmt3a* conditional knockout mice were used to investigate the functional role of Dnmt3a *in vivo*. The *Dnmt3a*^{tm1a(KOMP)Wtsi} mouse strain was purchased from EMMA mouse repository. This mouse line originates from knockout mouse project (KOMP) ES clone EPD0332_1_C06. The targeting vector (PRPGS00153_B_B10) consists of a promoter-driven cassette inserted at a position on Chromosome 12 upstream of exon 13. The cassette is composed by a flipase recognition target (FRT) site, a β-galactosidase (lacZ) sequence, a bacteriophage P1-derived loxP site and a neomycin under the control of beta-action promoter followed by a second FRT site and a second loxP site (Figure 2.1). The targeted exons 13-17 are flanked by two loxP sites. The vector was introduced into C57BL/6N-derived JM8A1.N3 embryonic stem cells. Positive cells were microinjected into mouse blastocysts and transferred into pseudopregnant female mice. The resulting chimeras were bred with C57BL/6NJ for colony expansion. The resulting *Dnmt3a* conditional mice allow the generation of conditional knockout mice.

Since *DNMT3A* had been identified as a susceptibility gene for CD, *Dnmt3a* conditional knockout mice were generated, where the lack of *Dnmt3a* is restricted to intestinal epithelial cells (IECs) of the villi and crypt cells of the small and large intestine (*Dnmt3a*^{ΔIEC}). Since these mice have not undergone FLP deletion, they were crossed with Flp deleter mice (C57BL/6-Tg(CAG-Flpe)2Arte) for removal of selection markers.

For the generation of *Dnmt3a*^{ΔIEC} mice, *Dnmt3a*^{fl/fl} conditional mice were crossed with B6.SJL-Tg(Vil-cre)997Gum/J (villin-cre) mice. Villin-cre mice express the Cre recombinase under the control of the *villin 1* promoter, which leads to Cre-mediated recombination of loxP sites resulting in a tissue-specific deletion of *Dnmt3a*. Beside the mainly described expression of *villin 1* in intestinal epithelial cells, *villin 1* can also be found in cells of the kidney proximal tubulus and in the duct of pancreas and biliary system [117]. In this

study, heterozygous mice for *villin 1* were bred with *Dnmt3a^{fl/fl}* in order to generate *Dnmt3a^{ΔIEC}* and their wild-type littermates.

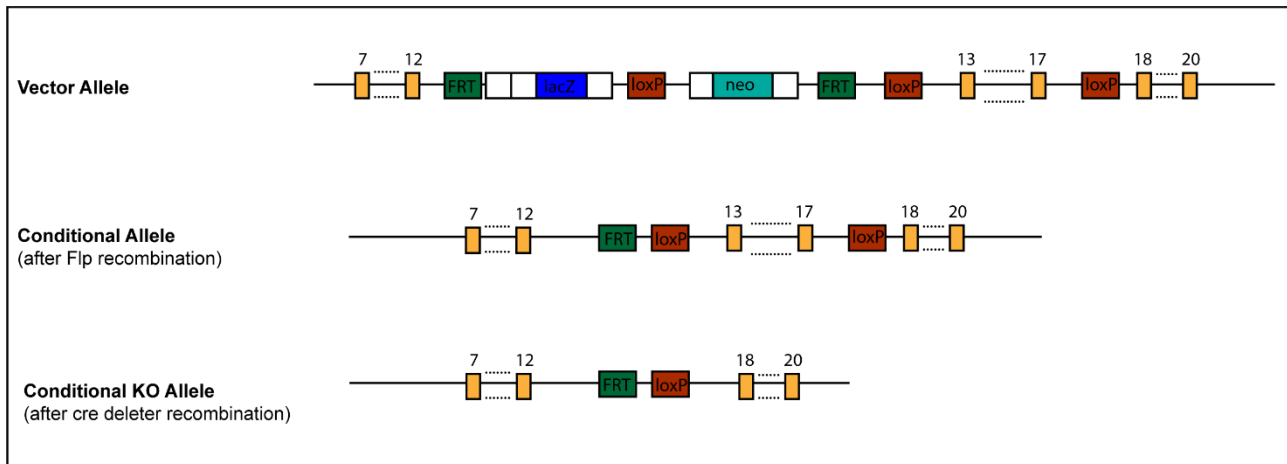


Figure 2.1: Targeting strategy for the generation of conditional *Dnmt3a* knockout allele.

For *Dnmt3a* deletion a targeting vector was designed to flank exon 13-17 by loxP sites and lacZ and a neomycin resistance cassette for positive selection. The lacZ and neomycin cassette was excised in vivo by breeding with Flp deleter mice. Mating of these mice with Cre deleter mice resulted in *Dnmt3a^{ΔIEC}* mice.

2.7.2 Animal housing and animal care

Mice were housed under specific pathogen-free conditions in individually ventilated cages at the Central Animal Facility of the Schleswig-Holstein University Hospital Kiel, Germany. Animals were maintained in a 12 h light-dark cycle under barrier conditions at 21°C ± 2°C and 60% ± 5% humidity and were provided with food and tap water *ad libitum*. All experiments were performed according to the German guidelines for animal care and protection. The animal research in this study was approved by the institutional review boards (Table 2.8).

Table 8: License number for approved animal research.

License number	Designated use
V 242-58854/2016 (32-3/16)	acute and chronic DSS-induced colitis

2.7.3 Genotyping

Genotyping was performed to distinguish between heterozygous mice and homozygous wild-type or knockout mice by performing PCR analyses of genomic DNA. The genomic DNA was extracted from tail biopsies of three to four weeks old mice. Isolation of genomic DNA was performed using the DNeasy Blood & Tissue Kit (Qiagen, Hilden, Germany) according to the manufacturer's protocol. For PCR analyses, GoTaq DNA polymerase (Promega, Mannheim, Germany) was applied. Components for the PCR reaction and thermocycler program are shown in (Table 9). Applied oligonucleotides are listed in the supplementary information (Table 18).

Table 9: PCR components and thermocycler program for genotyping.

Component	Amount	Number of cycles	Temp. (°C)	Time
DNA	1 µl	1	95	1 min
5X GoTaq Green Buffer	4 µl	35	95	30 sec
dNTP mix (10 Mm each)	0.5 µl		58	15 sec
Oligonucleotide for (10 µM)	0.25 µl		72	30 sec
Oligonucleotide rev (10 µM)	0.25 µl			
GoTaq Polymerase	0.25 µl	1	72	5 min
Nuclease-free water	13.5 µl			

The resulting amplicon lengths were determined by gel electrophoresis (as described in chapter 2.2.4) followed by exposure to UV light for visualization. The genotype of a mouse was determined by combining the received amplicon lengths of the two PCR analyses (Table 10).

Table 10: Overview of expected amplicon lengths after genotyping PCR.

Genotype	PCR cond	PCR cre
Dnmt3a ^{fl/fl}	389 bp	no band
Dnmt3a ^{ΔIEC}	389 bp	400 bp

2.7.4 Induction of chronic colitis

Chronic colitis in 8-12 weeks old female mice was induced by three cycles of 1.5% (for the first cycle) and 2% (for the second and third cycles) (w/v) DSS in autoclaved drinking water for five days, followed by regular drinking water for five days. Mice were exposed to water with or without DSS *ad libitum*. In every cycle, the mice were monitored and weighed at least every other day. Mice were sacrificed on day 30.

2.7.5 Disease activity index (DAI)

During chronic DSS-induced colitis experiments, the course of the disease was monitored and scored using the disease activity index (DAI), a combined score of stool blood, stool consistency and body weight loss. Scores were determined as indicated in Table 11.

Table 11: Scoring criteria for the determination of the disease activity index.

Score	Body weight loss (%)	Stool consistency	Fecal blood
0	0	Formed	Hemoccult negative
1	1-5	Formed but soft	Hemoccult slightly positive
2	6-10	Unformed /smeary	Hemoccult strongly positive
3	11-20		Blood visible by eye on pellet
4	>20	Diarrhea	Rectal bleeding

2.8 Statistical analysis

Statistical analysis was performed using the GraphPad Prism 5 software package (GraphPad Software Inc., La Jolla, USA). Unless otherwise stated, the Student's unpaired t-test was performed. Data are shown as mean ± standard error of the mean (SEM). A p-value of ≤ 0.05 was considered as significant (*). A p-value of ≤ 0.01 was considered as strongly significant (**) and p-value of ≤ 0.001 as highly significant (***).

3 Results

3.1 Protein expression analysis of DNMT3A in human and murine cell lines

The *DNMT3A* gene encodes two major isoforms known as DNMT3A1 and DNMT3A2. While both isoforms transfer a methyl group to cytosine nucleotide, their subcellular localization differs. Indeed, in mouse embryonic stem cells, fluorescence microscopy analysis of DNMT3A1 and DNMT3A2 showed that DNMT3A1 is mainly localized in the cell nucleus while DNMT3A2 can be found both in the nucleus and cytoplasm [50]. We were able to demonstrate DNMT3A expression in three intestinal derived epithelial cell lines including the human colonic carcinoma cells Caco-2 and HT-29 and the immortalized murine intestinal epithelial cell line Mode-K (Fig. 3.1 a). These cells are widely used to study intestinal epithelial properties *in vitro* [118]. DNMT3A1 has a predicted size of 130 kDa and is equally expressed in all three cell lines. Regarding DNMT3A2, Mode-K cells presented a band of 110 kDa, while the human cell lines revealed an additional band of 89 kDa, from here on named DNMT3A2_1 and DNMT3A_2, respectively (Fig. 3.1 a-b). To verify the specificity of the DNMT3A antibody, Caco-2 cells were transfected with siRNA targeting DNMT3A. All three bands recognized by the DNMT3A antibody decreased, supporting its specificity (Fig. 3.1 c-d).

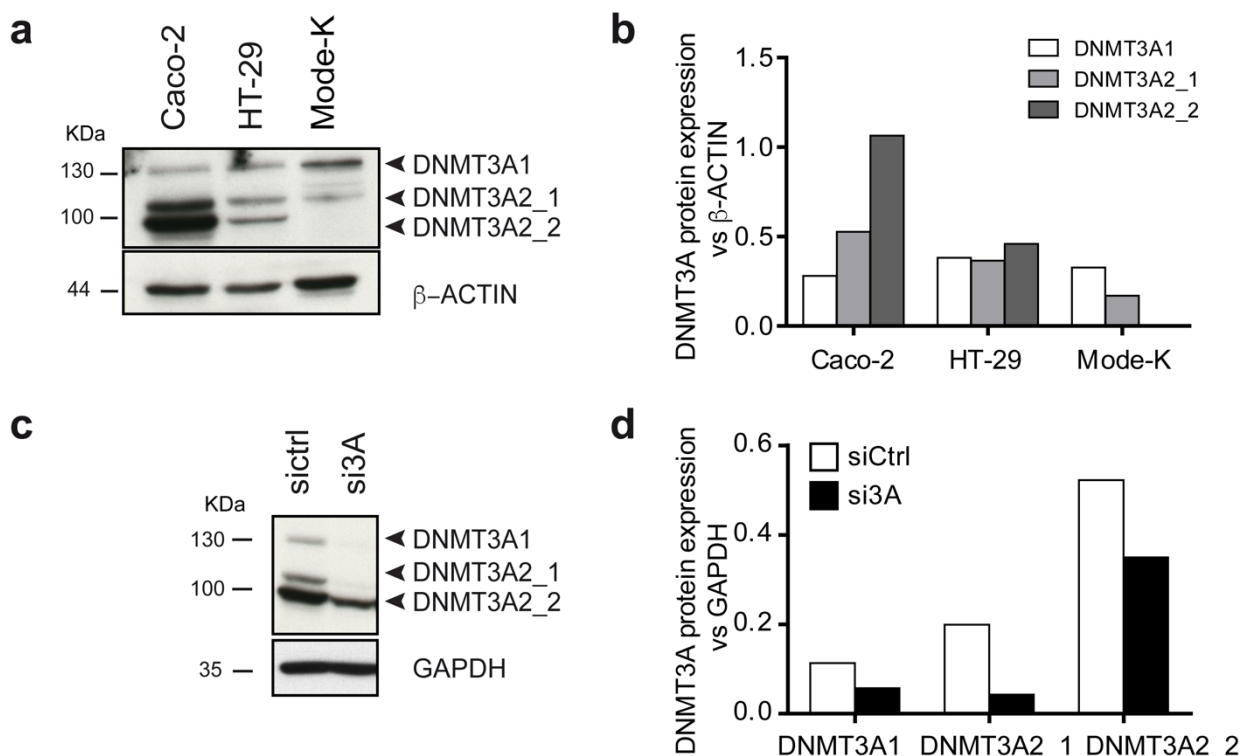


Figure 3.1: Human and murine intestinal epithelial cells express different levels of DNMT3A protein. (a) Western blot and (b) quantification of DNMT3A in the human cell lines Caco-2 and HT-29, and in the murine cell line Mode-K. β -Actin served as loading control. (c) Western blot and (d) quantification of DNMT3A in Caco-2 cells transfected with siRNA against DNMT3A and non-targeting control siRNA, respectively. GAPDH was used as loading control.

3.2 Generation of DNMT3A knock-out cells and reconstitution with single DNMT3A isoforms

DNA methylation is a dynamic process that is both cell type and tissue specific [119]. However, methylation and demethylation kinetics in differentiated cells remain poorly understood. As shown by Chen et al., deletion of *Dnmt3a* in mouse ESCs resulted in loss of methylation after a prolonged culture period, while inactivation of *Dnmt1*, responsible for DNA methylation maintenance, resulted in almost 90% loss of methylation [120]. In our study, we analysed transcriptional and DNA methylation changes upon prolonged ablation of DNMT3A. To this end, the Crispr/Cas9 genome editing technology was used to generate a *DNMT3A*-deficient Caco-2 cell line. Furthermore, individual DNMT3A isoforms were re-introduced in DNMT3A knock-out (KO) cells to generate stable cell lines encoding DNMT3A1 and DNMT3A2 isoforms, respectively.

Complete ablation of DNMT3A expression in the KO cell line and subsequent re-expression of DNMT3A1 and DNMT3A2 was confirmed by immunoblot detection (Fig. 3.2 a). Furthermore, knock-out and re-expression of the single isoforms on mRNA level was confirmed by RT-qPCR (Fig. 3.2 b). Additionally, the subcellular localization of DNMT3A was assessed by immunofluorescence staining using DNMT3A antibody and DAPI as nuclear counterstaining. As reported before [50], in wild-type (WT) cells DNMT3A was mainly confined to the nuclei (Fig. 3.2 c), while DNMT3A could not be detected in the KO cells (Fig. 3.2 b). Similar to the localization of DNMT3A in WT cells, in the cell lines encoding either the DNMT3A1 or the DNMT3A2 isoform, DNMT3A enzyme localized in the nuclei, confirming successful re-expression of the gene (Fig. 3.2 e-f).

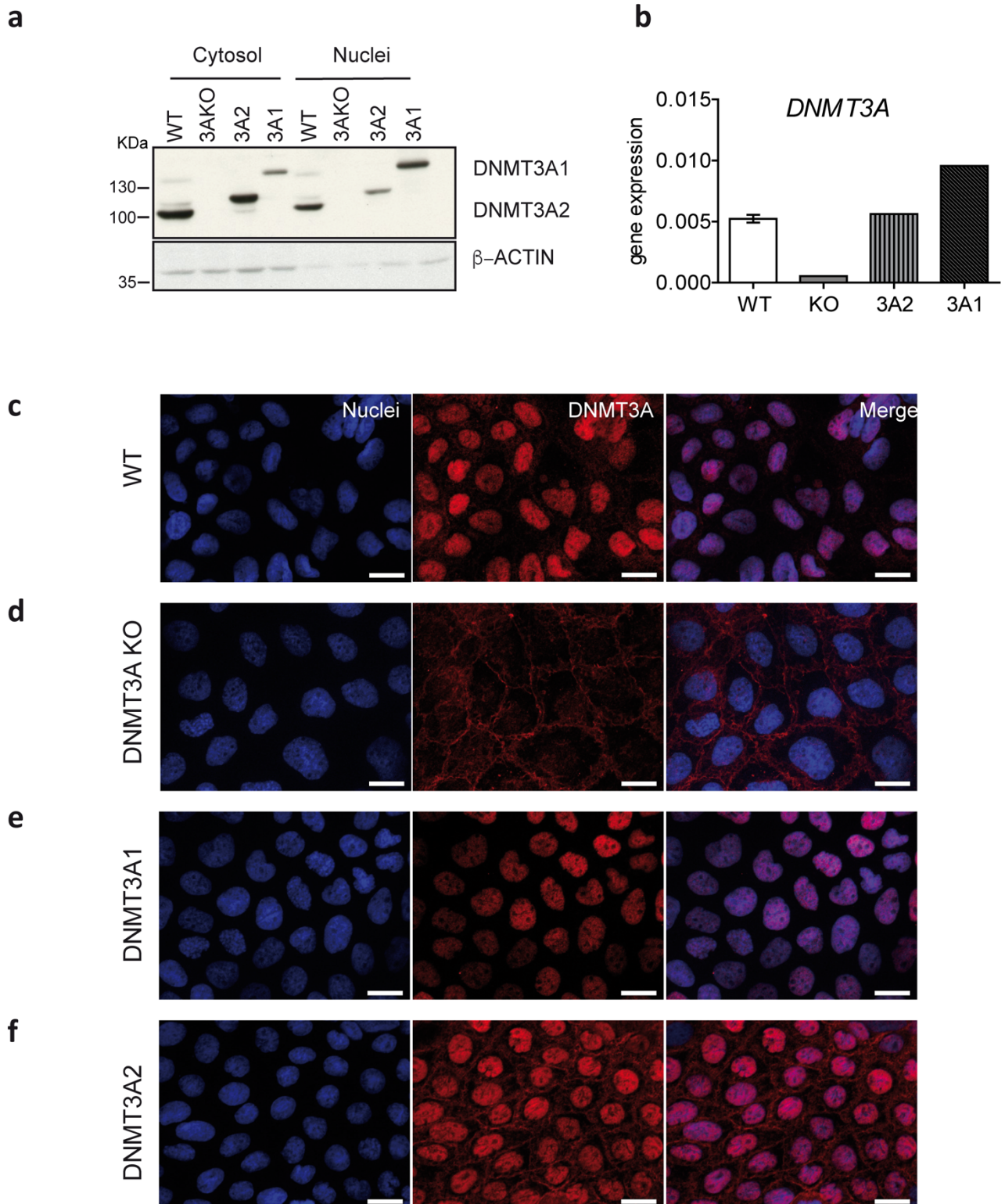


Figure 3.2: Characterization of DNMT3A KO, DNMT3A1 and DNMT3A2 cell lines.

(a) Western blot analysis of cytosolic and nuclear fractions and (b) gene expression levels of WT, DNMT3A KO, DNMT3A1 and DNMT3A2 cell lines. Actin was used as loading control. (c-f) Immunofluorescence staining for nuclei (blue) and DNMT3A (red) in WT, DNMT3A KO and DNMT3A1 and DNMT3A2 cell lines. Note a slight unspecific staining at the cell membrane, which is most prominent in the KO line. Scale bar 20 μ m.

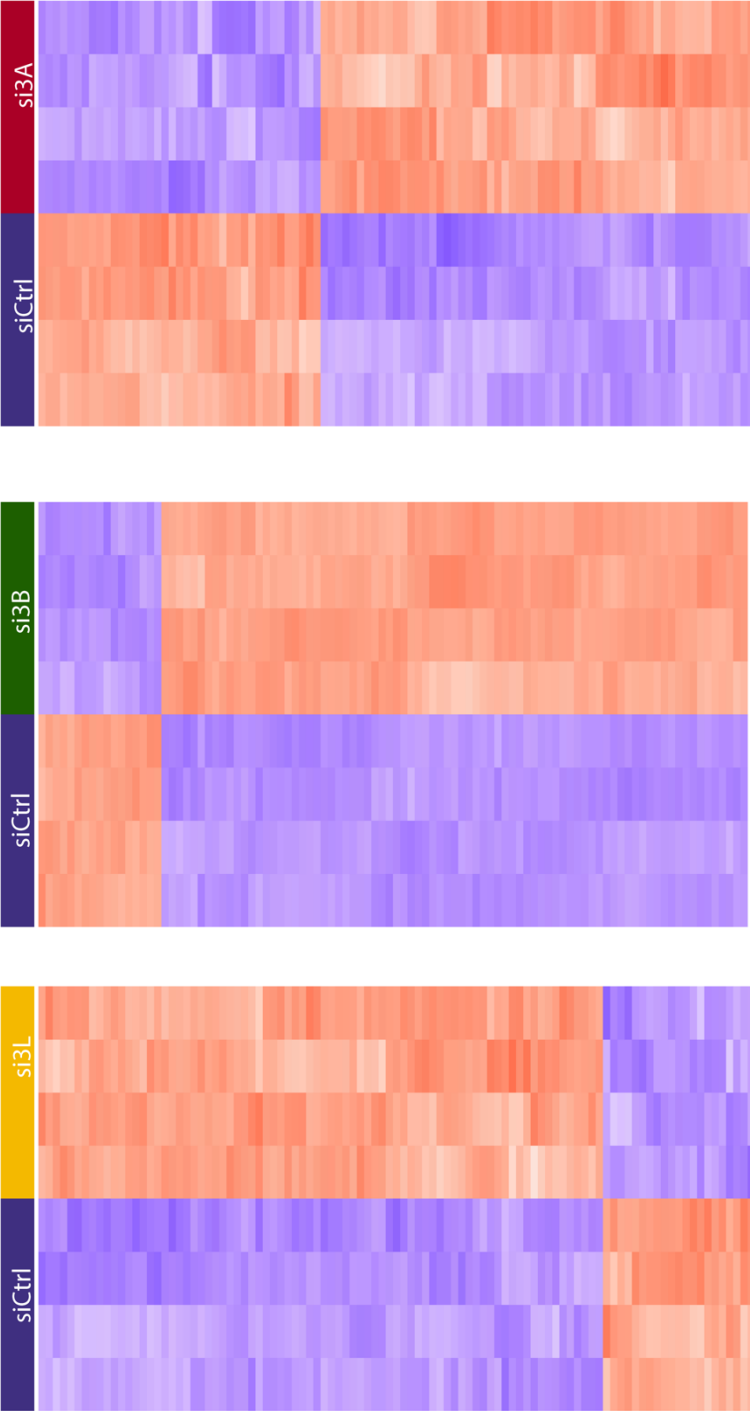
3.3 Downstream targets affected by short-term silencing of DNMT3A/B/L

In order to identify *DNMT3A*, *DNMT3B* and *DNMT3L* target genes, I used Caco-2 cells, in which the individual genes were silenced by siRNAs. 72 h post-transfection, RNA and DNA were isolated and used for RNA sequencing and 850k EPIC array, respectively.

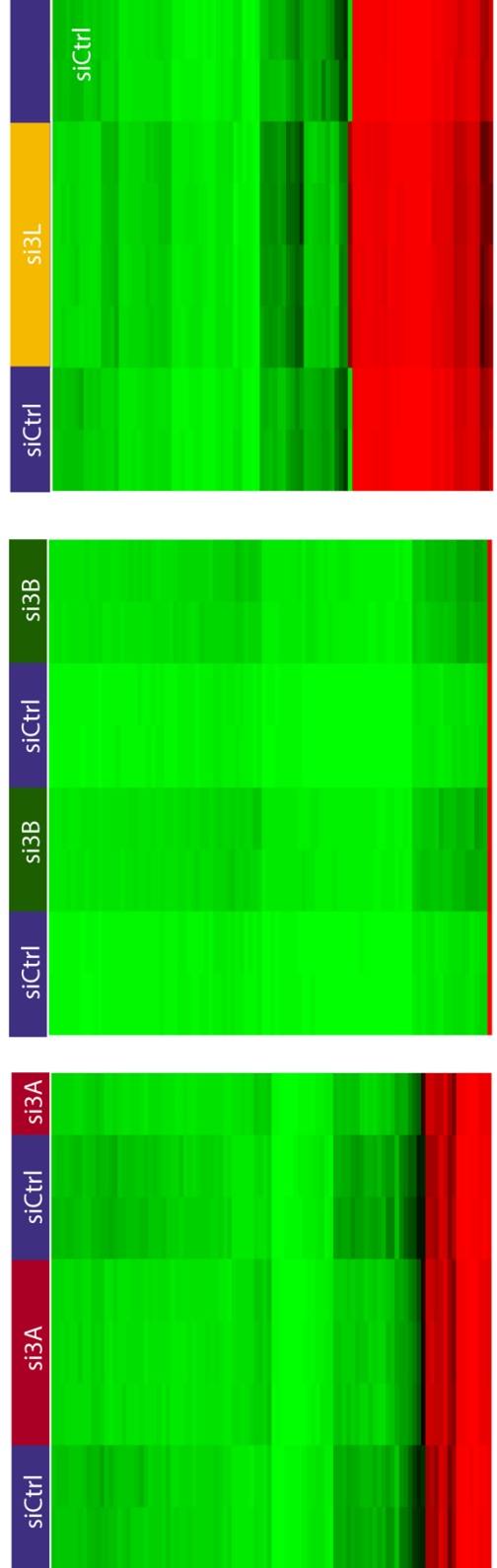
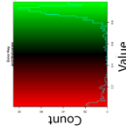
Transcriptome analysis was performed on siControl (siCtrl), siDNMT3A, siDNMT3B and siDNMT3L groups. Heat maps were created from the top 100 differentially expressed genes (DEGs) of siCtrl vs siDNMT3A, siCtrl vs siDNMT3B and siCtrl vs siDNMT3L (Fig. 3.3 a). An adjusted p-value (padj) smaller than 0.05 was used as cut-off. In total, we found 430 (siDNMT3A) vs 2618 (siDNMT3B) vs 368 (DNMT3L) uniquely upregulated genes and 276 (siDNMT3A) vs 2544 (siDNMT3B) vs 443 (DNMT3L) uniquely downregulated genes (Fig. 3.3 c). Next, GO term analysis (gene ontology of biological processes) was performed with the upregulated and downregulated genes from the siDNMT3A group. The analysis identified biological processes related to wound healing, cell-cell connection and cell migration to be induced (Fig. 3.3 d). Global DNA methylation was analysed using the 850k EPIC array that covers over 850.000 CpG positions. Surprisingly, statistical analysis of differentially methylated promoters (DMPs) showed no global changes on DNA methylation in any of the three groups (Fig. 3.3 b).

a

expression
2
1
0
-1
-2



b



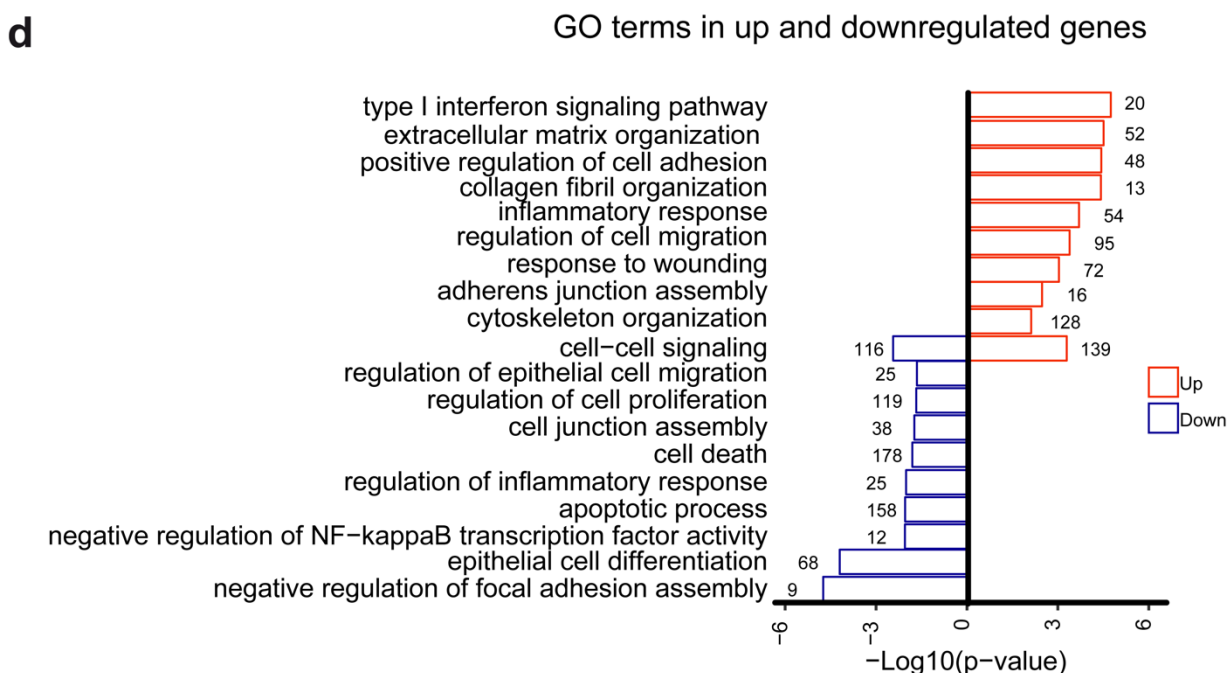
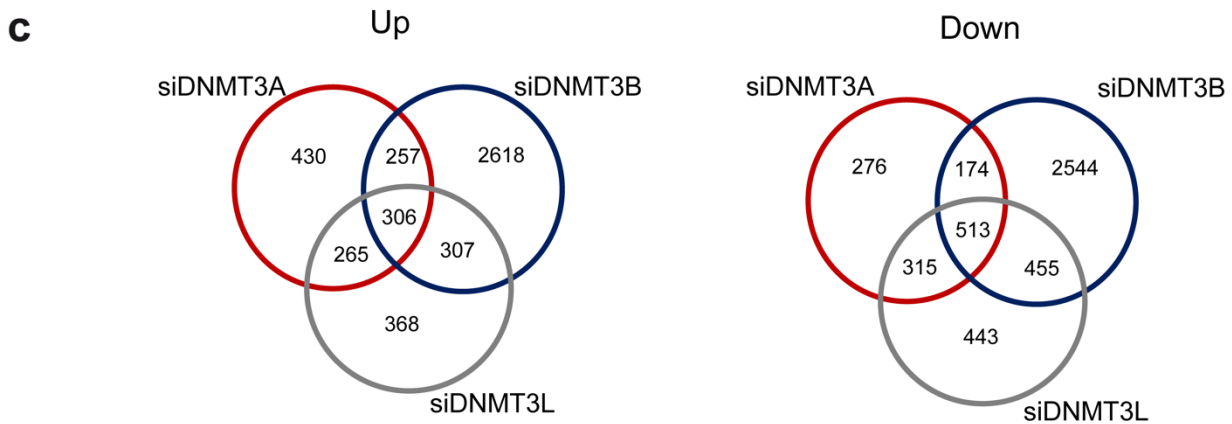
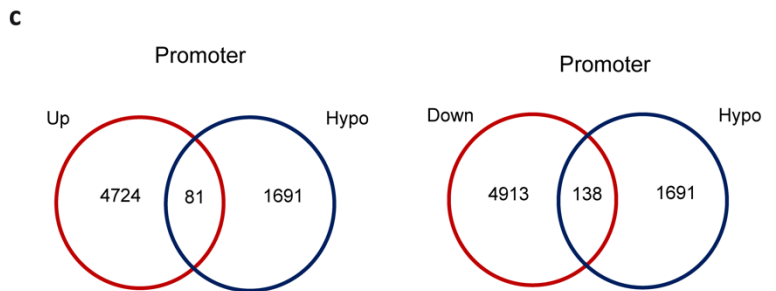
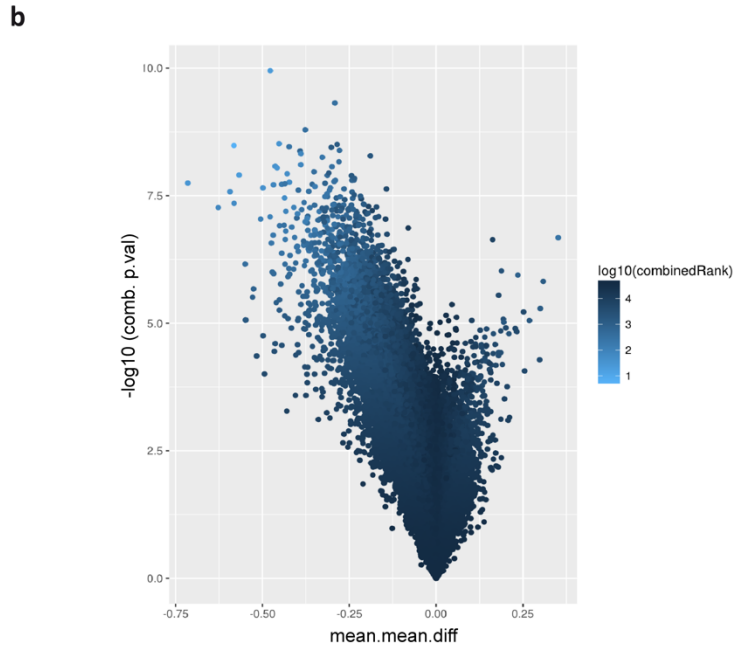
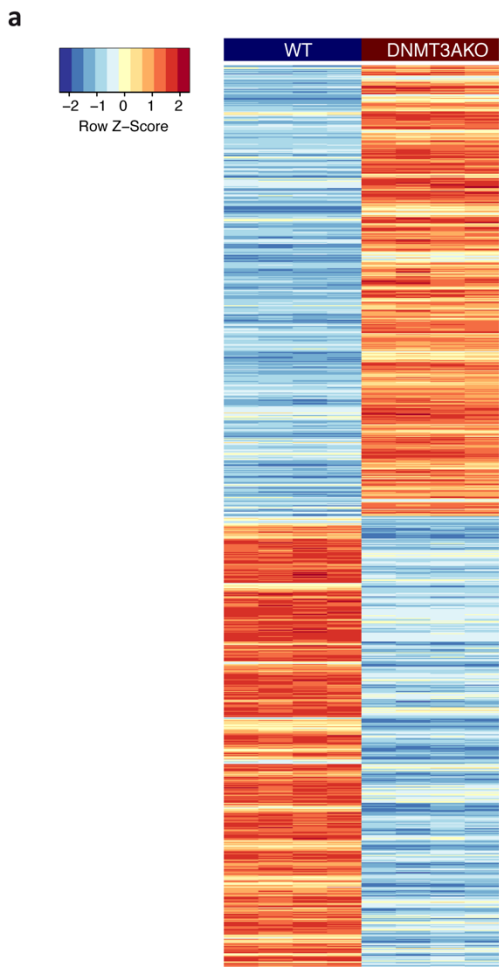


Figure 3.3: Short-term silencing of DNMT3s causes transcriptional changes without modifying global DNA methylation.

(a) Heat map of the top 100 differentially regulated transcripts and (b) heat map of differentially methylated promoters (DMPs) in Caco-2 cells transfected for 72 h with siRNA targeting DNMT3A, B and L and a siRNA control, respectively (c) Venn diagram of commonly up- and downregulated genes in siDNMT3A/B/L Caco2 cells. (d) GO term analysis for biological processes of upregulated and downregulated genes in siDNMT3A knock down cells. (n=4, two independent experiments).

3.4 Genomic deletion of *DNMT3A* alters transcriptome and methylome profiles in Caco-2 cells

DNA methylation regulates transcription via two independent mechanisms. One mechanism is the methylation of specific CpG nucleotides regulating the binding of transcription factors to the DNA. The second one is the recruitment of protein complexes to the DNA where methylation has occurred, leading to transcriptional repression [121]. In the previous paragraph, I could demonstrate that short-term silencing of DNMT3A induced transcriptional changes independent from an altered DNA methylation signature (Fig. 3.3 a-b). In this context, it has been proposed that loss of methylation upon ablation of DNMT3A might require a prolonged culture period [120]. Thus, our stable cell line lacking DNMT3A (Fig. 3.2) was used to investigate the effect of long-term loss of DNMT3A. RNA sequencing was employed to perform transcriptome analysis from DNMT3A KO and WT cells. Heat map analysis of the top 100 differentially expressed genes (DEGs) of WT vs DNMT3A KO was performed. The analysis identified over 4000 transcripts that were up- and downregulated (Fig. 3.4 a). Global DNA methylation was investigated using the 850k EPIC array. In contrast to the results shown in Fig. 3.3 b, volcano plot analysis of DMPs showed a global DNA promoter hypomethylation (Fig. 3.4 b). To identify genes, which are differentially expressed and might be regulated by methylation, genes presenting hypomethylated promoter and differential gene expression were analysed, depicted in the Venn diagram (Fig. 3.4 c). For the differentially expressed transcripts, we used as cut-off the adjusted p-value (p_{adj}) of 0.05. Regarding the hypomethylated promoter genes, a combined rank value smaller than 3584 was used. In total, I identified 81 up- and 138 downregulated genes. Both groups of genes revealed hypomethylation within the promoter region. Next, the commonly identified genes were used to perform GO term analysis for biological processes (Fig. 3.4 d). Interestingly, we identified new GO terms related to IL1-beta signaling (repressed) and regulation of T-cells (induced). Moreover, most of the GO terms identified during short-term silencing of DNMT3A (Fig. 3.3 c) were confirmed, such as response to wounding.



d GO terms in promoter hypomethylated and up and down regulated genes

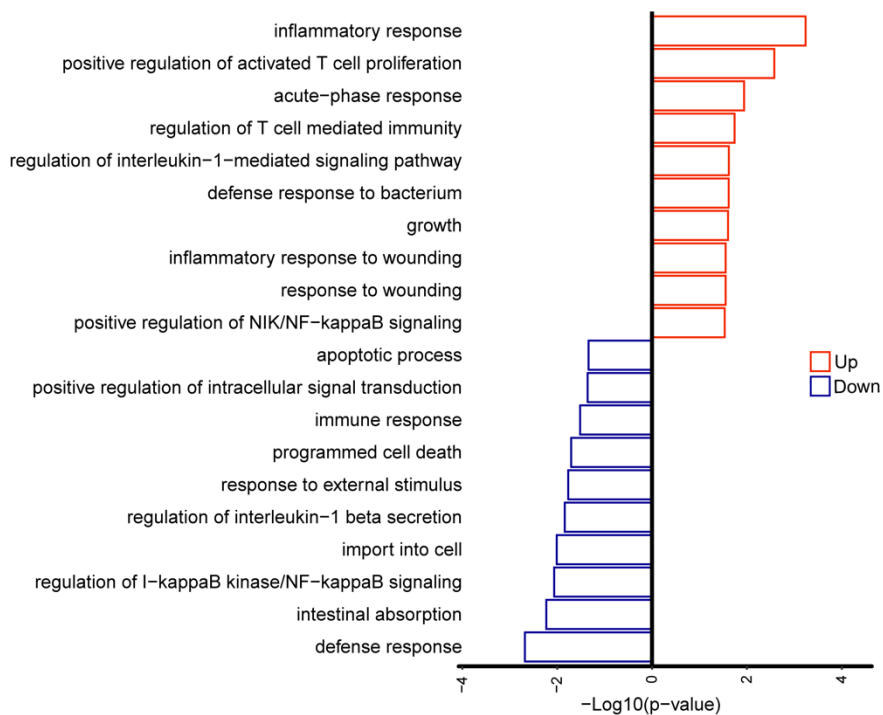


Figure 3.4: Genomic deletion of *DNMT3A* causes transcriptional changes with global DNA hypomethylation.

(a) Heatmap of top 100 differentially regulated transcripts and (b) volcano plot of differentially methylated promoters of Caco-2 cells WT and DNMT3A KO. (c) Venn diagram of common genes with hypomethylated promoters and up- or downregulated genes in DNMT3A KO and WT cells. (d) GO term analysis for biological processes of hypomethylated promoters and up- or downregulated genes. (n=4, two independent experiments).

3.5 Identification of target genes rescued by re-expression of DNMT3A isoforms

DNMT3A isoforms show distinct subcellular localization and they differ in genomic binding and DNA methylation activity in mouse ES cells [52, 120]. So far, we identified genes with a dysregulated transcriptome and methylome upon ablation of DNMT3A (Fig. 3.4). To investigate whether re-expression of DNMT3A isoforms restores DNA methylation and gene expression levels, the stable cell lines encoding DNMT3A1 and DNMT3A2 isoforms were investigated. Transcriptome and DNA methylation profiles were analysed using RNA sequencing and 850k EPIC array, respectively.

Venn diagrams show up- and downregulated genes rescued by re-expression of the DNMT3A isoforms (Fig. 3.5 a). For the differentially expressed genes, I used as cut-off the adjusted p-value (padj) of 0.001. In total, we found 978 up- and 842 downregulated rescued transcripts. Furthermore, the identified genes showed restored expression levels similar to the wild-type cells (Fig. 3.5 b). Next, I performed gene ontology analysis of biological processes exclusively associated with the rescued genes. The analysis identified significantly induced processes related to cell cycle, tumor necrosis factor (TNF) signaling, cellular response to lipopolysaccharides (LPS) and response to interferon. In contrast, the repressed processes were related to chromatin remodelling, histone modification and the Wnt signaling pathway (Fig. 3.5 c).

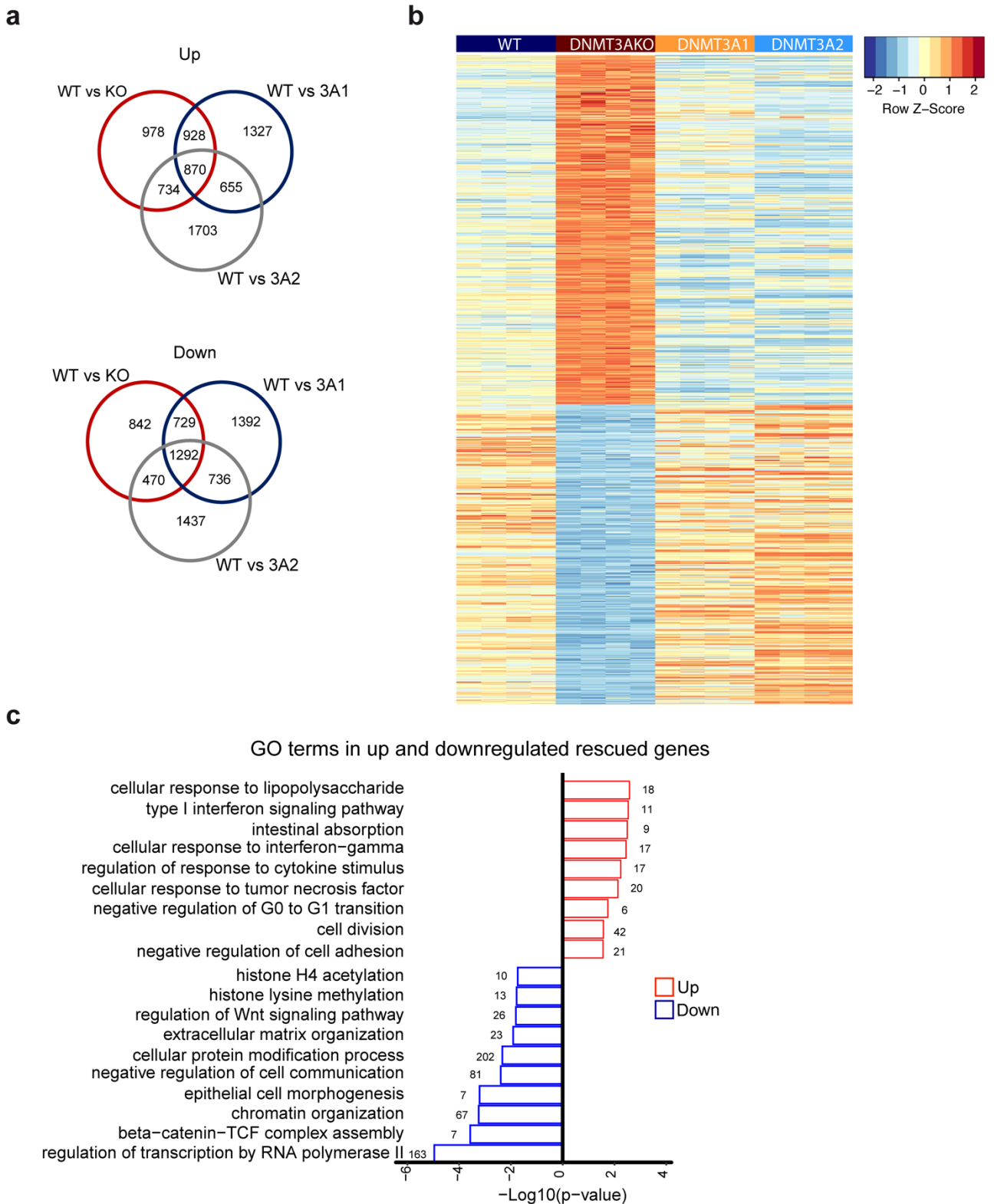


Figure 3.5: Transcriptome analysis of rescued genes.

(a) Venn diagram of up- and downregulated DEGs in DNMT3A, DNMT3A1 and DNMT3A2 Caco-2 cells. (b) Heatmap of up- and downregulated rescued genes. (c) GO term for biological processes analysis of up- or downregulated rescued genes. (n=4, two independent experiments).

So far, this study revealed that re-introduction of DNMT3A isoforms restores the expression of a set of genes to wild-type level, identifying them as DNMT3A specific target genes (Fig. 3.5). Since prolonged loss of DNMT3A causes global promoter hypomethylation, we investigated whether the methylation profile can be restored, as observed for the transcriptome. Expression of DNMT3A1 and DNMT3A2 restored methylation of 1617 genes at the promoter level (Fig. 3.6 a). For this analysis, a combined rank value smaller than 5584, 1937 and 1919 were used for DNMT3AKO, DNMT3A1 and DNMT3A2 cell lines, respectively.

Next, we asked whether restoration of DNA promoter methylation correlates with gene expression. Thus, I compared transcriptionally rescued genes identified in Fig. 3.5 and genes with restored promoter DNA methylation identified in Fig. 3.6 a. In total, 14 down- and 31 upregulated rescued genes were identified. Both groups of genes demonstrate a restored promoter DNA methylation (Fig. 3.6 b). From the 45 identified genes, based on their role in inflammatory response, the following genes were chosen as an example of DNMT3A targets: *trefoil factor 3 (TFF3)*, *interleukin 1 receptor, type I (IL1R1)* and *caspase 1 (CASP1)*. As shown in Fig. 3.6 c, *IL1R1* gene expression was restored by both isoforms. On the contrary, gene expression levels of *TFF3* and *CASP1* were only restored by DNMT3A1 and DNMT3A2, respectively. Similarly, promoter methylation profiles were rescued when comparing them to the levels in the WT (Fig. 3.7d). In summary, this study identified a set of genes specifically regulated by DNMT3A. Moreover, we could demonstrate that gene expression correlates with promoter DNA methylation.

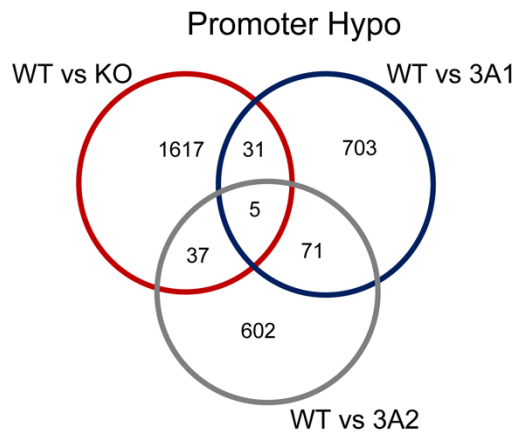
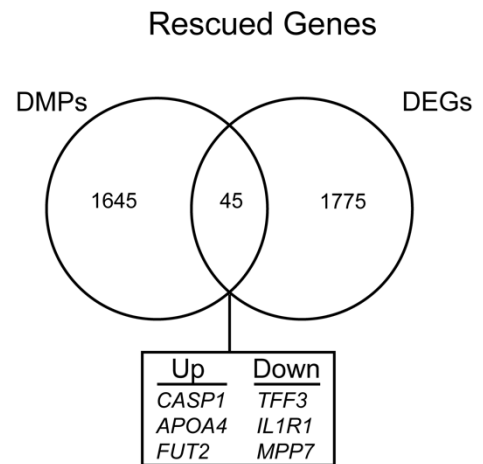
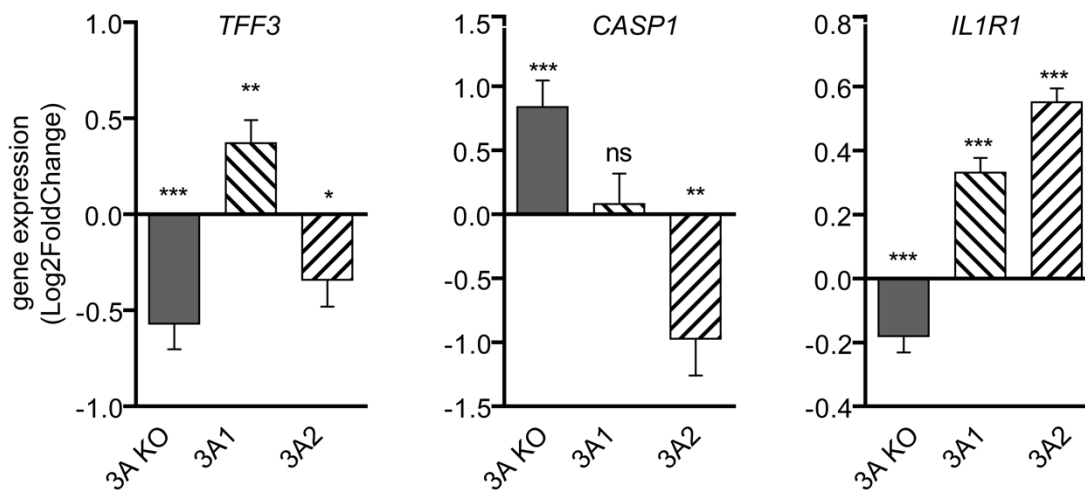
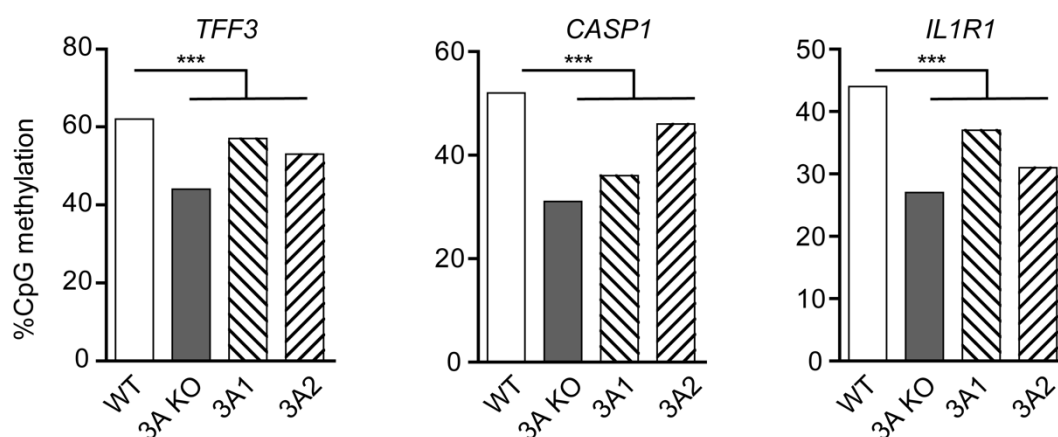
a**b****c****d**

Figure 3.6: Re-expression of DNMT3A isoforms restores promoter DNA methylation and gene expression.

(a) Venn diagram showing the number of rescued genes based on their promoter hypomethylation. (b) Venn diagram shows common genes where gene expression and promoter methylation are restored to wild-type level. Gene expression analysis, shown as Log2FoldChange (c) and %CpG methylation (d) of identified target genes *TFF3*, *CASP1*, *IL1R1*. Log2FoldChange was determined using RNA-seq (n=4). Error bars represent logfoldchangeStandard Error value (lfcSE); ***padj<0.001, **padj<0.01, *padj<0.05 vs WT.

3.6 Gene expression analysis of DNMTs

DNMT3A together with DNMT3B and the regulatory unit DNMT3L are members of the so called “DNMT3 family”. DNMT3A/B/L enzymes are responsible for the *de novo* methylation pattern. They form a protein complex that interacts with the DNA via the binding of DNMT3L to the unmethylated histone H3 tail [122]. In contrast, maintenance of the DNA methylation pattern after replication is performed by DNMT1. We raised the question whether short-term silencing of individual *DNMT3* genes or prolonged ablation of DNMT3A causes a reciprocal transcriptional regulation. Thus, I used RNA-seq data from chapters 3.3/3.4 and analysed DNMT3A/B/L and DNMT1 expression. DNMT3B knock-down caused a significant downregulation of DNMT3A and DNMT1, whereas silencing of DNMT3L resulted in a significant downregulation of DNMT3A and DNMT1 and an upregulation of DNMT3B (Fig. 3.7 a). Knock-down of DNMT3A resulted in a significant upregulation of DNMT3L, while no changes on DNMT3B and DNMT1 gene expression were detected. In contrast, long term ablation of DNMT3A significantly downregulated DNMT3B while DNMT3L and DNMT1 gene expression were not affected (Fig. 3.7 b). In conclusion, co-regulation rather than compensatory upregulation by the other DNMT occurs upon silencing of DNMT3A,-3B and -3L.

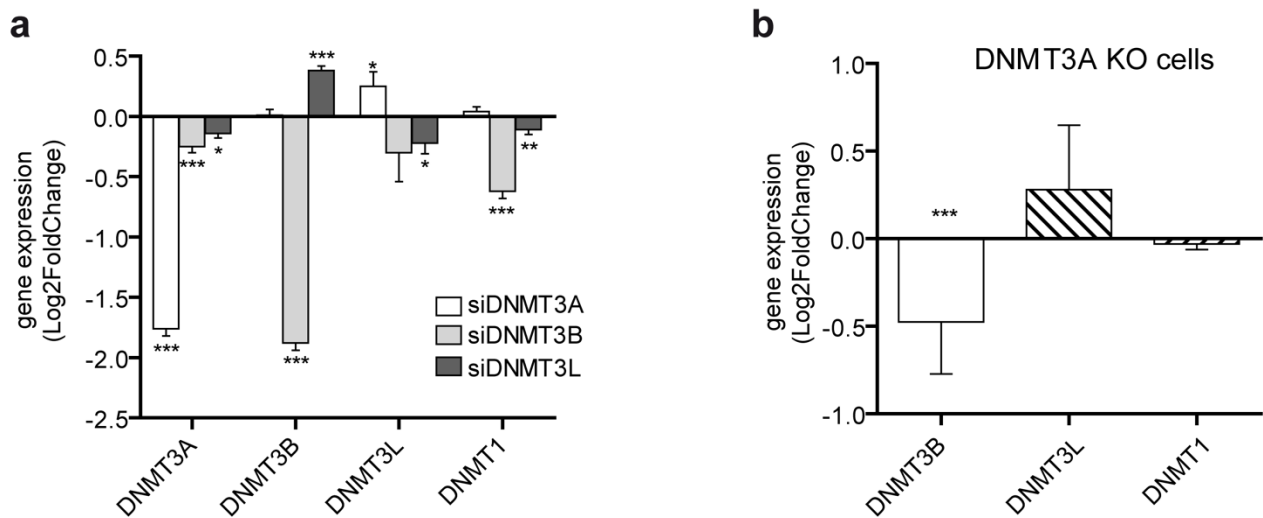


Figure 3.7: Reciprocal transcriptional regulation of DNMT3 family.

(a) Log2FoldChange of DNMT3A, B, L and DNMT1 in Caco-2 cells transfected with siRNA targeting DNMT3A, B and L, respectively, for 72 h. (b) Gene expression levels of DNMT3B, L and DNMT1 in DNMT3A knockout Caco-2 cell. Log2FoldChange was determined using RNA-seq (n=4). Error bars represent lfcSE; ****p*adj<0.001, ***p*adj<0.01, **p*adj<0.05

3.7 Characterization of DNMT3A KO spheroids morphology

Caco-2 cells can be cultured as undifferentiated cells, polarized cells and as spheroid-like structure. The latter is characterized by an inner lumen enclosed by a single layer of polarized cells. This 3D organization mimics the *in vivo* gut architecture. In order to investigate the role of DNMT3A in a 3D culture system, WT, DNMT3A KO, DNMT3A1 and DNMT3A2 cell lines were seeded in a 3D matrix. Wild-type spheroids were able to form the expected spheroid-like structure with a lumen surrounded by a single layer of cells. In contrast, *DNMT3A*-deficient spheroids were not able to form a lumen and they displayed an altered structural organization compared to the WT control (Fig. 3.8 a). The spheroid area (μm^2) was measured, and DNMT3A KO spheroids were around 50% smaller than the WT, suggesting a reduced cell proliferation rate. Furthermore, DNMT3A KO spheroids less often formed a lumen, only 20% of the DNMT3A KO spheroids were able to form it compared to 45% in the wild-type (Fig. 3.8 c). These morphological observations in the DNMT3A KO spheroids were partially rescued in the spheroids expressing the single isoform. DNMT3A1 and DNMT3A2 spheroids size, as well as the percentage of spheroids with lumen, was similar to values obtained for the WT spheroids, suggesting that DNMT3A drives altered spheroid-like structure formation (Fig. 3.8 b-c).

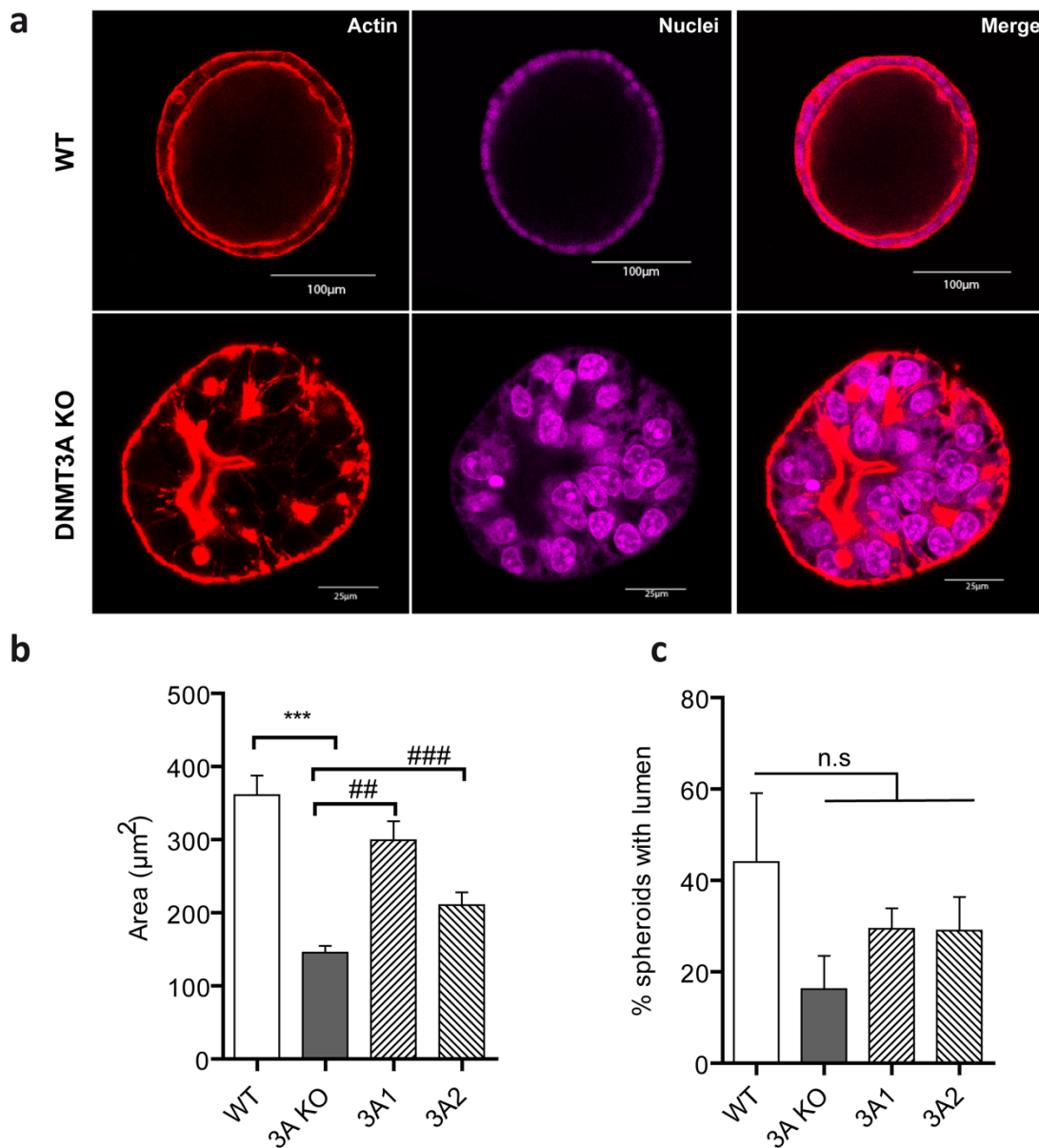


Figure 3.8: DNMT3A KO spheroids have an abnormal structural organization.

(a) Representative images of DNMT3A KO and WT spheroids cultured in 3D matrix for 14 days. Confocal microscopy was used to analyse spheroid organization. Phalloidin (red) and DRAQ5 (purple) was used to visualize actin filaments and nuclei, respectively. Spheroids size (μm^2) (b) and the percentage of spheroids with a lumen (c) were determined in WT, DNMT3A KO, DNMT3A2 and DNMT3A1 spheroids (n=30). Data represent mean \pm SEM of two independent experiments. *** $p < 0.001$ vs WT; ### $p < 0.001$ ## $p < 0.01$ vs 3A KO.

3.8 Role of DNMT3A in intestinal permeability

The integrity of the intestinal barrier is crucial for the maintenance of intestinal homeostasis. Altered cell-cell junction organization is one of the causes of impaired intestinal permeability [77]. Based on our transcriptomic data, GO term analysis identified repressed processes related to “cell-cell junction assembly” or “intestinal absorption” (Fig. 3.4). Therefore, we investigated on the consequences of DNMT3A-deficiency on barrier permeability.

To assess the barrier function of DNMT3A KO cells, three different assays were used. Paracellular permeability was evaluated with the use of two fluorescence dyes, namely Lucifer Yellow (LY) and 4 kDa fluorescein isothiocyanate-dextran (FITC-4D). Caco-2 cells were cultured as monolayer in a transwell system, and paracellular permeability was quantified by measuring the flux of LY from the upper chamber of the transwell to the lower chamber. DNMT3A KO monolayer showed an increased permeability indicated by higher LY levels in the lower chamber compared to the WT control (Fig. 3.9 a). Additionally, cell monolayer integrity was determined by measuring the trans-epithelial electrical resistance (TEER). DNMT3A KO monolayer showed significantly reduced TEER (Fig. 3.9 b). Furthermore, we studied the barrier function in a 3D environment system. Hence, I used WT and DNMT3A KO spheroids treated with FITC-4D for 24 h. After 24 h, fluorescence intensity at the luminal and the basolateral side was measured by confocal microscopy. In agreement with our 2D experiments (Fig. 3.9 a), DNMT3A KO spheroids were more permeable to the FITC-4D dye compared to the WT control (Fig. 3.9 c). To further elucidate whether the observed phenotype is due to a structural defect of the monolayer, we analysed the cellular contact zone by transmission electron microscopy (TEM). In differentiated DNMT3A KO monolayer, the cellular contact zone length, which includes tight junctions, adherens junctions and desmosomes, was reduced (Fig. 3.9 d) compared to the WT. Taken together, our data suggest a regulatory function of DNMT3A in paracellular permeability *in vitro*.

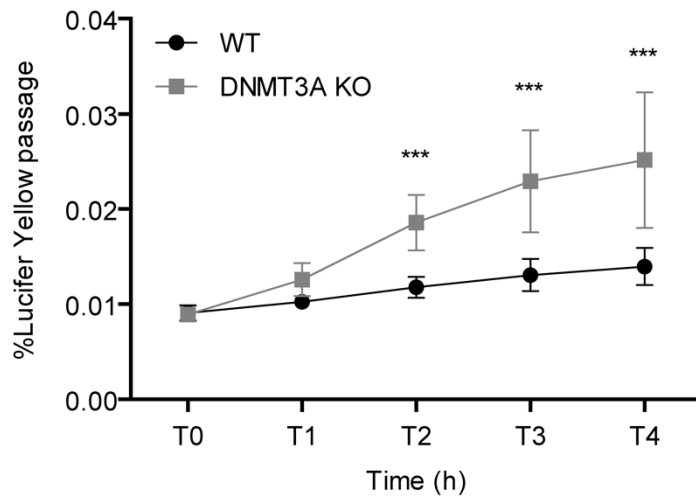
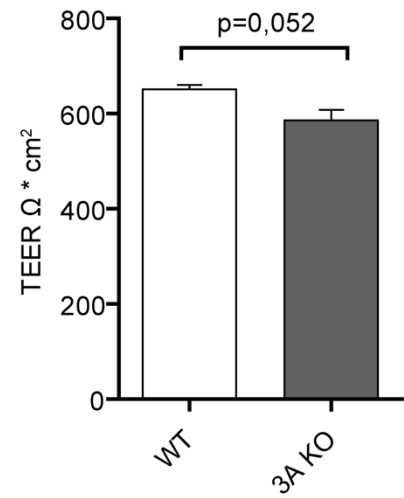
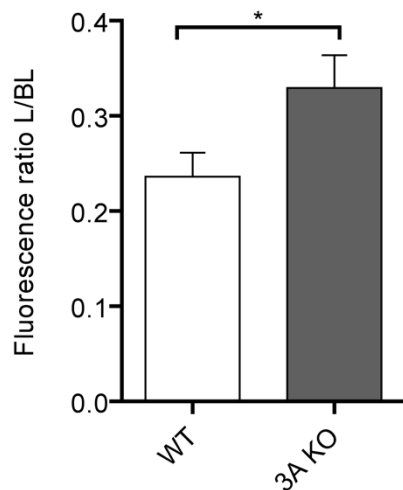
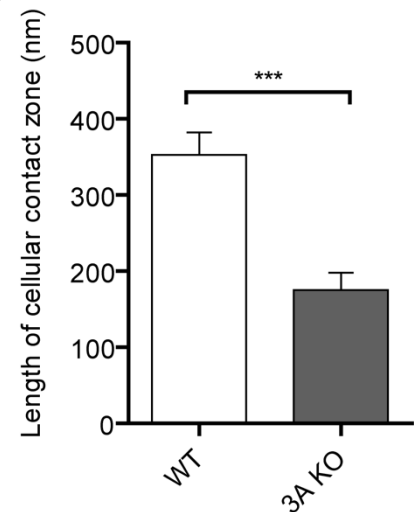
a**b****c****d**

Figure 3.9: Loss of DNMT3A results in defective paracellular permeability.

(a) Percentage of Lucifer Yellow passage in differentiated DNMT3A KO and WT Caco-2 cells at different time points. (b) TEER measurements of differentiated DNMT3A KO and WT Caco-2 cells. (c) Fluorescence intensity ratio between the luminal (L) and basolateral (BL) side of Caco-2 spheroids, WT and DNMT3A KO, incubated with FITC for 24 h. (d) Cellular contact zone length quantification of differentiated Caco-2 WT and DNMT3A KO cells visualized by Transmission electron microscopy (TEM). The values represent mean \pm SEM from three independent experiments. *** $p < 0.001$, * $p < 0.05$ vs. WT.

3.9 Role of DNMT3A in epithelial wound healing

Wound healing is a dynamic and complex tissue response to external damage. Epigenetic modifications have been shown to control the expression levels of several known repair genes, and thus serve as modulators of wound healing [123]. The transcriptome analyses of DNMT3A KO cells suggest a role of DNMT3A in the epithelial wound healing response, as well as in Wnt signaling pathway (Fig. 3.4 d). Wnt signaling is involved in several processes, including epithelial proliferation at the wound edges upon injury [124]. To study wound healing *in vitro*, WT and DNMT3A KO Caco-2 cells were plated into a culture insert containing four compartments. After 24 h, the insert was removed and the wound area was measured at 0 h and 24 h after establishing the wound. As shown in Fig. 3.10 a, cell migration was clearly delayed by lack of DNMT3A. Loss of DNMT3A significantly delayed wound closure by 20 % compared to the WT control (Fig. 3.10 b). To confirm the regulatory role of DNMT3A in wound healing, the observed phenotype was rescued by stable re-expression of the individual DNMT3A isoforms. In both cell lines, wound closure was almost restored to WT levels (Fig. 3.10 c). In accordance to our previous experiment (Fig. 3.10 b), the percentage of wound closure in the KO was 20 % less compared to the WT. Interestingly, both DNMT3A1 and DNMT3A2 cell lines showed an increased wound closure compared to the KO, similar to the percentage seen in the WT control (Fig. 3.10 d), suggesting a functional redundancy of DNMT3A isoforms in this process.

In order to understand whether Wnt signaling activity is impaired upon deletion of DNMT3A, I employed a Wnt reporter activity assay, termed TOP/FOP luciferase reporter assay, indicative for beta-catenin nuclear translocation and binding to its TCF binding region. As showed in Fig. 3.10 e, deletion of DNMT3A caused a reduced beta-catenin translocation in the nucleus, resulting in reduced Wnt signaling activity. In summary, these observations point towards a function of DNMT3A in regulating intestinal epithelial regeneration, and impaired Wnt activity might contribute to the observed phenotype.

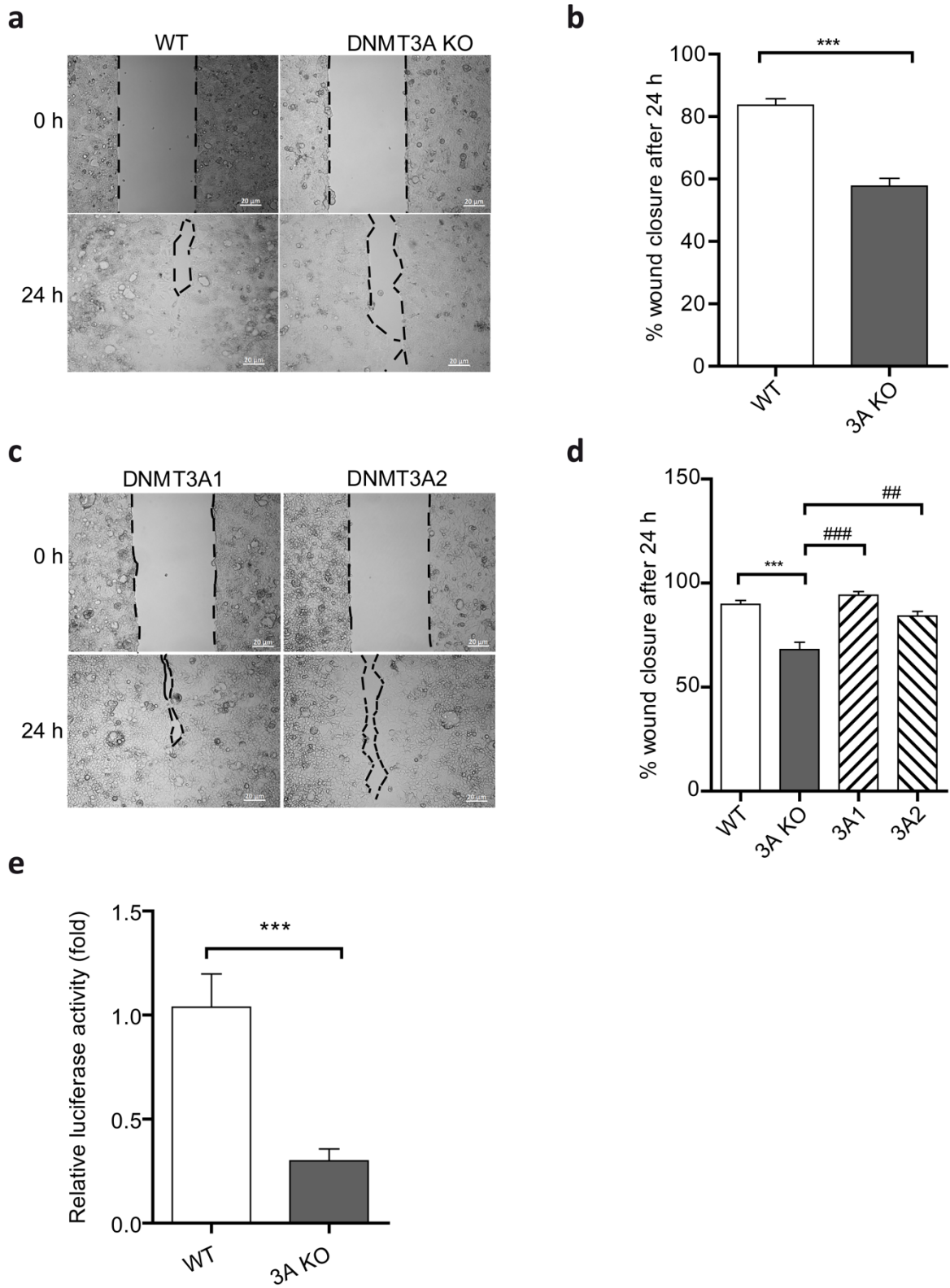


Figure 3.10: Loss of DNMT3A impairs epithelial wound healing *in vitro* and it is rescued by re-expression of DNMT3A single isoforms.

Representative images of Caco-2 cells, WT and DNMT3A KO (a) and DNMT3A1 and DNMT3A2 (c), at 0 h and 24 h after inducing the gap. The percentage of wound closure after 24 h was measured with a phase-contrast microscope, using the absolute wound area normalized to the corresponding value at 0 h (b-d). (e) TOP/FOP luciferase reporter assay of Caco-2 WT and DNMT3A KO. The values represent mean \pm SEM from three independent experiments. *** $p < 0.001$ vs. WT. ### $p < 0.001$, ## $p < 0.01$ vs. 3AKO.

3.10 DNMT3A modulates NF- κ B signaling in intestinal epithelial cells

NF- κ B (nuclear factor kappa-light-chain-enhancer of activated B cells) is a family of transcription factors. This family includes p50/p105, p52/p100, RelA (p65), c-Rel and RelB. In the inactive state, they are bound to an inhibitor (I κ B). Several stimuli can rapidly activate these transcription complexes, releasing them from their inhibitor and allowing the translocation to the nucleus [125]. The NF- κ B signaling play a critical role in inflammation enhancing the expression of pro-inflammatory cytokines such as TNF α , IL1 β or IL6 [126]. Our GO term analysis (biological processes) of RNA-seq data in chapter 3.5 has revealed that the loss of DNMT3A leads to the induction of processes related to LPS response, TNF response or IL1beta signaling. Strikingly, these induced molecular responses are activators of NF- κ B transcription factors [125]. As an example, IL1 β is one of the inducers of NF- κ B signaling activation [127]. Here, I analysed the role of DNMT3A in modulating NF- κ B signaling. While stimulation with IL1 β resulted in a pronounced NF- κ B promoter activity in WT cells, DNMT3A KO cells displayed less NF- κ B induction (Fig. 3.11 a). To further elucidate impaired NF- κ B signaling, we analysed the production of the proinflammatory cytokine IL8 (interleukin 8), a known NF- κ B target. In line with our findings, IL8 production of DNMT3A KO cells stimulated with IL1 β was significantly reduced compared to the WT control (Fig. 3.11 b). Likewise, *Dnmt3a*^{ΔIEC} colonic organoids stimulated with IL1 β showed less phosphorylated p65 and I κ B α compared to the control organoids indicating impaired NF- κ B activation (Fig. 3.11 c). This study suggests a role of DNMT3A in regulating NF- κ B activity, both in *in vitro* and *ex-vivo* models.

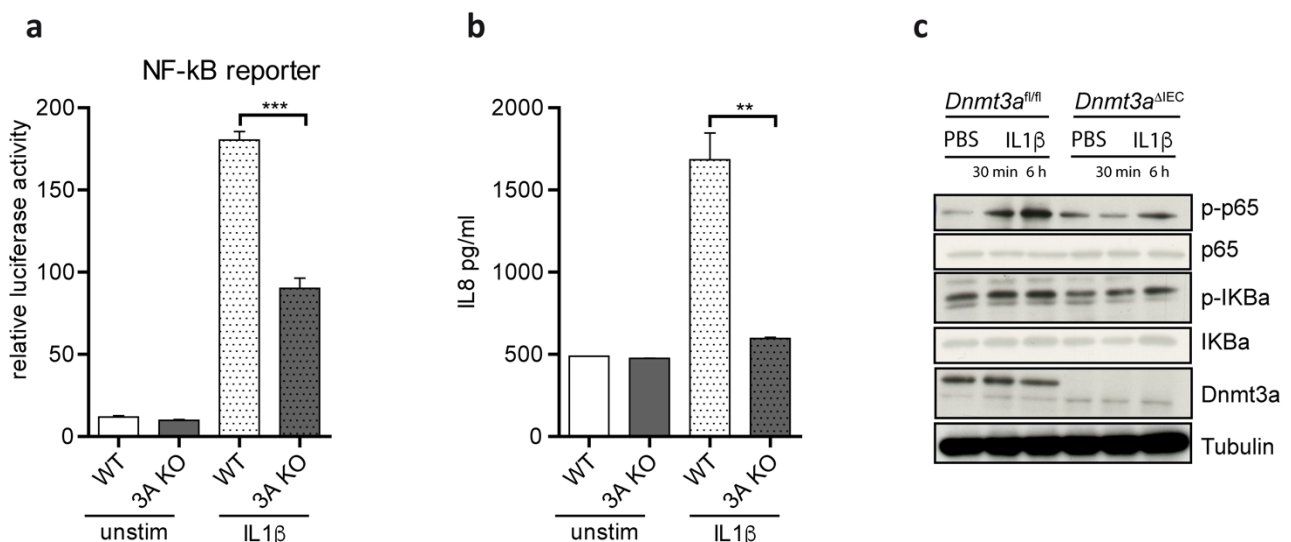


Figure 3.11: Loss of DNMT3A impairs NF- κ B activity.

(a) NF- κ B promoter activity in Caco-2 cells, WT and DNMT3A KO, quantified by dual luciferase reporter assays. Caco-2 cells were co-transfected with the firefly luciferase reporter pNF- κ B and a Renilla luciferase for normalization. After 24 h, cells were left untreated or stimulated with IL1 β (100 ng/ml) for additional 24 h (n=6). (b) Caco-2 WT and DNMT3A KO cells were stimulated with IL1 β (100 ng/ml) for 24 h. Supernatants were harvested for measurements of IL8 production by ELISA (n=3). (c) Immunoblot of colonic organoids from wild-

type and *Dnmt3a*^{ΔIEC} mice stimulated with IL1 β (100 ng/ml) for 30 min and 6 h, respectively. Tubulin was used as loading control. Data represent mean \pm SEM, ***p<0.001, **p<0.01

3.11 DNMT3A gene expression is downregulated during intestinal inflammation

DNMTs, as DNA methyltransferases, are involved in regulation of gene expression, however little is known about their transcriptional regulation. In particular, it is not clear how inflammatory conditions may modulate their expression. Dextran sodium sulfate (DSS)-induced colitis is the most used murine model to study IBD pathogenesis [128]. To monitor expression levels of DNMT3A, 3B and 3L in intestinal inflammation, wild-type mice were exposed to DSS, and epithelial and lamina propria fractions were isolated. Gene expression analysis by RT-qPCR identified a significant downregulation of *Dnmt3a* and *Dnmt3b* genes in the DSS-treated animals compared to the water control group, in both the epithelial and the lamina propria fraction (Fig. 3.12 a), pointing to a more general influence of inflammation. *Dnmt3l* was only expressed in the lamina propria fraction (data not shown). Although we observed a significant downregulation of *Dnmt3a* transcript, we did not find any differences on protein level, both in the epithelial and lamina propria fraction (data not shown). In addition, we quantified the expression of the human *DNMT3A* and *DNMT3B* by RT-qPCR analyses in whole biopsy tissue from 20 healthy, 20 UC and 20 CD individuals. In line with the murine data, *DNMT3A* and *DNMT3B* gene expression were significantly downregulated in UC and CD compared to the healthy individuals, while mRNA of *DNMT3L* was not detected (Fig. 3.12 b). In summary, both DNMT3A and -3B genes are significantly downregulated during inflammation, in both the murine model and in human diseased tissue. Therefore, we can hypothesize that the reduced expression of *DNMT3A/B* genes during inflammation might contribute to altered DNA methylation observed in inflammatory diseases, such as IBD.

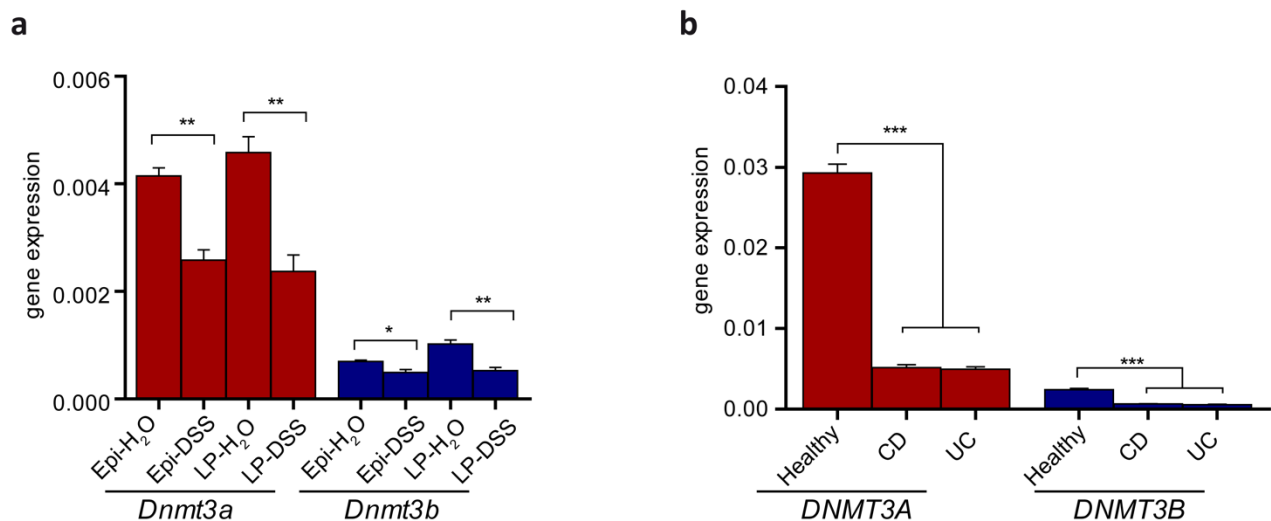


Figure 3.12: DNMT3A is downregulated under inflammatory conditions in patient biopsies and in a murine chemical colitis model.

(a) Gene expression analysis of *Dnmt3a* and *3b* genes in the intestinal epithelial (Epi) and the lamina propria (LP) fractions of mice treated with DSS (n=5) or water (n=5), respectively. (b) Gene expression analysis of

DNMT3A and *DNMT3B* whole biopsy tissue from CD (n=20), UC (n=) and healthy individuals (n=). Data represent mean ± SD. ***p<0.001, **p<0.01, *p<0.05

3.12 Characterization of *Dnmt3a*^{ΔIEC} mice

To study the specific role of DNMT3A in intestinal epithelial cells, a conditional knockout model with a deletion of *Dnmt3a* only in IECs was generated (*Dnmt3a*^{ΔIEC} mice) (see chapter 2.7.1). The resulting conditional mouse model was investigated under baseline and challenged conditions.

3.12.1 Basal phenotype of *Dnmt3a*^{ΔIEC} mice

For the validation of the IEC-specific deletion of *Dnmt3a*, mRNA expression levels of *Dnmt3a* were investigated in isolated crypts by RT-qPCR. As expected, *Dnmt3a* mRNA was not expressed in IECs of small intestine and colon tissues isolated from *Dnmt3a*^{ΔIEC} mice (Fig. 3.13 a). Furthermore, we analysed protein expression in IECs and lamina propria cells by immunoblotting. In *Dnmt3a*^{ΔIEC} mice, no expression of the DNMT3A protein was detected in the IECs fraction, whereas in the lamina propria fraction, DNMT3A protein expression in *Dnmt3a*^{ΔIEC} mice was similar to the protein levels detected in the control *Dnmt3a*^{fl/fl} littermates (Fig. 3.13 b), confirming the intestinal epithelial specific knockout of DNMT3A. Additionally, we quantified mRNA expression of the other DNA methyltransferase enzymes. While *Dnmt3l* was not expressed in IECs (data not shown), we did not observe any compensatory upregulation of neither *Dnmt3b* nor *Dnmt1* (Fig. 3.13 c-d).

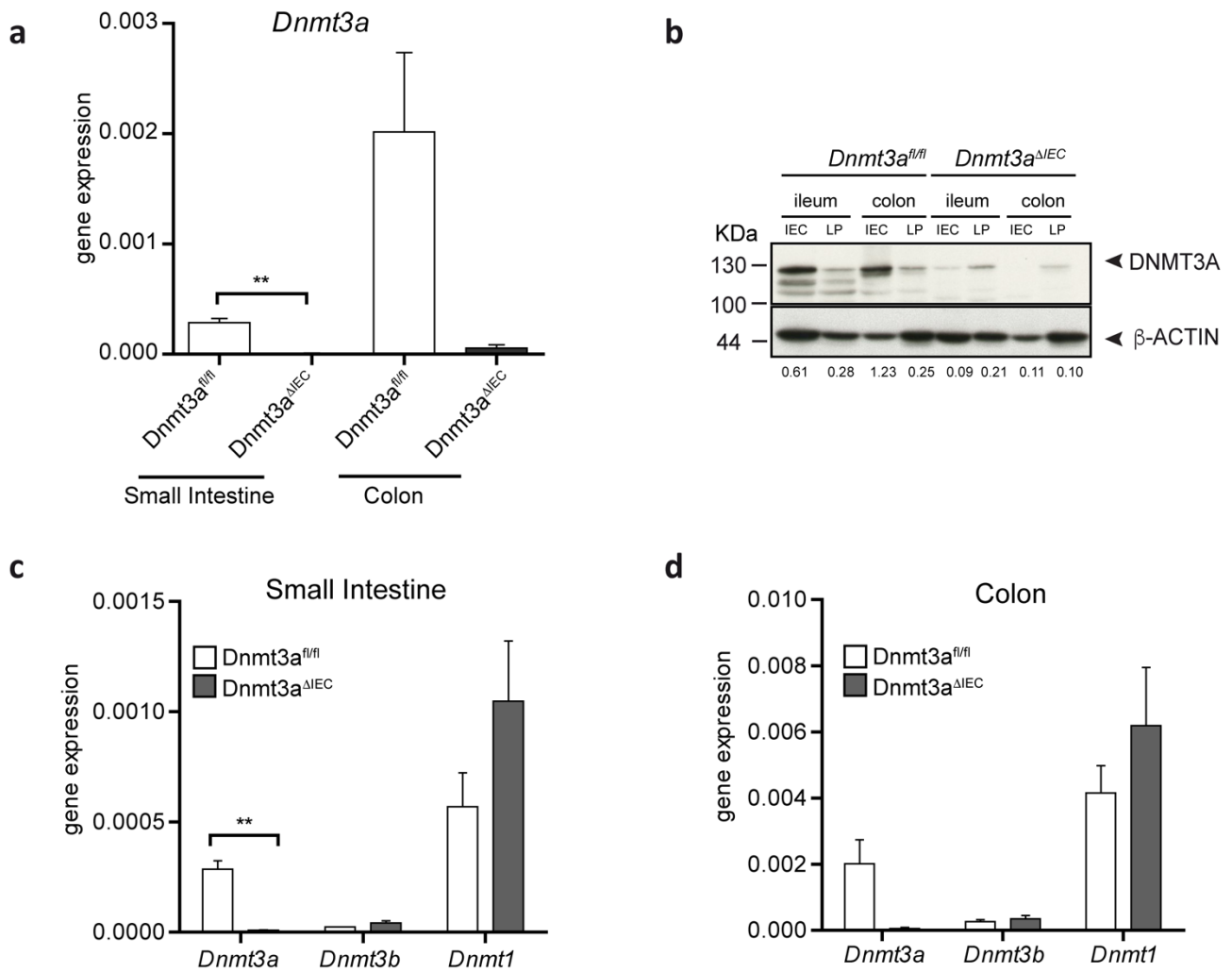


Figure 3.13: mRNA and protein levels of *Dnmt3a* in *Dnmt3a*^{ΔIEC} mice and control mice.

(a) Gene expression analysis of *Dnmt3a* in IECs isolated from small intestinal and colonic crypts. (b) Cell lysates of IECs and LP fractions isolated from ileal and colonic tissues were analysed by immunoblotting using antibodies against DNMT3A. β-Actin was used as loading control. (c-d) mRNA expression of *Dnmt3a*, *Dnmt3b* and *Dnmt1* were analysed in IECs isolated from small intestinal and colonic crypts of *Dnmt3a*^{ΔIEC} and wild-type littermates. Data represent mean ± SEM of n=4 per group. **p<0.01

For basal phenotyping of *Dnmt3a*^{ΔIEC} mice, 10 week old female and male mice were used. We did not observe any differences in body weight in *Dnmt3a*^{ΔIEC} mice compared to their control littermates. However, we observed a slight increase of colon length in *Dnmt3a*^{ΔIEC} compared to wild-type animals. No difference in small intestine length was detected under basal conditions (Fig. 3.14 a-c).

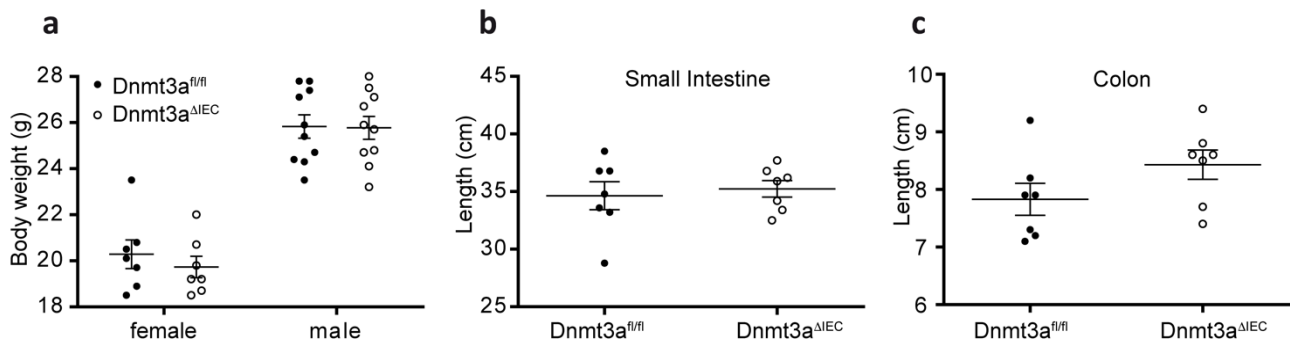


Figure 3.14: Basal phenotype of *Dnmt3a*^{ΔIEC} mice.

(a) Body weight of 10 week old male and female wild-type and *Dnmt3a*^{ΔIEC} mice (n=7 per group for females, n=10 for males). Small intestinal length (b) and colon (c) length of 10 week old mice was measured. Data represent mean ± SEM.

To study the impact of loss of *Dnmt3a* on the intestinal architecture, tissue of 10 weeks old mice was stained with haematoxylin and eosin for histological examinations. *Dnmt3a*^{ΔIEC} mice showed reduced crypts length compared to wild-type mice (Fig. 3.15 a). Since crypt and villus length are determined by cell proliferation and cell migration [129], we quantified cell proliferation by injecting 10 week old mice with bromodeoxyuridine (BrdU) for 1 h. Histological analysis of the BrdU staining showed no differences in the number of BrdU positive cells between *Dnmt3a*^{ΔIEC} and wild-type mice (Fig. 3.15 b). These findings suggest a normal cell proliferation phenotype at the crypt bottom. IECs derived from the stem cell niche migrate along the crypt-villus axis. Therefore, I investigated the capability of the transient amplifying cells to migrate towards the tip of the villus. To this end, BrdU was administrated to the mice overnight. *Dnmt3a*^{ΔIEC} mice exhibited less BrdU positive cells compared to wild-type mice (Fig. 3.15 c), suggesting that the reduced cell migration can cause the observed shorter crypts in the *Dnmt3a*^{ΔIEC} mice.

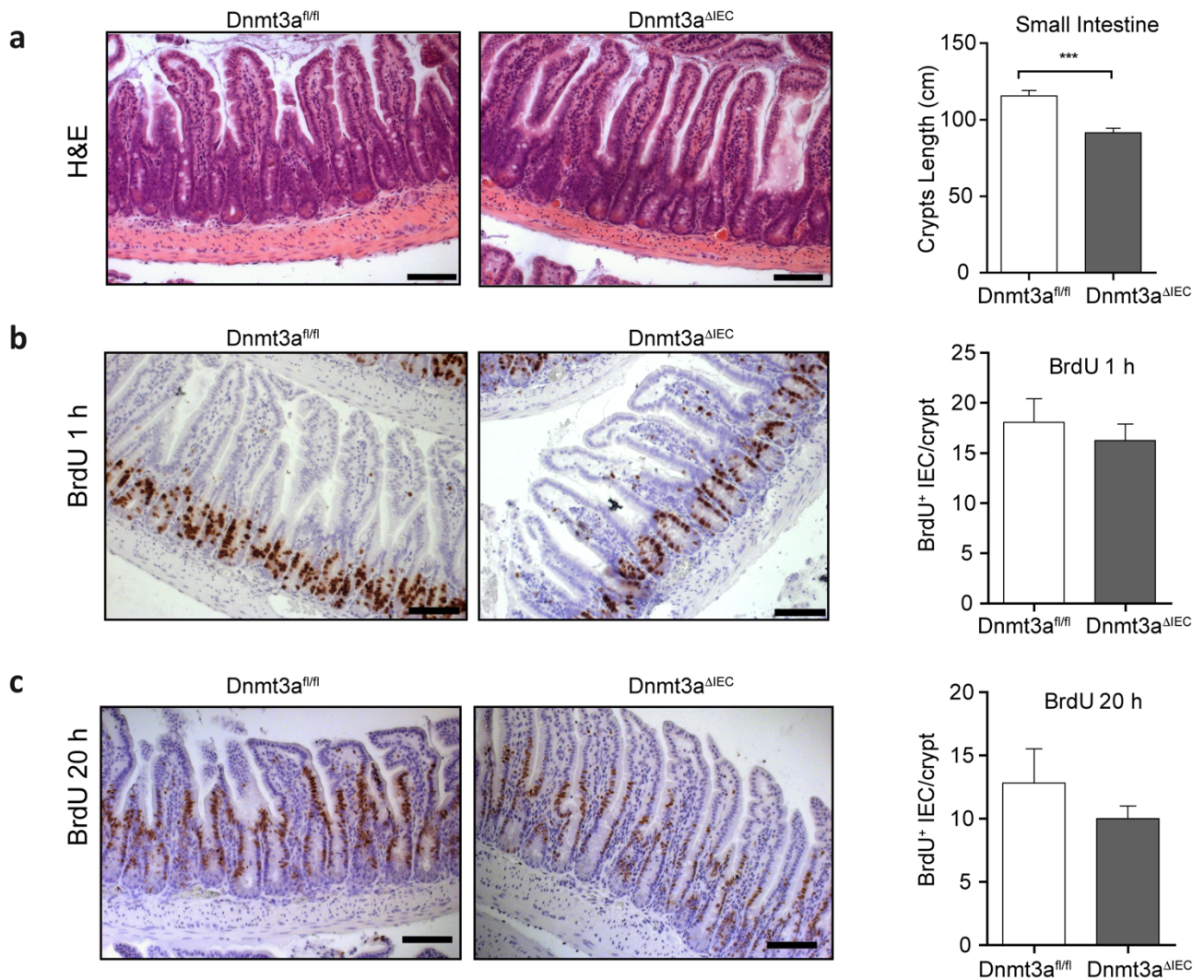


Figure 3.15: Small intestinal architecture of *Dnmt3a^{ΔIEC}* mice.

(a) Representative images of ileal tissue stained for haematoxylin and eosin (H&E) and measurements of small intestinal crypt lengths. For crypt length measurements, 30 crypts per animal were assessed ($n=6$ per genotype). Representative pictures of small intestinal section stained for BrdU and quantification of positive stained cells. Mice were injected with BrdU and sacrificed after 1 h (b) and 20 h (c), respectively ($n=3$ per genotype). Data represent mean \pm SEM. *** $p<0.001$

3.12.2 *Dnmt3a^{ΔIEC}* mice are more susceptible to chronic DSS-induced colitis

To investigate the role of *Dnmt3a* in IECs in the context of inflammation, *Dnmt3a^{ΔIEC}* mice were exposed for three cycles of DSS as described by Chassaing et al [130]. During the first cycle mice were treated with 1.5 % DSS in their drinking water for five days, followed by five days of normal drinking water. For the second and third cycles 2 % DSS was used. Disease activity scoring was performed every 5 days (see chapter 2.7.5 for details). After the first cycle of DSS treatment, no differences in body weight loss were observed between *Dnmt3a^{ΔIEC}* and wild-type mice. However, during the first regeneration phase (days 7-10), the recovery of *Dnmt3a^{ΔIEC}* mice was impaired as indicated by less weight gain compared to their wild-type littermates. In the course of the second and third DSS administration (days 10-15 and days 20-25, respectively), *Dnmt3a^{ΔIEC}*

mice performed consistently worse than their wild-type counterparts illustrated by a reduced body weight. These results indicate that *Dnmt3a*^{ΔIEC} mice are more susceptible to a chronic DSS-induced colitis (Fig. 3.16 a). Disease activity index (DAI) scoring was performed at the beginning and at the end of each DSS cycles (days 0,5,10,15,20,25,30). In accordance with the more severe body weight loss, *Dnmt3a*^{ΔIEC} mice had a significant higher DAI score compared to their wild-type littermates at day 15 and day 25 (Fig. 3.16 b). Measurements of colon length and spleen weight at the end of the chronic colitis did not reveal any significant differences between *Dnmt3a*^{ΔIEC} and wild-type mice in DSS-induced chronic colitis (Fig. 3.16 c-d).

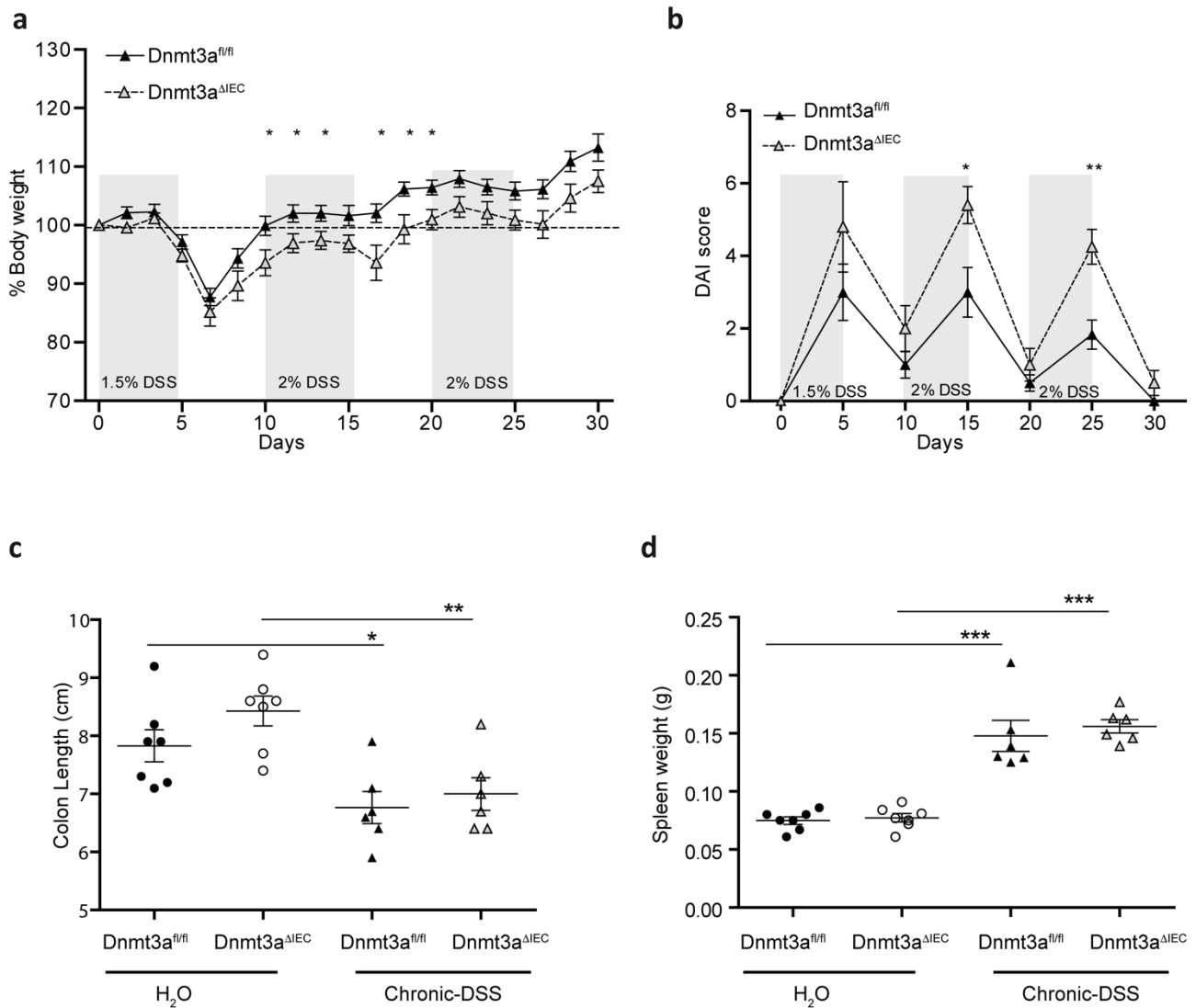


Figure 3.16: Conditional *Dnmt3a* deficiency increases susceptibility to chronic DSS-induced colitis. (a) Percentage of body weight changes of DSS treated *Dnmt3a*^{ΔIEC} and control mice. (b) Disease activity was assessed every 5 days using the disease activity score (DAI). Colon length (c) and spleen weight (d) of untreated and DSS-treated mice were measured. Data represent mean ± SEM of n=6/7 per group. ***p<0.001, **p<0.01, *p<0.05

3.12.3 Role of DNMT3A in cell-cell junction architecture

A defective mucosal barrier is a hallmark in IBD, and it can result in altered intestinal permeability [85]. Defects in paracellular permeability may arise from an altered expression of proteins involved in cell-cell junction [77]. Based on our previous *in vitro* data (Fig. 3.9), we aimed to investigate whether deletion of *Dnmt3a* in the intestinal epithelium affects cell-cell junction architecture. We applied transmission electron microscopy (TEM) to examine cell-cell junction organization of enterocytes from ileal tissue (Fig. 3.18 a). The obtained images revealed an altered architecture of the adherens junctions. A reduced length and increased width of the zonula adherens (white triangles) was observed in *Dnmt3a* deficient mice compared to the control mice (Fig. 3.18 b). To further validate these observations, we analysed gene expression levels of the two major components of the adherent junctions, namely E-cadherin (*Cdh1*) and β -catenin (*Ctnnb1*) by RT-qPCR. Both genes were downregulated in *Dnmt3a* ^{Δ IEC} mice compared to *Dnmt3a*^{fl/fl} mice and these differences became even more pronounced during chronic DSS-induced colitis (Fig. 3.18 c-d).

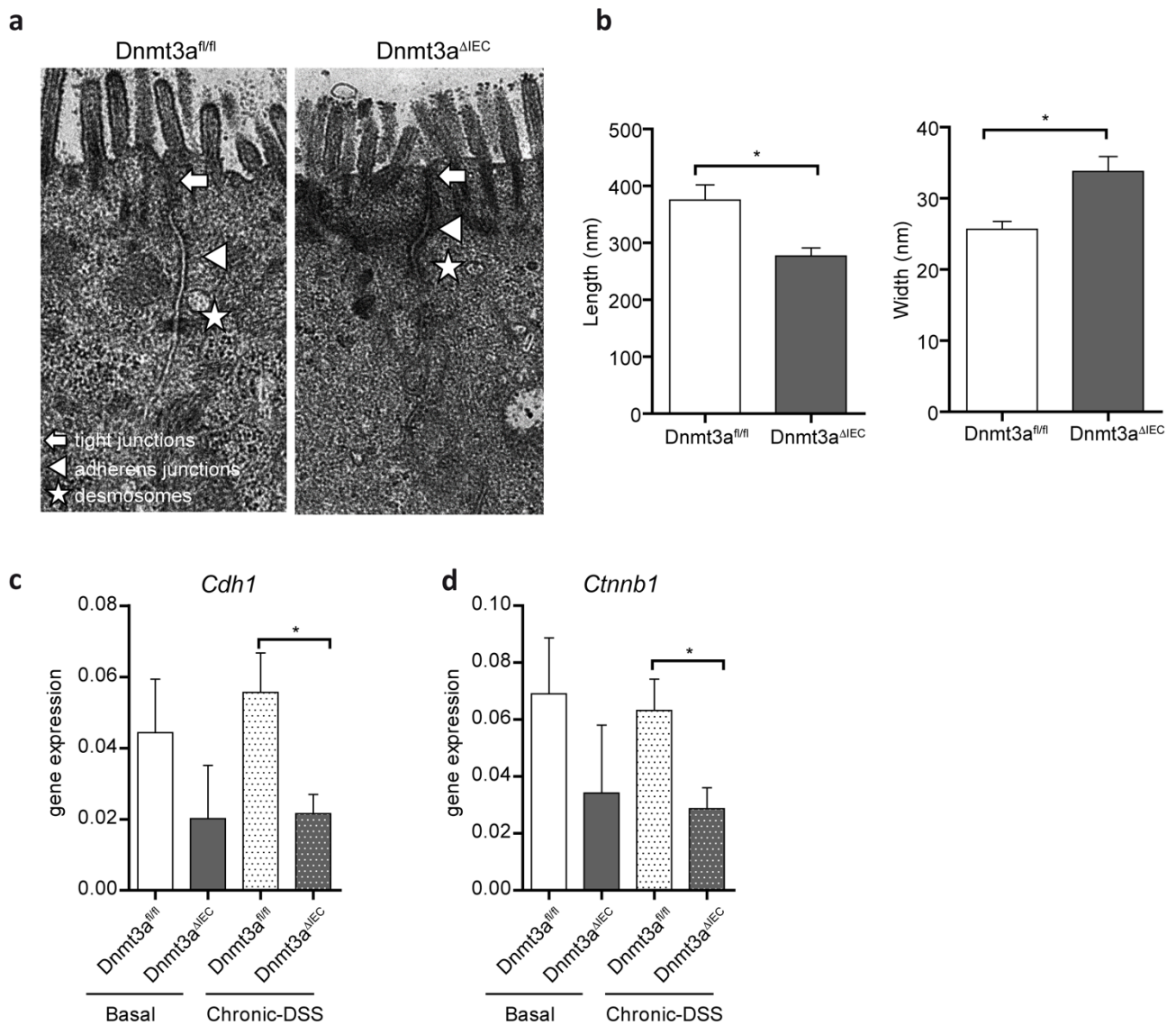


Figure 3.17: DNMT3A alters intestinal epithelial cell-cell junction.

(a) Transmission electron microscopy (TEM) of small intestinal crypts of 10-week old *Dnmt3a^{ΔIEC}* mice and wild-type littermates. Arrows indicate tight junctions, triangles indicate adherens junctions and stars indicate desmosomes. Scale bar, 500 nm. (b) Length and (c) width of adherens junctions were measured. $n=3$ per group. Gene expression analysis of the two major components of adherens junctions, *Cdh1* (b) and *Ctnnb1* (c) from small intestinal crypts of untreated and DSS-treated mice. Data represent mean \pm SEM of $n=6$ per group. * $p<0.05$

4 Discussion

DNA methylation, as an epigenetic mark, regulates genome architecture and gene expression, and it is involved in the regulation of cellular development, differentiation, and homeostasis [65, 131]. Although several studies suggest a role for epigenetics in IBD [132], our understanding of the involved molecular mechanisms remains limited. Numerous studies suggest that information on the epigenome might improve disease diagnosis, contribute to our understanding of IBD aetiology, and most importantly, provide new therapeutic approaches [133]. Epigenome-wide association studies (EWAS), analysing whole tissue intestinal biopsies or peripheral blood, have identified differentially methylated loci, including some loci involved in the regulation of immune responses [55, 57, 58]. Importantly, genome-wide association study (GWAS) identified an association between IBD and genetic variants in the *DNMT3A* gene [45]. While there are many studies that implicate DNA methylation in IBD pathogenesis, the role of DNMT3A in intestinal epithelial cells homeostasis has not been investigated.

4.1 DNMT3A is expressed in intestinal epithelial cell lines

The *de novo* DNA methyltransferase genes were identified by Okano et al. in 1998 [134]. The human *DNMT3A* and *DNMT3B* genes are highly homologous with the corresponding murine genes [134]. *Dnmt3a* is highly expressed in mouse embryonic stem cells (ESCs), whereas its expression decreases in adult tissues [135]. The role of the DNA methyltransferase enzymes has been extensively studied in ESCs, however little is known about their function in intestinal epithelial cells. Our studies revealed that the protein expression pattern of DNMT3A isoforms differs between human and murine cell lines. Although DNMT3A2 is the major isoform detected in mouse ES cells [50], DNMT3A1 is the mainly expressed isoform in the murine intestinal epithelial cell line Mode-K. On the contrary, DNMT3A2 is the major isoform in IEC lines of human origin, HT-29 and Caco-2. Few studies have focused on the question whether DNMT3A isoforms exhibit specific or redundant roles in intestinal epithelium homeostasis. In mouse embryonic stem cells, DNMT3A isoforms manifest specific genomic binding preferences [52]. Nevertheless, studies on DNMT3A isoforms in adult tissue have not been conducted.

Caco-2 cells, when cultured under specific conditions, can differentiate and polarize similarly to enterocytes of the small intestine, making them an excellent *in vitro* model for intestinal biology research. Thus, Caco-2 cell line was chosen for better elucidate the role of DNMT3A, and their isoforms, in intestinal epithelial cells. DNMT3A was deleted in Caco-2 cells followed by subsequent re-expression of the individual isoforms. Deletion of DNMT3A resulted in a viable and morphologically normal cell line as determined by microscopical observations, indicating that DNMT3A is dispensable for Caco-2 cell viability. DNMT3A2 cell line presented

protein and mRNA expression of DNMT3A similar to Caco-2 wild-type cells, while re-expression of DNMT3A1 isoform in DNMT3A KO cells resulted in higher protein and mRNA expression of DNMT3A. Nevertheless, cell viability was unaffected, and microscopical examinations resulted in no morphological alterations. Our DNMT3A-deficient Caco-2 cell line together with the stable cell lines expressing the individual isoforms, provide a useful tool to study cell-state driven epigenetic effects in intestinal epithelial cells.

4.2 Deletion of DNMT3A induces a complex dysregulation of the transcriptional signatures of IECs

The link between DNA methylation and gene expression is complex, and how DNA methylation affects transcriptional activity is only partially understood. DNA methylation is canonically associated with transcriptional repression by interfering with the binding of transcription factors [136]. Moreover, DNA methylation in gene promoters is well known to be associated with gene silencing [137]. However, DNA methylation has also been implicated with enhanced gene transcription. Indeed, gene body methylation is positively correlated with expression [138]. It has been reported that deletion of *Dnmt1* results in almost 90% reduction of global DNA methylation. In contrast, loss of DNA methylation, induced by *Dnmt3a/Dnmt3b* deletion, can only be seen after prolonged culturing [120, 139]. In our study, short-term silencing of the individual *DNMT3A*, *DNMT3B* and *DNMT3L* by siRNA resulted in significant changes on the transcriptome level. However, the DNA methylation profiles were unchanged. This might be due to incomplete knockdown efficiency and the limited duration of the assay. Thus, siRNA silencing might not be the suitable approach to observe DNA methylation changes, especially when considering the time-dependency of DNA demethylation. In agreement with other studies [120, 139], we have shown that loss of DNA methylation can only be observed after prolonged period of deletion of the *de novo* methyltransferases enzymes, DNMT3A -3B and 3L.

Even though short-term silencing of *DNMT3A/B/L* did not alter the DNA methylation profile, we did observe significant transcriptional changes. Thus, we raised the question whether DNMT3A/B/L proteins have an additional role that does not require enzymatic activity for transcriptional regulation. The N-terminal regions of Dnmt3a and Dnmt3b are involved in transcriptional repression in association with HDAC (histone deacetylase) activity [140], which could explain the observed methylation-independent transcriptional dysregulation. In this context, the generation of a stable cell line expressing a mutated, catalytically inactive DNMT3A protein might elucidate the methylation-independent functions of DNMT3A on transcriptional regulation.

Since DNMT3A and -3B have differential DNA binding preferences [141, 142] and DNMT3L acts as DNMT3A/B regulator [143], we hypothesized that they may regulate different subsets of genes. The majority of the identified differentially expressed genes (DEGs) were uniquely regulated by the individual DNMT3A/B/L. Considering the unchanged DNA methylation pattern, the observed unique transcriptional regulation could

be attributed to their specific genomic binding preferences. As another possible explanation, differential gene expression may arise from the preferential co-localization of DNMT3A/B/L with specific chromatin remodelling proteins, such as heterochromatin protein 1 α [140].

The fact that DNA demethylation, as a consequence of *Dnmt3a* genomic deletion in mouse ESCs, can only be observed after a prolonged culture period [120], led us to the assumption that long-term genomic ablation of DNMT3A in IECs could alter DNA methylation pattern. To this end, DNMT3A knock-out cells, generated by CRISPR/Cas, were used. Consistent with other studies [131, 139], we observed a global reduction of DNA methylation in DNMT3A KO cells. We found that DNA hypomethylation at the promoter region correlates with both up- and downregulation of gene expression. In addition, the identified DEGs are involved in biological processes such as “intestinal absorption”, “IL1 signaling” and “inflammatory response”. Interestingly, GO term analysis of differentially expressed genes of siRNA versus CRISPR deletion of DNMT3A revealed shared biological processes, such as “response to wounding” or “inflammation”. How exactly DNMT3A mediates transcriptional regulation remains unclear. One might speculate on a possible cross-talk/interference of DNMT3A with the organization of histones. A more detailed investigation on the distribution of histones throughout the DNA may elucidate a possible interplay between DNMT3A and histone organization and the consequences on modulating gene transcription.

Collectively, this study shows a role of DNMT3A in regulating gene expression and DNA methylation profile. The latter depends on deletion of DNMT3A in a time-dependent manner. The biological relevance, resulting from the omics data, proposes a role of DNMT3A in IECs homeostasis and inflammatory responses.

4.3 DNMT3A isoforms exhibit overlapping functions

The *DNMT3A* gene encodes for two main isoforms. In 2002 Chen et al. identified a novel isoform generated from an alternative promoter, known as *Dnmt3a2*. This isoform has *de novo* methylation activity similar to *Dnmt3a1*, but it localizes to the euchromatin [50]. In 2017, Baubec et al. investigated the activity and localization of individual DNMT3A isoforms in mouse embryonic stem cells. They could demonstrate that *Dnmt3a1* and *Dnmt3a2* exhibit a different binding activity throughout the genome. In particular, *Dnmt3a1* preferentially localizes to genomic sites enriched for H3K27me3 at the CpG island shores, while *Dnmt3a2* showed a more global binding activity throughout the whole genome [52].

In this study, we have identified genes that are transcriptionally dysregulated by deletion of all DNMT3A isoforms. Moreover, we validated these candidate genes by rescuing their expression. Indeed, re-expression of DNMT3A1 and DNMT3A2 restored the gene transcription and DNA methylation of a set of genes resembling wild-type levels. GO term analysis of the rescued genes revealed that DNMT3A is engaged in cell

cycle progression, shown by an upregulation of genes involved in controlling the cell cycle, including cyclin-dependent kinase inhibitor 1 (*CDKN1A*), cyclin-dependent kinase inhibitor 1C (*CDKN1C*), cyclin D3 (*CCND3*) and growth arrest and DNA damage inducible alpha (*GADD45A*). These findings are supported by other studies suggesting a function of DNMT3A in regulation of cell proliferation by interfering with the G1/S checkpoint in gastric carcinogenesis [144]. Moreover, it has been shown that DNMT3A interacts with the tumor suppressor gene p53. It can induce the expression of *CDKN1A*, known as the p21 protein, thereby causing a G1 arrest [145]. Interestingly, overexpression of DNMT3A results in p21 reduction via suppression of p53 transactivation and is not dependent on any methylation activity [146].

Repressed biological processes identified by GO term analysis including “chromatin organization” and “histone modifications” suggest a role of DNMT3A in chromatin remodelling by regulating genes encoding enzymes responsible for histone modifications. The latter are post-translational modifications of the histone proteins. The amino acid of the N-terminal histone tail can be subjected to different modifications, including acetylation and methylation [27]. Loss of DNMT3A resulted in downregulation of genes involved in histone modifications, including histone-lysine-N-methyltransferase (*SETDB1*), euchromatic histone-lysine-N-methyltransferase 1 (*EHMT1*), and lysine acetyltransferase (*KAT6A*).

Noteworthy, our findings strongly indicate that DNMT3A contributes to the regulation of processes involved in inflammation. As an example, “cellular response to LPS” was one of the induced GO term analysis for biological processes. LPS (lipopolysaccharide) is a large molecule found in the outer membrane of Gram-negative bacteria [147]. It binds to the toll-like receptor4 (*TRL4*) activating either the NF- κ B signaling and the interferon response [148]. Additionally, genes belonging to the GO term “cellular response to LPS”, including caspase 1 (*CASP1*), C-X-C motif chemokine 10 (*CXCL10*), toll-like receptor 2 (*TLR2*) were upregulated, and their expression was rescued by re-introducing DNMT3A. In IBD patients, increased levels of circulating LPS have been found to correlate with disease activity [149]. Furthermore, exposure to LPS leads to the activation of a strong immune response and the release of pro-inflammatory cytokines and acute phase proteins in IBD patients [150]. Given the biological relevance of the LPS response, our data suggest a potential implication of DNMT3A in modulating key genes involved in the response to LPS, and generally in inflammation.

Integration analyses of DMPs and DEGs identified 45 candidate genes, that have gene expression and promoter DNA methylation rescued. Of interest, the trefoil factor 3 (*TFF3*) gene was found to be downregulated and its promoter hypomethylated upon deletion of DNMT3A, resulting in a positive correlation between DNA methylation and gene transcription. In addition, only the DNMT3A1 isoform was able to rescue gene expression and DNA methylation. TFF3 is a mucin associated peptide and its expression is enhanced in serum of IBD patients, proposing TFF3 as a biomarker to evaluate mucosal healing [151]. Moreover, promoter methylation of the *TFF3* gene has been investigated in prostate cancer as a potential

biomarker for prognosis [152]. Several studies have investigated the correlation between promoter methylation and gene expression of *TFF3*. Indeed, hypomethylation of specific CpGs positions at the promoter leads to overexpression of *TFF3* in human hepatocellular carcinoma [153], indicating that *TFF3* gene expression is epigenetically regulated.

Integration analyses for the *CASP1* gene showed negative correlation of gene expression and DNA methylation. Furthermore, the DNMT3A2 isoform but not DNMT3A1 restored both the expression and DNA methylation profile of *CASP1*. This gene encodes a member of the caspase family that acts as cysteine protease with a specific role in immunity. It cleaves and activates the inactive precursor of IL1, a pro-inflammatory cytokine involved in processes such as inflammation and wound healing [154-156].

In addition to isoform-specific target genes, we have identified transcripts that are regulated by both isoforms, such as interleukin 1 receptor 1 (*IL1R1*) gene. The latter was downregulated and its promoter hypomethylated. Indeed, re-expression of either isoforms resulted in upregulation of both promoter methylation status and gene expression resembling level detected in the wild-type control, resulting in a positive correlation between DNA methylation and gene transcription. The *IL1R1* gene encodes a cytokine receptor that belongs to the IL1 receptor family. It binds IL1 α , IL1 β and their receptor antagonist IL1Ra. Interestingly, the *IL1R1* gene is located within a CD-associated locus that is directly adjacent to an UC-associated region where *IL2R1* is located. GWAS identified SNPs within these regions. However, it is still unclear whether these SNPs tag two separate loci or one locus, suggesting *IL1R1/IL1R2* as IBD risk genes [157]. The IL1 pathway plays an important role in regulation of immune responses during inflammation [158]. For instance, high levels of IL1 β are detected in the colonic mucosa of IBD patients [159] correlating with diseases severity [160]. Loss of IL1 signaling components, such as *IL1R1* or IL1 β results in a more severe phenotype upon DSS-induced colitis in mice [161, 162], supporting the importance of this pathway in regulating inflammatory responses.

In summary, we identified genes that are regulated by DNMT3A. Furthermore, we confirmed our target genes by reintroducing DNMT3A isoforms and we were able to depict set of genes rescued by an individual isoform or by both isoforms, respectively.

4.4 DNMT3A modulates intestinal barrier homeostasis *in vitro*

A functional intestinal epithelial barrier is extremely important, not only for the efficient absorption of nutrients but also as a primary mechanism of defence against invading pathogens. In addition, an appropriate epithelial regeneration response is required for proper barrier homeostasis. In this study, we investigated

the effects of DNMT3A deletion on intestinal barrier homeostasis focusing on intestinal permeability and regenerative properties.

IECs are characterized by a polarized organization, with an apical and a basolateral membrane. Cell polarity plays an important role for barrier formation, uptake and transport of nutrients. Candidate IBD genes are involved in regulation of several features of the epithelial barrier, including cell polarity, cell adhesion and tight junction assembly [163]. Caco-2 cells have been widely used to study intestinal barrier properties [118]. We used Caco-2 cells as a model to study spheroid-like structure formation, representing the physiological gut organization. We showed an implication of DNMT3A in regulating spheroid architecture, illustrated by a defect in lumen expansion in DNMT3A KO spheroids. The observed phenotype might be due to defective cell proliferation or cell polarity as well as impaired ion/water transport. It has been shown that inhibition of actin filament polymerization results in impaired spheroid formation [164], indicating that, spheroid formation may also be dependent on the organization of the actin cytoskeleton and the interaction with the underlying extracellular matrix. Additionally, epithelial morphogenesis requires cell-substrate interaction to allow cell polarization. Extracellular matrix (ECM) components are secreted by epithelial cells, and the cell-ECM interaction contributes to cell polarity and consequently to spheroids formation [164, 165]. In this study, GO analysis revealed as repressed the term “extracellular matrix organization”. Genes encoding laminins and collagen components were downregulated and their expression was rescued by re-expression of DNMT3A. In fact, re-introducing DNMT3A in the KO cells resulted in increased lumen formation and spheroids size compared to DNMT3A null spheroids. Taking together, loss of DNMT3A results in an abnormal structural organization of spheroids and this may be due to the dysregulation of genes responsible for cell-ECM interaction and cell-cell contact. It is unclear if the lumen defect is caused by a pleiotropic dysregulation of this group of genes or whether specific genes can be pinpointed as main culprits. Therefore, additional experiments are required to test the individual contribution of these genes.

Gut barrier integrity is maintained by intercellular epithelial junctions, that are critical for epithelial barrier functions. Most IBD patients present epithelial barrier dysfunction [166, 167], attributed to a dysregulation of proteins involved in epithelial junctional organization [168, 169]. In our study, we discover a possible role of DNMT3A in regulating intestinal permeability. Loss of DNMT3A resulted in increased permeability to paracellular markers, in both 2D and 3D *in vitro* models. Measurements of the trans-epithelial resistance (TEER), indicative for membrane integrity [170], showed reduced TEER values in DNMT3A KO cells suggesting an impaired monolayer integrity. E-cadherin and β -catenin are the two major proteins involved in adherens junction formation, and loss of E-cadherin in the intestinal epithelium increases the susceptibility to DSS-induced colitis *in vivo* [171]. Among the IBD risk genes related to intestinal barrier defects, the *CDH1* gene,

encoding E-cadherin, has been associated with ulcerative colitis [172]. Strikingly, electron microscopy analysis revealed altered adherens junction complexes, in both our *in vitro* and *in vivo* models. Normally, IBD patients are characterized by low expression of β -catenin and E-cadherin [173, 174]. *In vivo*, deletion of Dnmt3a in the intestinal epithelium resulted in a decreased expression of β -catenin and E-cadherin both under basal conditions and during chronic intestinal inflammation. Our findings propose a role for DNMT3A in regulating epithelial intercellular junction proteins. Importantly, the lack of DNMT3A leads to impaired barrier permeability, probably due to altered cellular adhesion, and eventually increased susceptibility to inflammation.

Mucosal damage and impaired epithelial regeneration are commonly observed in IBD [95]. Our data show for the first time a role of DNMT3A in regulating epithelial wound healing *in vitro*. Loss of DNMT3A delays the regeneration process. In addition, impaired healing was restored by re-expression of *DNMT3A*, indicating that the observed phenotype is caused by the absence of DNMT3A. One of the identified differentially expressed genes in DNMT3A KO cells was *TFF3*. It is downregulated in DNMT3A KO cells, and its expression is rescued by re-expression of the DNMT3A1 isoform, revealing *TFF3* as DNMT3A1 target gene. The TFFs family have an essential role in intestinal epithelial healing, specifically during the restitution phase where epithelial cells migrate to the wounded area [175]. TFFs gene expression is regulated by methylation of their promoters and it is tissue-specific. In murine small intestinal tissue, the *Tff3* promoter is partially demethylated (10-25 %) and the methylation status corresponds to gene expression levels [176]. Mice lacking *Tff3* have impaired mucosal healing with poor epithelial regeneration capacity after injury [177]. Epithelial wound healing is also dependent on cell proliferation, which restores the intestinal epithelial cell number. In this context, the Wnt signaling pathway, involved in numerous cellular processes, is critical for proliferation, and when it is aberrantly activated leads to tumor development [178]. As mentioned in the results section, β -catenin is downregulated both *in vitro* and *in vivo* in DNMT3A null IECs compared to the wild-type. Importantly, β -catenin not only modulates cell adhesion but is also a known master regulator of Wnt signaling, and silencing of β -catenin leads to impaired cell migration [179]. It has been shown that Dnmt3a inhibits Wnt signaling and promotes differentiation by repression of Wnt inhibitory factor 1 (*WIF1*) gene, in cardiac progenitor cells [180]. In contrast, our GO term analysis identified as repressed term “Wnt signaling pathway” upon deletion of DNMT3A, supported by reduced expression of β -catenin and three members of the Wnt-Frizzled domains (*FZD3*, *FZD4*, *FZD7*), while *WIF1* gene expression was unaffected. Additionally, a luciferase reporter assay showed a reduced activation of the β -catenin/TCF complex in DNMT3A KO cells, demonstrating reduced Wnt activity. We can speculate that intestinal epithelial cells undergo a different DNMT3A-mediated epigenetic control compared to cardiac cells, regulating therefore a different set of genes. Several studies have reported an implication of Wnt signaling in IBD [181, 182]. While tissue

regeneration requires cell proliferation, the contribution of Wnt signaling to injury repair is not completely understood. Our data illustrate a role of DNMT3A in regulating wound healing, still the precise mechanism remains unclear. Indeed, altered Wnt signaling might not be the major cause, since other genes that are related to wound healing, such as *TFF3*, are dysregulated as well in DNMT3A null intestinal epithelial cells.

NF- κ B signaling in the intestinal epithelium represents a critical regulator of epithelial integrity and intestinal immune homeostasis [183], indicating its crucial role for the maintenance of tissue homeostasis. As transcriptional regulator, NF- κ B regulates immune responses and is implicated in the onset of inflammation [184]. In IBD patients, activation of NF- κ B signaling is enhanced, resulting in an increased expression of various pro-inflammatory cytokines [185]. In the absence of any stimuli, NF- κ B is maintained in an inactive state via its binding to I κ B. Upon inflammatory stimuli, phosphorylation of I κ B results in its degradation releasing NF- κ B from its inhibition. NF- κ B translocates to the nucleus where it acts as transcriptional regulator of its target genes [186]. It is well established that the NF- κ B signaling pathway has pro-inflammatory capacities by inducing the expression of various cytokines. However, recent studies in mouse models have proposed that NF- κ B inhibition in intestinal epithelial cells leads to spontaneous development of inflammation suggesting a protective function of NF- κ B in this cell type [187]. So far, epigenetic regulations of NF- κ B signaling have not been well investigated. Here, we analysed the role of DNMT3A in regulating NF- κ B signaling pathway. Stimulation with IL1 β resulted in reduced nuclear translocation of NF- κ B and less IL8 cytokine production in *DNMT3A*-deficient Caco-2 cells. Furthermore, reduced phosphorylation of p65 was observed in *Dnmt3a*-deficient organoids stimulated with IL1 β , suggesting impaired NF- κ B activation compared to the wild-type. Interestingly, for DNMTs, an epigenetic regulation on I κ B-alpha expression in HCT116 intestinal epithelial cells has been proposed. The authors show that loss of DNMTs results in a reduced NF- κ B activation, indicated by less IL8 production [188]. Our data suggest a possible implication of DNMT3A in regulating NF- κ B activity, and therefore interfere with its pro-inflammatory response. Nevertheless, how exactly DNMT3A acts is not completely clear yet.

In conclusion, our *in vitro* and *in vivo* functional studies support our omics data providing insights into the function of DNMT3A in intestinal epithelial cells. We therefore hypothesize that dysregulation of DNMT3A impairs intestinal epithelial cells homeostasis, compromising the physiology of the gastrointestinal tract.

4.5 The role of DNMT3A during intestinal homeostasis and inflammation

The three methyltransferase enzymes Dnmt1, Dnmt3a and Dnmt3b are required for development, as their deletion is embryonically and postnatally lethal [135, 189]. Dnmt3a has been implicated in tumorigenesis. Indeed, targeted deletion of Dnmt3a in the intestine results in inhibition of tumor progression [47], whereas

transgenic expression of Dnmt3a promotes tumor formation [190]. While the contribution of Dnmt3a tumorigenesis has been demonstrated [47], little is known on Dnmt3a and its role in intestinal homeostasis and inflammation *in vivo*. In this study, we demonstrate that the conditional deletion of Dnmt3a in intestinal epithelial cells does not result in spontaneous inflammation. *Dnmt3a*^{ΔIEC} mice were born at the expected Mendelian ratios and did not show any significant differences neither in body weight, nor in colon and small intestine length. In contrast with the lethal phenotype of the full body knockout animals, loss of *Dnmt3a* in IECs did not impair the development of the mice. Likewise, in our DNMT3A KO cell line, deletion of the gene resulted in viable and morphologically normal cells.

Compensatory upregulation of Dnmt3b, but not Dnmt3a, has been reported in IECs of *Dnmt1*-deficient mice [191]. In our study, mRNA of both *Dnmt3b* and *Dnmt1* was unchanged in colon and small intestine of Dnmt3a-deficient mice compared to their wild-type littermates. On the contrary, during chronic DSS-induced colitis, their gene expression levels were decreased in the small intestine of the knockout mice compared to the wild-type (data not shown). We observed the same tendency for both short and long-term deletion of DNMT3A in Caco-2 cell line. Thus, there is no compensatory upregulation of *Dnmt3b* and *Dnmt1*, instead absence of Dnmt3a causes a down-regulation of the other *Dnmt* genes.

DNMT3A and *DNMT3B* are both downregulated during DSS-induced colitis in mice and in IBD patients, indicating that a pro-inflammatory environment might trigger transcriptional dysregulation of these genes. It has been shown that the miR-29 family directly targets *DNMT3A* and *DNMT3B* leading to down-regulation of these genes, thereby causing DNA hypomethylation in both lung cancer and acute myeloid leukemia [192, 193]. Noteworthy, microRNAs are strongly associated with IBD pathogenesis [194]. Interestingly, elevated levels of miR-29a/b have been identified in mucosal tissue and peripheral blood of UC and CD patients [195]. Therefore, we propose a possible link between higher levels of miR-29 and a low expression of DNMT3A/B in the context of IBD. However, no correlation analysis has been done so far. Therefore, more experiments are needed to elucidate how a pro-inflammatory landscape regulates DNMT3A/B expression.

4.5.1 Deletion of Dnmt3a alters crypt homeostasis

It has been demonstrated that loss of Dnmt1, both in perinatal and mature intestinal epithelium, results in decreased proliferation and enhanced DNA damage followed by apoptosis [191, 196]. Here, we show that the crypt architecture is disturbed in small intestine of *Dnmt3a*^{ΔIEC} mice, indicated by a decreased crypt length. Since crypt and villus length are determined by cell proliferation and cell migration, we hypothesized that this phenomenon might be attributed to a reduced cell proliferation or impaired cell migration. Several studies have shown a role of Dnmt3a in tumorigenesis by regulating cell proliferation. On one side, deletion

of Dnmt3a has been proposed to result in inhibition of melanoma growth via regulation of cell cycle-related genes [197], and silencing of Dnmt3a activates the tumor suppressor gene PTEN, suppressing cell proliferation in hepatocellular carcinoma [198]. On the other side, Dnmt3a has been shown to promote cell proliferation in gastric cancer by disrupting the G1/S checkpoint [144]. Our *in vitro* data support a role of DNMT3A in regulating cell cycle progression, reinforcing our hypothesis. Surprisingly, we detected a normal cell proliferation rate after 1 h BrdU administration, suggesting no impairment of cell proliferation at the crypt niche. In contrast, upon 20 h BrdU exposure, we did observe a reduced number of BrdU positive cells, corresponding to the trans amplifying cells, in *Dnmt3a*^{AIEC} mice. BrdU is incorporated into newly synthesized DNA of dividing cells during the S phase and it can be transmitted to daughter cells [199]. Therefore, despite the normal cell proliferation at the crypt niche, we observed a reduced number of migrating cells. We are still investigating which signaling pathways are contributed to this phenotype. Deletion of Dnmt3a in intestinal epithelial cells might affect cell proliferation via altering cell cycle progression. It is known that the tumor suppressor gene p53, with a key role in cell cycle regulation [145], interacts with DNMT3A [146]. Hence, future studies are warranted, which will investigate whether and how deletion of DNMT3A acts on cell cycle progression and proliferation of IECs.

4.5.2 Mice lacking *Dnmt3a* in the intestine are more susceptible to chronic chemically-induced colitis

Our *in vitro* transcriptomic data suggested a role of DNMT3A in processes such as inflammation and response to wounding. Furthermore our *in vitro* functional assays suggest a protective role of DNMT3A in maintaining intestinal homeostasis, since loss of DNMT3A impairs epithelial healing and barrier permeability. Importantly, while DNMT3A has been identified as a risk gene for CD [45], its role during intestinal inflammation has not been investigated. In this study, we performed a chronic DSS-induced colitis, partially mimicking human IBD pathogenesis, to study the role of DNMT3A in intestinal inflammation. Thus, mice with a genetic deletion of *Dnmt3a* in IECs were used. In agreement with our *in vitro* findings, suggesting an impaired gut barrier and epithelial regeneration, *Dnmt3a*^{AIEC} mice were more susceptible to chronic DSS-induced colitis, illustrated by a slower regeneration and higher disease activity scores.

Overall, our findings indicate a protective function of Dnmt3a in IECs in (chronic) intestinal inflammation. Indeed, loss of Dnmt3a impairs regeneration upon chemically induced colitis, suggesting a role of Dnmt3a in facilitating healing processes. These results are supported by our *in vitro* data, that reveal a crucial role of DNMT3A in regulating permeability and healing in intestinal epithelial cells.

5 Conclusions and future perspectives

IBD patients exhibit an abnormal DNA methylation profile [57]. Based on DNA methylation analysis, it is possible to distinguish between diagnosis (CD, UC or healthy) [66]. Thus, DNA methylation profile can be used as potential biomarker. Genome-wide association studies (GWAS) have identified *DNMT3A* as a genetic risk factor of CD [45], raising the hypothesis of a critical role of DNMT3A in IBD pathogenesis.

In our study, we elucidate the function of DNMT3A in intestinal epithelium homeostasis and its role during chronic inflammation. Our analysis reveals that genomic deletion of DNMT3A alters transcription of a set of genes involved in several processes, leading to impaired intestinal barrier properties. I validated my findings by reintroducing DNMT3A isoforms back to DNMT3A null cells. Indeed, transcriptome analysis identified a set of genes which were specifically dysregulated by DNMT3A, and their expression was restored by re-expression of *DNMT3A* isoforms. In parallel, I performed the same investigation on promoter DNA methylation pattern, and we demonstrated a global DNA hypomethylation upon loss of DNMT3A. In line with the gene expression analysis, I could demonstrate either positive and negative correlation between gene expression and promoter DNA methylation dependent of DNMT3A. In addition, we could show that the DNMT3A-dependent loss of DNA methylation is time-dependent, indicated by unaffected DNA methylation pattern upon short-term silencing of DNMT3A. Therefore, it will be interesting to elucidate the mechanism beyond methylation-independent functions of DNMT3A on transcriptional regulation. In particular, how DNMT3A induces transcriptional changes without modify DNA methylation. Therefore, chromatin immunoprecipitation sequencing (ChIP-seq) analysis will elucidate DNA binding preferences of DNMT3A, and thereby clarify transcriptional regulation driven by DNMT3A in intestinal epithelial cells.

In addition to our transcriptome and methylome analysis, we investigated the functional consequences of deletion of DNMT3A *in vitro*. Overall, deletion of DNMT3A dysregulates intestinal permeability. Cell-cell contacts of differentiated monolayers were disturbed in the absence of DNMT3A, compromising barrier function. In addition to permeability, wound healing was also impaired *in vitro*. While the process of wound healing is characterized by several phases, it remains unclear which specific stage is regulated by DNMT3A. Hence, the use of mouse derived organoid monolayers provides a suitable tool for studying the role of DNMT3A in intestinal barrier functions *ex vivo*. Furthermore, co-culture methods of organoid monolayers and immune cells will shed light on the influence of DNMT3A on intestinal barrier properties and the consequences on the interplay between IECs and immune cells, in homeostatic and inflammatory conditions. Moreover, our *in vitro* findings indicate defective NF- κ B signaling, illustrated by reduced nuclear translocation of NF- κ B and IL8 cytokine production in DNMT3A null cells. It may be of great interest to investigate the role of DNMT3A in regulating NF- κ B signaling by employing other experimental mouse models, such as *in vivo* LPS

exposure. Since NF- κ B signaling plays a key role in immune cells, a mouse model where *Dnmt3a* is specifically deleted only in myeloid cell is suitable to study the role of DNMT3A in NF- κ B signaling pathway.

This study shows a transcriptional dysregulation of DNMT3A during inflammatory condition. In DSS-induced colitis model, *Dnmt3a* mRNA expression is reduced. Likewise, in whole biopsy tissue from IBD patients *DNMT3A* gene expression is repressed. In the context of inflammation, little is known about the transcriptional regulation of *DNMT3A*. Therefore, the usage of several pro-inflammatory stimuli might help understanding which inflammatory triggers, and which molecular mechanism, are responsible for the transcriptional dysregulation of DNMT3A.

While the conditional deletion of *Dnmt3a* in IECs did not result in spontaneous inflammatory phenotype, the small intestinal crypt architecture is altered in our mouse model. In addition, *Dnmt3a*^{ΔIEC} mice were more susceptible to chronic inflammation, underlining the critical role of DNMT3A in inflammatory conditions. So far, it is not fully clear how deletion of DNMT3A increases the susceptibility to chronic inflammation. Further *in vivo* investigations, including wound healing experiments and measurements of the intestinal epithelial permeability in challenged and unchallenged conditions, will elucidate the role of DNMT3A during intestinal inflammation.

6 Summary

DNA methylation is one of the epigenetic modifications which regulates gene transcription in a cell-type and tissue-specific manner. By interfering with the accessibility of transcription factor binding sites or the chromatin state, methylation of the DNA typically results in gene silencing. DNA methyltransferases (DNMTs) are responsible for the establishment and maintenance of the DNA methylation profile. Deletion of *DNMTs* genes causes embryonic lethality, highlighting the importance of DNA methylation during development. While the effects of DNA methylation in intestinal development and homeostasis have been extensively investigated, the specific role of DNA (cytosine-5)-methyltransferase 3A (DNMT3A) in intestinal homeostasis and inflammation is still not clear. Notably, genetic variants in the human *DNMT3A* gene have been associated with an increased risk of inflammatory bowel disease (IBD) and aberrant DNA methylation has been extensively observed in several diseases, including IBD. However, while epigenome-wide association studies (EWAS) have reported several disease-associated loci, the mechanistic dysregulation of DNA methylation has remained elusive. In this thesis, we study the function of DNMT3A in intestinal homeostasis, focusing on the mechanisms by which DNMT3A regulates gene transcription and DNA methylation.

In this study, we elucidate the transcriptional and functional consequences of genomic ablation of *DNMT3A* in intestinal epithelial cells. Long-term ablation of *DNMT3A* resulted in transcriptional dysregulation and global DNA hypomethylation, whereas short-term silencing caused transcriptome dysregulation but no changes in the DNA methylation profile. More specifically, we found 45 genes which were regulated in a methylation-dependent way. In contrast, we detected a group of genes that were transcriptionally dysregulated despite unchanged promoter methylation, resulting in DNMT3A methylation-independent regulation. These results suggest that DNMT3A regulates gene expression both in a methylation-dependent and independent manner. On a function level, our transcriptome analysis revealed a role for DNMT3A in biological processes such as cell cycle progression, Wnt signaling, intestinal absorption or response to lipopolysaccharides (LPS), supporting the importance of DNMT3A in maintaining intestinal homeostasis.

In line with these findings, our *in vitro* analysis identifies a critical role of DNMT3A in two crucial epithelial features, permeability and wound healing. We find that intestinal permeability is impaired in *DNMT3A* null cells. Notably, lack of DNMT3A increased cell permeability and resulted in reduced cellular contact zones characterized by a higher inter-cellular distance *in vitro*. Furthermore, we identified a role for DNMT3A in wound repair. The impaired healing was restored by re-expression of *DNMT3A* gene, indicating that the observed phenotype is driven by the absence of DNMT3A.

We find that mice that lack *Dnmt3a* in Intestinal epithelial cells (IECs) are more susceptible to chronic chemically-induced colitis. *Dnmt3a* deficiency in the intestinal epithelium affects the structure of adherens junctions along with reduced expression of β -catenin and E-cadherin, suggesting a compromised mucosal barrier mechanism.

In our study, we report for the first time an inflammation-dependent *DNMT3A* expression, more precisely, we observed a downregulation of *DNMT3A* in both IBD patients and in a murine chronic colitis model. Furthermore, upon deletion of *DNMT3A* there is no compensatory regulation by *DNMT3B* or *DNMT1* neither *in vitro* nor *in vivo* and, suggesting a unique role of the gene in establishing *DNMT3A*-specific transcriptome and methylome signatures.

In conclusion, this thesis provides insights into the role of *DNMT3A* in intestinal epithelium homeostasis, with a particular emphasis on gene expression, DNA methylation and mucosal barrier properties. These findings indicate a critical importance of *DNMT3A* transcriptional regulation during homeostasis and inflammation. Thereby, altered expression of *DNMT3A* or its target genes could be used as alternative biomarkers to screen intestinal epithelial barrier defect and develop new potential therapeutic molecules.

7 Zusammenfassung

Bei der DNA-Methylierung handelt es sich um eine epigenetische Veränderung, die die Transkription von Genen zelltyp- und gewebespezifisch reguliert. Eine Methylierung der DNA beeinträchtigt die Bindung von Transkriptionsfaktoren oder den Chromatinstatus und führt dadurch typischerweise zur Inaktivierung eines Gens. DNA-Methyltransferasen (DNMTs) sind für die *de novo* sowie für die Erhaltungs-Methylierung verantwortlich. Die Deletion von *DNMTs* ist embryonal lethal und unterstreicht damit die Bedeutung der DNA-Methylierung bei der Embryonalentwicklung. Während die Rolle der DNA-Methylierung bei der intestinalen Entwicklung und Homöostase bereits intensiv untersucht wurde, ist die spezifische Funktion der DNA-Methyltransferase 3 (DNMT3A) bei der Aufrechterhaltung der intestinalen Homöostase und im Kontext von intestinaler Entzündung bisher unzureichend verstanden. Im Menschen sind genetische Varianten im *DNMT3A* Gen mit einem erhöhten Risiko für die Entstehung von chronisch-entzündlichen Darmerkrankungen (CED) assoziiert. Darüberhinaus wurde das Auftreten von abberanten Veränderungen der DNA-Methylierung in zahlreichen Krankheiten beschrieben, darunter auch bei CED. Zwar konnten *Epigenom-Weite-Assoziations-Studien* (EWAS) zahlreiche krankheitsassoziierte Loci identifizieren, allerdings ist die mechanistische Dysregulation der DNA Methylierung nur schlecht verstanden. In dieser Thesis untersuchen wir die Rolle von DNMT3A bei der intestinalen Homöostase, dabei wird insbesondere der Einfluss von DNMT3A auf die Regulation der Gentranskription und DNA Methylierung untersucht.

In dieser Arbeit werden zunächst die transkriptionellen und funktionalen Konsequenzen einer genomischen Ablation von DNMT3A in intestinalen Epithelzellen untersucht. Die langfristige Ablation von DNMT3A führt zu einer transkriptionellen Dysregulation und zu einer globalen DNA-Hypomethylierung. Dagegen bewirkt eine kurzzeitiges *silencing* von DNMT3A eine transkriptionelle Modulation, aber keine Veränderung des Methylierungsstatus. Bei unseren Analysen konnten wir 45 Gene identifizieren, die methylierungsabhängig reguliert wurden. Interessanterweise konnten wir auch eine Gruppe von Genen ausmachen, die eine abweichende Transkription aufwiesen, gleichzeitig aber keine veränderte Methylierung zeigten. Diese Beobachtungen implizieren, dass DNMT3A die Genexpression sowohl methylierungsabhängig als auch -unabhängig reguliert. Auf funktioneller Ebene offenbaren unsere Transkriptomanalysen eine Rolle von DNMT3A bei der Regulation des Zellzyklusverlaufes, dem Wnt-Signalweg, der intestinalen Absorption und der Antwort auf bakterielles Lipopolysaccharid (LPS). Diese Ergebnisse unterstreichen die Bedeutung von DNMT3A bei der Aufrechterhaltung der intestinalen Homöostase.

In Übereinstimmung mit diesen Beobachtungen zeigen unsere *in vitro* Daten, dass DNMT3A eine kritische Rolle für die Integrität des intestinalen Epithels und bei der Wundheilung spielt. Wir konnten beobachten,

dass die intestinale Permeabilität in DNMT3A-defizienten Zellen beeinträchtigt ist. Dabei führt das Fehlen von DNMT3A *in vitro* zu einer erhöhten Zellpermeabilität und einer verminderten Ausprägung der Kontaktzonen zwischen den Zellen. Darüberhinaus konnten wir eine Rolle von DNMT3A bei der Wundheilung feststellen. Bemerkenswerterweise konnte die Wundheilung durch die Reexpression von *DNMT3A* wieder hergestellt werden. Diese Beobachtung verdeutlicht, dass der beobachtete Phänotyp durch die DNMT3A-Defizienz verursacht ist.

In vivo konnten wir zeigen, dass Mäuse mit einer DNMT3A-Defizienz im intestinalen Epithel anfälliger für eine chemisch-induzierte Colitis sind. Das Fehlen von DNMT3A im intestinalen Epithel beeinträchtigt die Struktur der Adhärenzverbindungen und führt zu einer reduzierten Expression von β -Catenin und E-Cadherin. Diese Ergebnisse implizieren eine Beeinträchtigung der Barrierefunktion des intestinalen Epithels.

Außerdem konnten wir erstmals eine entzündungsabhängige Expression von *DNMT3A* beobachten. Sowohl in CED-Patienten als auch in einem murinen Colitis-Modell detektierten wir eine Herabregulation von *DNMT3A*. Interessanterweise wurde weder *in vitro* noch *in vivo* eine kompensatorische Hochregulation von DNMT3B oder DNMT1 beobachtet. Dies legt nahe, dass DNMT3A eine einzigartige Rolle sowohl bei der Regulation des Transkriptoms als auch des Methyloms spielt.

Zusammenfassend liefert diese Thesis Einblicke in die Funktion von DNMT3A bei der Regulation der Genexpression, der DNA Methylierung und übergeordnet bei der Homöostase des intestinalen Epithels. Unsere Ergebnisse weisen auf eine kritische Funktion von DNMT3A bei der transkriptionellen Regulation sowohl unter basalen Bedingungen als auch bei einer intestinalen Entzündung hin. Eine veränderte Expression von DNMT3A und deren Zielgene könnte als alternativer Biomarker fungieren um Defekte der Barrierefunktion des intestinalen Epithels zu detektieren. Auch könnte eine gezielte Manipulation von DNMT3A und deren Zielgene zur Entwicklung neuerer Therapieansätze beitragen.

8 References

1. Baumgart, D.C. and S.R. Carding, *Inflammatory bowel disease: cause and immunobiology*. The Lancet, 2007. **369**(9573): p. 1627-1640.
2. Jean-Fre´de´ric Colombel, A.J.M.W., Markus F Neurath, *The 10 remaining mysteries of inflammatory bowel disease*. Gut, 2008. **Vol 57 No 4**.
3. Xavier, R.J. and D.K. Podolsky, *Unravelling the pathogenesis of inflammatory bowel disease*. Nature, 2007. **448**(7152): p. 427-34.
4. THAD WILKINS, K.J., JIGNESHKUMAR PATEL, *Diagnosis and Management of Crohn's Disease*. American Family Physician, 2011. **Volume 84**.
5. Isgar, B., et al., *Symptoms of irritable bowel syndrome in ulcerative colitis in remission*. Gut, 1983. **24**(3): p. 190-2.
6. Andersen, N.N. and T. Jess, *Has the risk of colorectal cancer in inflammatory bowel disease decreased?* World J Gastroenterol, 2013. **19**(43): p. 7561-8.
7. Bandzar, S., S. Gupta, and M.O. Platt, *Crohn's disease: a review of treatment options and current research*. Cell Immunol, 2013. **286**(1-2): p. 45-52.
8. Peyrin-Biroulet, L., *Advances in the treatment of ulcerative colitis*. Gastroenterol Hepatol (N Y), 2013. **9**(12): p. 827-9.
9. Ordás, I., et al., *Ulcerative colitis*. The Lancet, 2012. **380**(9853): p. 1606-1619.
10. Molodecky, N.A., et al., *Increasing incidence and prevalence of the inflammatory bowel diseases with time, based on systematic review*. Gastroenterology, 2012. **142**(1): p. 46-54 e42; quiz e30.
11. Ng, S.C., et al., *Worldwide incidence and prevalence of inflammatory bowel disease in the 21st century: a systematic review of population-based studies*. Lancet, 2018. **390**(10114): p. 2769-2778.
12. Thia, K.T., et al., *An update on the epidemiology of inflammatory bowel disease in Asia*. Am J Gastroenterol, 2008. **103**(12): p. 3167-82.
13. Renz, H., et al., *Gene-environment interactions in chronic inflammatory disease*. Nat Immunol, 2011. **12**(4): p. 273-7.
14. Hugot, J.P., et al., *Mapping of a susceptibility locus for Crohn's disease on chromosome 16*. Nature, 1996. **379**(6568): p. 821-3.
15. Hugot, J.P., et al., *Association of NOD2 leucine-rich repeat variants with susceptibility to Crohn's disease*. Nature, 2001. **411**(6837): p. 599-603.
16. Jostins, L., et al., *Host-microbe interactions have shaped the genetic architecture of inflammatory bowel disease*. Nature, 2012. **491**(7422): p. 119-24.
17. Duerr, R.H., et al., *A genome-wide association study identifies IL23R as an inflammatory bowel disease gene*. Science, 2006. **314**(5804): p. 1461-3.
18. Hampe, J., et al., *A genome-wide association scan of nonsynonymous SNPs identifies a susceptibility variant for Crohn disease in ATG16L1*. Nat Genet, 2007. **39**(2): p. 207-11.
19. Festen, E.A., et al., *Genetic variants in the region harbouring IL2/IL21 associated with ulcerative colitis*. Gut, 2009. **58**(6): p. 799-804.
20. Kaplan, N.A.M.a.G.G., *Environmental Risk Factors for Inflammatory Bowel Disease*. Gastroenterology & Hepatology, 2010. **6**(5).
21. Hou, J.K., B. Abraham, and H. El-Serag, *Dietary Intake and Risk of Developing Inflammatory Bowel Disease: A Systematic Review of the Literature*. American Journal of Gastroenterology, 2011. **106**(4): p. 563-573.

22. Petronis, A. and R. Petroniene, *Epigenetics of inflammatory bowel disease*. Gut, 2000. **47**(2): p. 302-6.
23. Wang, J., et al., *Quantifying the Waddington landscape and biological paths for development and differentiation*. Proc Natl Acad Sci U S A, 2011. **108**(20): p. 8257-62.
24. Morris, C.-t.W.a.J.R., *Genes, Genetics, and Epigenetics: A Correspondence*. SCIENCE, 2001. **293**.
25. Bernstein, B.E., A. Meissner, and E.S. Lander, *The mammalian epigenome*. Cell, 2007. **128**(4): p. 669-81.
26. Jones, P.A., *Functions of DNA methylation: islands, start sites, gene bodies and beyond*. Nat Rev Genet, 2012. **13**(7): p. 484-92.
27. Cedar, H. and Y. Bergman, *Linking DNA methylation and histone modification: patterns and paradigms*. Nat Rev Genet, 2009. **10**(5): p. 295-304.
28. Deaton, A.M. and A. Bird, *CpG islands and the regulation of transcription*. Genes Dev, 2011. **25**(10): p. 1010-22.
29. Lister, R., et al., *Human DNA methylomes at base resolution show widespread epigenomic differences*. Nature, 2009. **462**(7271): p. 315-322.
30. Salhab, A., et al., *A comprehensive analysis of 195 DNA methylomes reveals shared and cell-specific features of partially methylated domains*. Genome Biology, 2018. **19**.
31. Li, E., *Chromatin modification and epigenetic reprogramming in mammalian development*. Nat Rev Genet, 2002. **3**(9): p. 662-73.
32. Reik, W., W. Dean, and J. Walter, *Epigenetic reprogramming in mammalian development*. Science, 2001. **293**(5532): p. 1089-93.
33. Rollins, R.A., et al., *Large-scale structure of genomic methylation patterns*. Genome Res, 2006. **16**(2): p. 157-63.
34. Suzuki, M.M. and A. Bird, *DNA methylation landscapes: provocative insights from epigenomics*. Nat Rev Genet, 2008. **9**(6): p. 465-76.
35. Kantarjian, H., et al., *Decitabine improves patient outcomes in myelodysplastic syndromes: results of a phase III randomized study*. Cancer, 2006. **106**(8): p. 1794-803.
36. Hermann, A., H. Gowher, and A. Jeltsch, *Biochemistry and biology of mammalian DNA methyltransferases*. Cell Mol Life Sci, 2004. **61**(19-20): p. 2571-87.
37. Guo, X., et al., *Structural insight into autoinhibition and histone H3-induced activation of DNMT3A*. Nature, 2015. **517**(7536): p. 640-4.
38. Lyko, F., *The DNA methyltransferase family: a versatile toolkit for epigenetic regulation*. Nat Rev Genet, 2017.
39. Jeltsch, A. and R.Z. Jurkowska, *Allosteric control of mammalian DNA methyltransferases - a new regulatory paradigm*. Nucleic Acids Res, 2016. **44**(18): p. 8556-8575.
40. Mary Grace Goll, F.K., 2 Keith A. Magerl, 3 Jeffrey A. Yoder, 4 Chih-Lin Hsieh, 5 Xiaoyu Zhang, 6 Kent G. Golic, 7 Steven E. Jacobsen, 6 Timothy H. Bestor^{1*}, *Methylation of tRNA^{Asp} by the DNA Methyltransferase Homolog Dnmt2*. SCIENCE, 2006. **VOL 311**.
41. Jia, D., et al., *Structure of Dnmt3a bound to Dnmt3L suggests a model for de novo DNA methylation*. Nature, 2007. **449**(7159): p. 248-51.
42. Ooi, S.K., et al., *DNMT3L connects unmethylated lysine 4 of histone H3 to de novo methylation of DNA*. Nature, 2007. **448**(7154): p. 714-7.
43. Turek-Plewa, J. and P.P. Jagodzinski, *The role of mammalian DNA methyltransferases in the regulation of gene expression*. Cell Mol Biol Lett, 2005. **10**(4): p. 631-47.

44. Vojta, A., et al., *Repurposing the CRISPR-Cas9 system for targeted DNA methylation*. Nucleic Acids Res, 2016. **44**(12): p. 5615-28.
45. Franke, A., et al., *Genome-wide meta-analysis increases to 71 the number of confirmed Crohn's disease susceptibility loci*. Nat Genet, 2010. **42**(12): p. 1118-25.
46. Masaki Okano, D.W.B., Daniel A. Haber, and En Li, *DNA Methyltransferases Dnmt3a and Dnmt3b Are Essential for De Novo Methylation and Mammalian Development*. Cell, 1999. **99**: p. 247–257.
47. Weis, B., et al., *Inhibition of intestinal tumor formation by deletion of the DNA methyltransferase 3a*. Oncogene, 2015. **34**(14): p. 1822-30.
48. Dai, Y.J., et al., *Conditional knockin of Dnmt3a R878H initiates acute myeloid leukemia with mTOR pathway involvement*. Proc Natl Acad Sci U S A, 2017. **114**(20): p. 5237-5242.
49. Shaoping Xie , Z.W., Masaki Okano, Masahiro Nogami , Yuan Li , Wei-Wu He , Katsuzumi Okumura ,En Li *Cloning, expression and chromosome locations of the human DNMT3 gene family*. Gene, 1999: p. 87–95.
50. Chen, T., et al., *A novel Dnmt3a isoform produced from an alternative promoter localizes to euchromatin and its expression correlates with active de novo methylation*. J Biol Chem, 2002. **277**(41): p. 38746-54.
51. Irizarry, R.A., et al., *The human colon cancer methylome shows similar hypo- and hypermethylation at conserved tissue-specific CpG island shores*. Nat Genet, 2009. **41**(2): p. 178-186.
52. Manzo, M., et al., *Isoform-specific localization of DNMT3A regulates DNA methylation fidelity at bivalent CpG islands*. EMBO J, 2017. **36**(23): p. 3421-3434.
53. Low, D., A. Mizoguchi, and E. Mizoguchi, *DNA methylation in inflammatory bowel disease and beyond*. World J Gastroenterol, 2013. **19**(32): p. 5238-49.
54. Gloria, L., et al., *DNA hypomethylation and proliferative activity are increased in the rectal mucosa of patients with long-standing ulcerative colitis*. Cancer, 1996. **78**(11): p. 2300-6.
55. Nimmo, E.R., et al., *Genome-wide methylation profiling in Crohn's disease identifies altered epigenetic regulation of key host defense mechanisms including the Th17 pathway*. Inflamm Bowel Dis, 2012. **18**(5): p. 889-99.
56. Kitamura, E., et al., *Analysis of tissue-specific differentially methylated regions (TDMs) in humans*. Genomics, 2007. **89**(3): p. 326-37.
57. Hasler, R., et al., *A functional methylome map of ulcerative colitis*. Genome Res, 2012. **22**(11): p. 2130-7.
58. Cooke, J., et al., *Mucosal genome-wide methylation changes in inflammatory bowel disease*. Inflamm Bowel Dis, 2012. **18**(11): p. 2128-37.
59. McDermott, E., et al., *DNA Methylation Profiling in Inflammatory Bowel Disease Provides New Insights into Disease Pathogenesis*. Journal of Crohns & Colitis, 2016. **10**(1): p. 77-86.
60. Sadler, T., et al., *Genome-wide analysis of DNA methylation and gene expression defines molecular characteristics of Crohn's disease-associated fibrosis*. Clin Epigenetics, 2016. **8**: p. 30.
61. Taman, H., et al., *Genome-wide DNA Methylation in Treatment-naive Ulcerative Colitis*. J Crohns Colitis, 2018. **12**(11): p. 1338-1347.
62. Ventham, N.T., et al., *Integrative epigenome-wide analysis demonstrates that DNA methylation may mediate genetic risk in inflammatory bowel disease*. Nature Communications, 2016. **7**.
63. Okamoto, R. and M. Watanabe, *Role of epithelial cells in the pathogenesis and treatment of inflammatory bowel disease*. J Gastroenterol, 2016. **51**(1): p. 11-21.
64. Sheaffer, K.L., et al., *DNA methylation is required for the control of stem cell differentiation in the small intestine*. Genes & Development, 2014. **28**(6): p. 652-664.

65. Howell, K.J., et al., *DNA Methylation and Transcription Patterns in Intestinal Epithelial Cells From Pediatric Patients With Inflammatory Bowel Diseases Differentiate Disease Subtypes and Associate With Outcome*. *Gastroenterology*, 2017.
66. Kraiczky, J., et al., *Assessing DNA methylation in the developing human intestinal epithelium: potential link to inflammatory bowel disease*. *Mucosal Immunol*, 2016. **9**(3): p. 647-58.
67. Lora V. Hooper, D.R.L., Andrew J. Macpherson, *Interactions Between the Microbiota and the Immune System*. *SCIENCE* 2012 **VOL 336**.
68. Maynard, C.L., et al., *Reciprocal interactions of the intestinal microbiota and immune system*. *Nature*, 2012. **489**(7415): p. 231-41.
69. Peterson, L.W. and D. Artis, *Intestinal epithelial cells: regulators of barrier function and immune homeostasis*. *Nat Rev Immunol*, 2014. **14**(3): p. 141-53.
70. REHFELD, J.F., *The New Biology of Gastrointestinal Hormones*. *PHYSIOLOGICAL REVIEWS*, 1998. **78**.
71. Hansson, G.C., *Role of mucus layers in gut infection and inflammation*. *Curr Opin Microbiol*, 2012. **15**(1): p. 57-62.
72. Kim, Y.S. and S.B. Ho, *Intestinal goblet cells and mucins in health and disease: recent insights and progress*. *Curr Gastroenterol Rep*, 2010. **12**(5): p. 319-30.
73. Clevers, H.C. and C.L. Bevins, *Paneth cells: maestros of the small intestinal crypts*. *Annu Rev Physiol*, 2013. **75**: p. 289-311.
74. Stappenbeck, T.S. and D.P.B. McGovern, *Paneth Cell Alterations in the Development and Phenotype of Crohn's Disease*. *Gastroenterology*, 2017. **152**(2): p. 322-326.
75. Tschurtschenthaler, M., et al., *Defective ATG16L1-mediated removal of IRE1alpha drives Crohn's disease-like ileitis*. *J Exp Med*, 2017. **214**(2): p. 401-422.
76. Farquhar, M.G. and G.E. Palade, *Junctional Complexes in Various Epithelia*. *Journal of Cell Biology*, 1963. **17**(2): p. 375-&.
77. Groschwitz, K.R. and S.P. Hogan, *Intestinal barrier function: molecular regulation and disease pathogenesis*. *J Allergy Clin Immunol*, 2009. **124**(1): p. 3-20; quiz 21-2.
78. Van Itallie, C.M. and J.M. Anderson, *Claudins and epithelial paracellular transport*. *Annu Rev Physiol*, 2006. **68**: p. 403-29.
79. Alan S. Fanning, B.J.J., Lynne A. Jesaitis, and James Melvin Anderson, *The Tight Junction Protein ZO-1 Establishes a Link between the Transmembrane Protein Occludin and the Actin Cytoskeleton*. *THE JOURNAL OF BIOLOGICAL CHEMISTRY*, 1998.
80. Valeri Vasioukhin, C.B., Mei Yin, and Elaine Fuchs, *Directed Actin Polymerization Is the Driving Force for Epithelial Cell–Cell Adhesion*. *Cell*, 2000. **Vol. 100, 209–219**.
81. Mirna Perez-Moreno, C.J.a.E.F., *Sticky Business: Orchestrating Cellular Signals at Adherens Junctions*. *Cell*, 2003,. **112, 535–548**.
82. Kowalczyk, A.P. and K.J. Green, *Structure, function, and regulation of desmosomes*. *Prog Mol Biol Transl Sci*, 2013. **116**: p. 95-118.
83. Kleessen, B., et al., *Mucosal and invading bacteria in patients with inflammatory bowel disease compared with controls*. *Scand J Gastroenterol*, 2002. **37**(9): p. 1034-41.
84. Pullan, R.D., et al., *Thickness of adherent mucus gel on colonic mucosa in humans and its relevance to colitis*. *Gut*, 1994. **35**(3): p. 353-9.
85. Welcker, K., et al., *Increased intestinal permeability in patients with inflammatory bowel disease*. *Eur J Med Res*, 2004. **9**(10): p. 456-60.
86. Moreira, A.P., et al., *Influence of a high-fat diet on gut microbiota, intestinal permeability and metabolic endotoxaemia*. *Br J Nutr*, 2012. **108**(5): p. 801-9.

87. MARC PEETERS, Y.G., BART MAES, MARTIN HIELE, KAREL GEBOES, GASTON VANTRAPPEN, and PAUL RUTGEERTS, *Increased Permeability of Macroscopically Normal Small Bowel in Crohn's Disease*. Digestive Diseases and Sciences, 1994. **39**, No. 10
88. Hollander, D., *Increased Intestinal Permeability in Patients with Crohn's Disease and Their Relatives*. Annals of Internal Medicine, 1986. **105**(6).
89. Zeissig, S., et al., *Changes in expression and distribution of claudin 2, 5 and 8 lead to discontinuous tight junctions and barrier dysfunction in active Crohn's disease*. Gut, 2007. **56**(1): p. 61-72.
90. van Bodegraven, A.A., et al., *Genetic Variation in Myosin IXB Is Associated With Ulcerative Colitis*. Gastroenterology, 2006. **131**(6): p. 1768-1774.
91. Wapenaar, M.C., et al., *Associations with tight junction genes PARD3 and MAGI2 in Dutch patients point to a common barrier defect for coeliac disease and ulcerative colitis*. Gut, 2008. **57**(4): p. 463-7.
92. Muise, A.M., et al., *Polymorphisms in E-cadherin (CDH1) result in a mis-localised cytoplasmic protein that is associated with Crohn's disease*. Gut, 2009. **58**(8): p. 1121-1127.
93. Sturm, A. and A.U. Dignass, *Epithelial restitution and wound healing in inflammatory bowel disease*. World Journal of Gastroenterology, 2008. **14**(3): p. 348-353.
94. Basson, M.D., *Mucosal healing and adaptation in the small intestine*. Curr Opin Gen Surg, 1994: p. 138-46.
95. Sturm, A. and A.U. Dignass, *Epithelial restitution and wound healing in inflammatory bowel disease*. World J Gastroenterol, 2008. **14**(3): p. 348-53.
96. Iizuka, M. and S. Konno, *Wound healing of intestinal epithelial cells*. World J Gastroenterol, 2011. **17**(17): p. 2161-71.
97. Pickert, G., et al., *STAT3 links IL-22 signaling in intestinal epithelial cells to mucosal wound healing*. J Exp Med, 2009. **206**(7): p. 1465-72.
98. Huebener, P. and R.F. Schwabe, *Regulation of wound healing and organ fibrosis by toll-like receptors*. Biochim Biophys Acta, 2013. **1832**(7): p. 1005-17.
99. Rakoff-Nahoum, S., et al., *Recognition of commensal microflora by toll-like receptors is required for intestinal homeostasis*. Cell, 2004. **118**(2): p. 229-241.
100. Eyking, A., D.K. Podolsky, and E. Cario, *Colitis-Associated Variant of TLR2 Causes Impaired Mucosal Repair Due to TFF3 Deficiency*. Gastroenterology, 2009. **136**(5): p. A54-A54.
101. Fukata, M., et al., *Toll-like receptor-4 is required for intestinal response to epithelial injury and limiting bacterial translocation in a murine model of acute colitis*. American Journal of Physiology-Gastrointestinal and Liver Physiology, 2005. **288**(5): p. G1055-G1065.
102. Veeman, M.T., et al., *Zebrafish prickles, a modulator of noncanonical Wnt/Fz signaling, regulates gastrulation movements*. Current Biology, 2003. **13**(8): p. 680-685.
103. Sato, T. and H. Clevers, *Growing Self-Organizing Mini-Guts from a Single Intestinal Stem Cell: Mechanism and Applications*. Science, 2013. **340**(6137): p. 1190-1194.
104. Sato, T., et al., *Single Lgr5 stem cells build crypt-villus structures in vitro without a mesenchymal niche*. Nature, 2009. **459**(7244): p. 262-U147.
105. Miyoshi, H. and T.S. Stappenbeck, *In vitro expansion and genetic modification of gastrointestinal stem cells in spheroid culture*. Nature Protocols, 2013. **8**(12): p. 2471-2482.
106. Lowry, O.H., et al., *Protein measurement with the Folin phenol reagent*. J Biol Chem, 1951. **193**(1): p. 265-75.
107. Laemmli, U.K., *Cleavage of structural proteins during the assembly of the head of bacteriophage T4*. Nature, 1970. **227**(5259): p. 680-5.

108. Towbin, H., T. Staehelin, and J. Gordon, *Electrophoretic transfer of proteins from polyacrylamide gels to nitrocellulose sheets: procedure and some applications*. 1979. *Biotechnology*, 1992. **24**: p. 145-9.
109. Schindelin, J., et al., *Fiji: an open-source platform for biological-image analysis*. *Nat Methods*, 2012. **9**(7): p. 676-82.
110. Schmidt, H., et al., *Enrichment and analysis of secretory lysosomes from lymphocyte populations*. *BMC Immunol*, 2009. **10**: p. 41.
111. Trapnell, C., et al., *Differential gene and transcript expression analysis of RNA-seq experiments with TopHat and Cufflinks*. *Nat Protoc*, 2012. **7**(3): p. 562-78.
112. Anders, S., P.T. Pyl, and W. Huber, *HTSeq--a Python framework to work with high-throughput sequencing data*. *Bioinformatics*, 2015. **31**(2): p. 166-9.
113. Love, M.I., W. Huber, and S. Anders, *Moderated estimation of fold change and dispersion for RNA-seq data with DESeq2*. *Genome Biol*, 2014. **15**(12): p. 550.
114. Chen, H. and P.C. Boutros, *VennDiagram: a package for the generation of highly-customizable Venn and Euler diagrams in R*. *BMC Bioinformatics*, 2011. **12**: p. 35.
115. M, C., *GO.db: A set of annotation maps describing the entire Gene Ontology. R package version 3.7.0*. 2018.
116. Assenov, Y., et al., *Comprehensive analysis of DNA methylation data with RnBeads*. *Nat Methods*, 2014. **11**(11): p. 1138-1140.
117. Robine S, H.C., Moll R, Sahuquillo-Merino C, Coudrier E, Zweibaum A, et al., *Can villin be used to identify malignant and undifferentiated normal digestive epithelial cells?* *Proc Natl Acad Sci U S A*, 1985. **Dec;82(24):8488–92**.
118. Rousset, M., *The human colon carcinoma cell lines HT-29 and Caco-2: two in vitro models for the study of intestinal differentiation*. *Biochimie*, 1986. **68**(9): p. 1035-40.
119. Ambrosi, C., M. Manzo, and T. Baubec, *Dynamics and Context-Dependent Roles of DNA Methylation*. *J Mol Biol*, 2017. **429**(10): p. 1459-1475.
120. Chen, T., et al., *Establishment and Maintenance of Genomic Methylation Patterns in Mouse Embryonic Stem Cells by Dnmt3a and Dnmt3b*. *Molecular and Cellular Biology*, 2003. **23**(16): p. 5594-5605.
121. Bird, A., *DNA methylation patterns and epigenetic memory*. *Genes Dev*, 2002. **16**(1): p. 6-21.
122. Law, J.A. and S.E. Jacobsen, *Establishing, maintaining and modifying DNA methylation patterns in plants and animals*. *Nat Rev Genet*, 2010. **11**(3): p. 204-20.
123. Ti, D., et al., *Causes and consequences of epigenetic regulation in wound healing*. *Wound Repair Regen*, 2014. **22**(3): p. 305-12.
124. Barrett, T.A., *Developmental biology. Intestinal wound healing requires a Wnt balancing act*. *Science*, 2012. **338**(6103): p. 51-2.
125. Pahl, H.L., *Activators and target genes of Rel/NF-kappaB transcription factors*. *Oncogene*, 1999. **18**(49): p. 6853-66.
126. Oeckinghaus, A. and S. Ghosh, *The NF-kappaB family of transcription factors and its regulation*. *Cold Spring Harb Perspect Biol*, 2009. **1**(4): p. a000034.
127. Glenn E. Croston, Z.C., and David V. Geoddel, *NF-κB Activation by Interleukin-1 (IL-1) Requires an IL-1 Receptor-associated Protein Kinase Activity*. *The Journal of Biological Chemistry*, 1995. **270**: p. 16514-16517.
128. Okayasu, I., et al., *A novel method in the induction of reliable experimental acute and chronic ulcerative colitis in mice*. *Gastroenterology*, 1990. **98**(3): p. 694-702.

129. Rijke, R.P.C., Meerfieig.Wv, and H. Galjaard, *Effect of Villus Length on Cell-Proliferation and Migration in Small Intestinal Epithelium*. Cell and Tissue Kinetics, 1974. **7**(6): p. 577-586.
130. Chassaing, B., et al., *Dextran sulfate sodium (DSS)-induced colitis in mice*. Curr Protoc Immunol, 2014. **104**: p. Unit 15 25.
131. Kaaij, L.T., et al., *DNA methylation dynamics during intestinal stem cell differentiation reveals enhancers driving gene expression in the villus*. Genome Biol, 2013. **14**(5): p. R50.
132. Loddo, I. and C. Romano, *Inflammatory Bowel Disease: Genetics, Epigenetics, and Pathogenesis*. Front Immunol, 2015. **6**: p. 551.
133. Yang, X., et al., *Targeting DNA methylation for epigenetic therapy*. Trends Pharmacol Sci, 2010. **31**(11): p. 536-46.
134. Okano, M., S. Xie, and E. Li, *Cloning and characterization of a family of novel mammalian DNA (cytosine-5) methyltransferases*. Nat Genet, 1998. **19**(3): p. 219-20.
135. Okano, M., et al., *DNA methyltransferases Dnmt3a and Dnmt3b are essential for de novo methylation and mammalian development*. Cell, 1999. **99**(3): p. 247-57.
136. Eden, S. and H. Cedar, *Role of DNA methylation in the regulation of transcription*. Curr Opin Genet Dev, 1994. **4**(2): p. 255-9.
137. Jones, P.A. and S.B. Baylin, *The fundamental role of epigenetic events in cancer*. Nat Rev Genet, 2002. **3**(6): p. 415-28.
138. Jjingo, D., et al., *On the presence and role of human gene-body DNA methylation*. Oncotarget, 2012. **3**(4): p. 462-74.
139. Liao, J., et al., *Targeted disruption of DNMT1, DNMT3A and DNMT3B in human embryonic stem cells*. Nat Genet, 2015. **47**(5): p. 469-78.
140. Bachman, K.E., M.R. Rountree, and S.B. Baylin, *Dnmt3a and Dnmt3b are transcriptional repressors that exhibit unique localization properties to heterochromatin*. J Biol Chem, 2001. **276**(34): p. 32282-7.
141. Baubec, T., et al., *Genomic profiling of DNA methyltransferases reveals a role for DNMT3B in genic methylation*. Nature, 2015. **520**(7546): p. 243-7.
142. Jeong, M., et al., *Large conserved domains of low DNA methylation maintained by Dnmt3a*. Nat Genet, 2014. **46**(1): p. 17-23.
143. Chedin, F., M.R. Lieber, and C.L. Hsieh, *The DNA methyltransferase-like protein DNMT3L stimulates de novo methylation by Dnmt3a*. Proc Natl Acad Sci U S A, 2002. **99**(26): p. 16916-21.
144. Cui, H., et al., *DNA methyltransferase 3A promotes cell proliferation by silencing CDK inhibitor p18INK4C in gastric carcinogenesis*. Sci Rep, 2015. **5**: p. 13781.
145. Shaw, P.H., *The role of p53 in cell cycle regulation*. Pathol Res Pract, 1996. **192**(7): p. 669-75.
146. Wang, Y.A., et al., *DNA methyltransferase-3a interacts with p53 and represses p53-mediated gene expression*. Cancer Biol Ther, 2005. **4**(10): p. 1138-43.
147. Zhang, G., T.C. Meredith, and D. Kahne, *On the essentiality of lipopolysaccharide to Gram-negative bacteria*. Curr Opin Microbiol, 2013. **16**(6): p. 779-85.
148. Bryant, C.E., et al., *The molecular basis of the host response to lipopolysaccharide*. Nat Rev Microbiol, 2010. **8**(1): p. 8-14.
149. Gardiner, K.R., et al., *Significance of systemic endotoxaemia in inflammatory bowel disease*. Gut, 1995. **36**(6): p. 897-901.
150. Pasternak, B.A., et al., *Lipopolysaccharide exposure is linked to activation of the acute phase response and growth failure in pediatric Crohn's disease and murine colitis*. Inflammatory Bowel Diseases, 2010. **16**(5): p. 856-869.

151. Srivastava, S., et al., *Serum human trefoil factor 3 is a biomarker for mucosal healing in ulcerative colitis patients with minimal disease activity*. J Crohns Colitis, 2015. **9**(7): p. 575-9.
152. Norgaard, M., et al., *Comprehensive Evaluation of TFF3 Promoter Hypomethylation and Molecular Biomarker Potential for Prostate Cancer Diagnosis and Prognosis*. Int J Mol Sci, 2017. **18**(9).
153. Okada, H., et al., *Frequent trefoil factor 3 (TFF3) overexpression and promoter hypomethylation in mouse and human hepatocellular carcinomas*. Int J Oncol, 2005. **26**(2): p. 369-77.
154. Thornberry, N.A., et al., *A Novel Heterodimeric Cysteine Protease Is Required for Interleukin-1-Beta Processing in Monocytes*. Nature, 1992. **356**(6372): p. 768-774.
155. Scott, A.M. and M. Saleh, *The inflammatory caspases: guardians against infections and sepsis*. Cell Death Differ, 2007. **14**(1): p. 23-31.
156. Rathinam, V.A.K. and F.K.-M. Chan, *Inflammasome, Inflammation, and Tissue Homeostasis*. Trends in Molecular Medicine, 2018. **24**(3): p. 304-318.
157. Anderson, C.A., et al., *Meta-analysis identifies 29 additional ulcerative colitis risk loci, increasing the number of confirmed associations to 47*. Nat Genet, 2011. **43**(3): p. 246-52.
158. Andus, T., et al., *Imbalance of the interleukin 1 system in colonic mucosa - association with intestinal inflammation and interleukin 1 receptor agonist genotype 2*. Gut, 1997. **41**(5): p. 651-657.
159. McAlindon, M.E., C.J. Hawkey, and Y.R. Mahida, *Expression of interleukin 1 beta and interleukin 1 beta converting enzyme by intestinal macrophages in health and inflammatory bowel disease*. Gut, 1998. **42**(2): p. 214-9.
160. Ludwiczek, O., et al., *Imbalance between interleukin-1 agonists and antagonists: relationship to severity of inflammatory bowel disease*. Clinical and Experimental Immunology, 2004. **138**(2): p. 323-329.
161. Bersudsky, M., et al., *Non-redundant properties of IL-1 alpha and IL-1 beta during acute colon inflammation in mice*. Gut, 2014. **63**(4): p. 598-609.
162. Gonzalez-Navajas, J.M., et al., *Interleukin 1 receptor signaling regulates DUBA expression and facilitates Toll-like receptor 9-driven antiinflammatory cytokine production*. J Exp Med, 2010. **207**(13): p. 2799-807.
163. McCole, D.F., *IBD candidate genes and intestinal barrier regulation*. Inflamm Bowel Dis, 2014. **20**(10): p. 1829-49.
164. Olson, A.D., T. Pysher, and R.S. Bienkowski, *Organization of Intestinal Epithelial-Cells into Multicellular Structures Requires Laminin and Functional Actin Microfilaments*. Experimental Cell Research, 1991. **192**(2): p. 543-549.
165. Yu, W., et al., *Beta1-integrin orients epithelial polarity via Rac1 and laminin*. Mol Biol Cell, 2005. **16**(2): p. 433-45.
166. Schmitz, H., et al., *Altered tight junction structure contributes to the impaired epithelial barrier function in ulcerative colitis*. Gastroenterology, 1999. **116**(2): p. 301-9.
167. Soderholm, J.D., et al., *Epithelial permeability to proteins in the noninflamed ileum of Crohn's disease?* Gastroenterology, 1999. **117**(1): p. 65-72.
168. Landy, J., et al., *Tight junctions in inflammatory bowel diseases and inflammatory bowel disease associated colorectal cancer*. World J Gastroenterol, 2016. **22**(11): p. 3117-26.
169. Mehta, S., et al., *Defects in the adherens junction complex (E-cadherin/ β -catenin) in inflammatory bowel disease*. Cell and Tissue Research, 2014. **360**(3): p. 749-760.
170. Srinivasan, B., et al., *TEER measurement techniques for in vitro barrier model systems*. J Lab Autom, 2015. **20**(2): p. 107-26.

171. Grill, J.I., et al., *Intestinal E-cadherin Deficiency Aggravates Dextran Sodium Sulfate-Induced Colitis*. *Dig Dis Sci*, 2015. **60**(4): p. 895-902.
172. Consortium, U.I.G., et al., *Genome-wide association study of ulcerative colitis identifies three new susceptibility loci, including the HNF4A region*. *Nat Genet*, 2009. **41**(12): p. 1330-4.
173. Karayiannakis, A.J., et al., *Expression of catenins and E-cadherin during epithelial restitution in inflammatory bowel disease*. *J Pathol*, 1998. **185**(4): p. 413-8.
174. Kucharzik, T., et al., *Neutrophil transmigration in inflammatory bowel disease is associated with differential expression of epithelial intercellular junction proteins*. *American Journal of Pathology*, 2001. **159**(6): p. 2001-2009.
175. Taupin, D. and D.K. Podolsky, *Trefoil factors: initiators of mucosal healing*. *Nat Rev Mol Cell Biol*, 2003. **4**(9): p. 721-32.
176. Ribieras, S., et al., *Mouse Trefoil factor genes: genomic organization, sequences and methylation analyses*. *Gene*, 2001. **266**(1-2): p. 67-75.
177. Mashimo, H., et al., *Impaired defense of intestinal mucosa in mice lacking intestinal trefoil factor*. *Science*, 1996. **274**(5285): p. 262-5.
178. Giles, R.H., J.H. van Es, and H. Clevers, *Caught up in a Wnt storm: Wnt signaling in cancer*. *Biochim Biophys Acta*, 2003. **1653**(1): p. 1-24.
179. Vlad-Fiegen, A., et al., *The Wnt pathway destabilizes adherens junctions and promotes cell migration via beta-catenin and its target gene cyclin D1*. *Febs Open Bio*, 2012. **2**: p. 26-31.
180. De Pauw, A., et al., *Dnmt3a-mediated inhibition of Wnt in cardiac progenitor cells improves differentiation and remote remodeling after infarction*. *JCI Insight*, 2017. **2**(12).
181. Moparthi, L. and S. Koch, *Wnt signaling in intestinal inflammation*. *Differentiation*, 2019.
182. You, J., et al., *Wnt pathway-related gene expression in inflammatory bowel disease*. *Dig Dis Sci*, 2008. **53**(4): p. 1013-9.
183. Nenci, A., et al., *Epithelial NEMO links innate immunity to chronic intestinal inflammation*. *Nature*, 2007. **446**(7135): p. 557-61.
184. Lawrence, T., *The nuclear factor NF-kappaB pathway in inflammation*. *Cold Spring Harb Perspect Biol*, 2009. **1**(6): p. a001651.
185. Atreya, I., R. Atreya, and M.F. Neurath, *NF-kappaB in inflammatory bowel disease*. *J Intern Med*, 2008. **263**(6): p. 591-6.
186. Wan, F. and M.J. Lenardo, *The nuclear signaling of NF-kappaB: current knowledge, new insights, and future perspectives*. *Cell Res*, 2010. **20**(1): p. 24-33.
187. Pasparakis, M., *Regulation of tissue homeostasis by NF-kappaB signalling: implications for inflammatory diseases*. *Nat Rev Immunol*, 2009. **9**(11): p. 778-88.
188. O'Gorman, A., et al., *Regulation of NF-kappaB responses by epigenetic suppression of IkappaBalpha expression in HCT116 intestinal epithelial cells*. *Am J Physiol Gastrointest Liver Physiol*, 2010. **299**(1): p. G96-G105.
189. Li, E., T.H. Bestor, and R. Jaenisch, *Targeted mutation of the DNA methyltransferase gene results in embryonic lethality*. *Cell*, 1992. **69**(6): p. 915-26.
190. Samuel, M.S., et al., *Elevated Dnmt3a Activity Promotes Polyposis in Apc(Min) Mice by Relaxing Extracellular Restraints on Wnt Signaling*. *Gastroenterology*, 2009. **137**(3): p. 902-913.
191. Elliott, E.N., K.L. Sheaffer, and K.H. Kaestner, *The 'de novo' DNA methyltransferase Dnmt3b compensates the Dnmt1-deficient intestinal epithelium*. *Elife*, 2016. **5**.
192. Fabbri, M., et al., *MicroRNA-29 family reverts aberrant methylation in lung cancer by targeting DNA methyltransferases 3A and 3B*. *Proc Natl Acad Sci U S A*, 2007. **104**(40): p. 15805-10.

193. Garzon, R., et al., *MicroRNA-29b induces global DNA hypomethylation and tumor suppressor gene reexpression in acute myeloid leukemia by targeting directly DNMT3A and 3B and indirectly DNMT1.* Blood, 2009. **113**(25): p. 6411-8.
194. Kalla, R., et al., *MicroRNAs: new players in IBD.* Gut, 2015. **64**(3): p. 504-17.
195. Fisher, K. and J. Lin, *MicroRNA in inflammatory bowel disease: Translational research and clinical implication.* World J Gastroenterol, 2015. **21**(43): p. 12274-82.
196. Elliott, E.N., et al., *Dnmt1 is essential to maintain progenitors in the perinatal intestinal epithelium.* Development, 2015. **142**(12): p. 2163-2172.
197. Deng, T., et al., *An essential role for DNA methyltransferase 3a in melanoma tumorigenesis.* Biochem Biophys Res Commun, 2009. **387**(3): p. 611-6.
198. Zhao, Z., et al., *Depletion of DNMT3A suppressed cell proliferation and restored PTEN in hepatocellular carcinoma cell.* J Biomed Biotechnol, 2010. **2010**: p. 737535.
199. Parker, A., et al., *Cell proliferation within small intestinal crypts is the principal driving force for cell migration on villi.* Faseb Journal, 2017. **31**(2): p. 636-649.

9 Supplement

9.1 List of Abbreviations

5-hmc	5-hydroxymethylcytosine
ADD	ATRIX-DNMT3A-DNMT3L
3D	three dimensional
AJ	adherens junction
AMPs	antimicrobial peptide
ATG16L1	autophagy related 16 like 1
BSA	bovine serum albumin
Cas9	CRISPR associated protein 9
CASP1	caspase 1
CD	Crohn's disease
cDNA	complimentary DNA
CGIs	cytosine guanine islands
ChIP-seq	chromatin immunoprecipitation DNA-sequencing
CpG	cytosine-phosphate-cuanine
CRISPR	clustered regularly interspaced short palindromic repeats
DAI	disease activity index
DEG	diferentially expressed genes
DMP	differentially methylated promoters
DNMT	DNA methylatransferase
dNTP	deoxyribonucleoside triphosphates
DSS	dextran sulfate sodium
DTT	ditriothreitol
<i>E. coli</i>	<i>Escherichia coli</i>
ECL	enhanced chemiluminescence
ECM	extracellular matrix
EDTA	ethylenediaminetetraacetic acid
EDTA	ethylenediaminetetraacetic acid
EWAS	epigenome-wide association study
FITC	Fluorescein isothiocyanate
GO	gene ontology

GWAS	genome-wide association studies
HE	hematoxylin and eosin
IBD	inflammatory bowel disease
IECs	intestinal epithelial cells
IESCs	intestinal epithelial stem cells
IHC	immunohistochemistry
IL	interleukin
IL1R1	interleukin-1 receptor 1
INF	interferon
kDA	kilodalton
KO	knockout
LPS	lipopolysaccharide
LY	lucifer yellow
MDS	myelodysplastic syndrome
mRNA	messenger ribonucleic acids
MUC2	mucin 2
NF- κ B	nuclear factor kappa-light-chain-enhancer of activated B cells
NOD2	nucleotide-binding oligomerization domain-containing protein 2
padj	adjusted p-value
PCA	principal component analysis
PCR	polymerase chain reactions
PVDF	polyvinylidene difluoride
PWWP	Pro-Trp-Trp-Pro
qPCR	quantitative real-time PCR
RT	reverse transcriptase
SAM	S-adenosyl-methionine
SDS-PAGE	sodium dodecyl sulfate polyacrylamide gel electrophoresis
SEM	standard error of the mean
siRNA	small interfering RNA
SNP	single nucleotide polymorphisms
TEER	transepithelial electrical resistance
TEM	transmission electron microscopy
TEMED	tetramethylethylenediamine
TFF3	trefoil factor 3

TJ	tight junction
TNF	tumor necrosis factor
TSS	transcription starting site
UC	ulcerative colitis
WT	wild-type
ZO	zonula occludens

9.2 Buffers and Solutions

Table 12: List of applied buffers and solutions.

buffer or solution	composition or company
10x TAE buffer	Carl Roth, Karlsruhe, Germany, cat. nr. T845.2
10x TBS	200 mM Tris (pH 7.6), 1.37 M sodium chloride
10x TGS buffer	25 mM Tris (pH 8.3), 192 mM glycine, 0.1 % (w/v) SDS
5x SDS loading dye	250 mM Tris (pH 6.8), 10 % (w/v) SDS, 50 % (v/v) glycerol, 500 mM DTT
Anode buffer 1	30 mM Tris, 20 % (v/v) methanol
Anode buffer 2	300 mM Tris, 20 % (v/v) methanol
Blocking solution	5 % (w/v) non-fat dry milk in TTBS
Cathode buffer	25 mM Tris, 20 % (v/v) methanol, 40 mM 6-amino-ncaproic acid
Cell fractionation 1	10 mM HEPES (pH 7.9), 10 mM potassium chloride, 1.5 mM magnesium chloride, 10 mM sodium fluoride
Cell fractionation 2	20 mM HEPES (pH 7.9), 420 mM sodium chloride, 1.5 mM magnesium chloride, 0.2 mM EDTA, 25 % (v/v) glycerol, 10 mM sodium fluoride
DNA loading dye	50 % (v/v) glycerol, 0.1 % (w/v) bromophenol blue, 0.1 % (w/v) xylene cyanol
ECL substrate	GE Healthcare, Freiburg, Germany, cat. nr. RPN2109
FCS	PAA Laboratories/ GE Healthcare, Freiburg, Germany, cat. nr. PAA A15-151
Loading gel	0.5 M Tris (pH 6.8), 0.4 % (w/v) SDS
MOPS SDS Running Buffer (20X)	Novex/Life Technologies, Darmstadt, Germany, cat. nr. NP001
OPTI-MEM	Gibco/Life Technologies, Darmstadt, Germany, cat. nr. 31985-047
PBS	8 g/l sodium chloride, 0.2 g/l potassium chloride, 1.56 g/l disodium phosphate, 0.24 g/l monopotassium phosphate, pH 7.4
RIPA	150 mM sodium chloride, 1 % (v/v) NP40, 0.5 % (w/v) deoxycholic acid, 0.1 % (w/v) SDS, 50 mM Tris (pH 8.0)
Separation buffer	1.5 M Tris (pH 8.8), 0.4 % (w/v) SDS
SmartLadder	Eurogentec, Cologne, Germany, cat. nr. MW-1700-10
Stacking buffer	0.5 M Tris (pH 8.8), 0.4 % (w/v) SDS
Stripping buffer	62.5 mM Tris (pH 6.8), 2 % (w/v) SDS
SYBR Safe DNA gel stain	Life Technologies, Darmstadt, Germany cat. nr. S33102
TEA	10 mM Tris, 1 mM EDTA
TTBS	1x TBS, 0,1 % (v/v) Tween20

9.3 Media

Table 13: List of applied media.

Media	Composition or company
DMEM	Gibco/Life Technologies, Darmstadt, Germany cat. nr. 41966-029
DMEM Glutamax	Gibco/Life Technologies, Darmstadt, Germany cat. nr. 61965-059
LB Agar	10 g/l tryptone, 5 g/l yeast extract, 5 g/l sodium chloride, 15 g/l agar
LB Medium	10 g/l tryptone, 5 g/l yeast extract, 5 g/l sodium chloride
NEAA, MEM	Invitrogen/Thermo Scientific, Bremen, Germany cat nr. 11140-035

9.4 Chemicals

Table 14: List of applied chemicals.

chemical	company
2-Mercaptoethanol	Sigma-Aldrich, Munich, Germany
6-amino-n-caproic acid	Sigma-Aldrich, Munich, Germany
Acrylamide Bis Sol.30%	Bio-Rad, Munich, Germany
Ammonium persulfate (APS)	Sigma-Aldrich, Munich, Germany
Amphotericin	PAA Laboratories/ GE Healthcare, Freiburg, Germany
Ampicillin	Sigma-Aldrich, Munich, Germany
Bovine serum albumin (BSA)	Carl Roth, Karlsruhe, Germany
Bromophenol blue	Sigma-Aldrich, Munich, Germany
Deoxycholic acid	Sigma-Aldrich, Munich, Germany
Dimethylsulfoxid (DMSO)	Sigma-Aldrich, Munich, Germany
Dithiothreitol (DTT)	Th. Geyer, Renningen, Germany
DSS reagent grade, molecular weight 36000-50000	MP Biomedicals, Illkirch Cedex, France
Dynabeads Protein G	Life Technologies, Darmstadt, Germany
EDTA	Sigma-Aldrich, Munich, Germany
Ethanol	Merck, Darmstadt, Germany
FITC-4D	TH Geyer
Glycerol	Carl Roth, Karlsruhe, Germany
Glycine	Carl Roth, Karlsruhe, Germany
HEPES	Sigma-Aldrich, Munich, Germany
Isopropanol	Merck, Darmstadt, Germany
LE Agarose	Biozyme, Hessisch Oldendorf, Germany
Lucifer yellow	Sigma-Aldrich, Munich, Germany
Magnesium chloride	Merck, Darmstadt, Germany
Methanol	Merck, Darmstadt, Germany
Monopotassium phosphate	Sigma-Aldrich, Munich, Germany
Non-fat dry milk (NFDM)	Bio-Rad, Munich, Germany
Nonidet p 40 substitute	Sigma-Aldrich, Munich, Germany

Penicilin/Streptomycin	Life Technologies, Darmstadt, Germany
Potassium chloride	Sigma-Aldrich, Munich, Germany
Potassium dihydrogen phosphate	Merck, Darmstadt, Germany
RNase-free water	Qiagen, Hilden, Germany
Sodium chloride	Merck, Darmstadt, Germany
Sodium dodecyl sulfate (SDS)	Carl Roth, Karlsruhe, Germany
Sodium fluoride	Sigma-Aldrich, Munich, Germany
Sodium phosphate dibasic	Sigma-Aldrich, Munich, Germany
SYBR safe	Life Technologies
Tetramethylethylenediamine (TEMED)	Sigma-Aldrich, Munich, Germany
TRIS	Merck, Darmstadt, Germany
Triton-X	Sigma-Aldrich, Munich, Germany
Tween20	Carl Roth, Karlsruhe, Germany
Xylene cyanol	Sigma-Aldrich, Munich, Germany

9.5 Enzymes

Table 15: List of applied enzymes.

enzyme	company
Endonuclease H	New England Biolabs
GoTaq™ polymerase	Promega, Mannheim, Germany
Proteinase K	Thermo Scientific, Bremen, Germany
RNase-free DNase Set	Qiagen, Hilden, Germany
Trypsin/EDTA	Life Technologies

9.6 Kits

Table 16: List of applied kits.

kit	company
Dual-luciferase® reporter assay system	Promega, Mannheim, Germany
GeneJET Plasmid Miniprep Kit	Thermo Scientific, Bremen, Germany
Maxima H Minus First Strand cDNA Synthesis Kit	Thermo Scientific, Bremen, Germany
PureLink® HiPure Plasmid Filter Midiprep Kit	Life Technologies, Darmstadt, Germany
QIAshredder	Qiagen, Hilden, Germany
Rapid DNA Ligation Kit	Roche, Mannheim, Germany
RNeasy Mini Kit	Qiagen, Hilden, Germany
Roti Histokit	Carl Roth, Karlsruhe, Germany
Taqman Universal PCR MasterMix	Life Technologies, Darmstadt, Germany
GeneArt® CRISPR Nuvlease Vector kit	Life Technologies, Darmstadt, Germany

9.7 Plasmids and oligonucleotides

Table 17: List of plasmids used in this study.

plasmid	generated by
M50 Super 8xTOPFlash	Veman <i>et al.</i> , 2003; purchased from Addgene, Cambridge, USA, cat. nr.12456
pPiggy-GFP-TY1-DNMT3A1	restriction enzyme based cloning using EcoRV and NotI
pPiggy-GFP-TY1-DNMT3A2	restriction enzyme based cloning using EcoRV and NotI
pCRISPR-CD4-DNMT3A	generated using GeneArt® CRISPR Nuvlease Vector kit
pNF-κB-Luc	purchased from Clontech, cat. nr, 631904
pRL-TK	purchased from Promega, Mannheim, Germany, cat. nr. E2241

All oligonucleotides were generated and desalted by Microsynth AG (Balgach, Switzerland). All sequences are shown from 5' to 3' direction.

Table 18: List of applied oligonucleotides with their sequences.

target	species	forward sequence	reverse sequence
Dnmt3a PCR cond	murine	TACCTTCATCTGCCAACCCC	AGAGTGAGTTCAAGGCCAGC
Dnmt3a PCR cre	murine	GTGTGGGACAGAGAACAAACC	ACATCTTCAGGTTCTGCGGG

Table 19: Overview of applied TaqMan probes.

target	species	company	catalog number
DNMT3A	human	Life Technologies, Darmstadt, Germany	01027166
DNMT3B	human	Life Technologies, Darmstadt, Germany	00171876
ACTIN	human	Life Technologies, Darmstadt, Germany	99999903
<i>Dnmt3a</i>	murine	Life Technologies, Darmstadt, Germany	00432881
<i>Dnmt3b</i>	murine	Life Technologies, Darmstadt, Germany	01240113
<i>Dnmt1</i>	murine	Life Technologies, Darmstadt, Germany	01151063
<i>Il1β</i>	murine	Life Technologies, Darmstadt, Germany	01336189
<i>Cdh1</i>	murine	Life Technologies, Darmstadt, Germany	01247357
<i>Cttnb1</i>	murine	Life Technologies, Darmstadt, Germany	00483039
<i>Gapdh</i>	murine	Life Technologies, Darmstadt, Germany	99999915
<i>Tnfa</i>	murine	Life Technologies, Darmstadt, Germany	00443258

9.8 Antibodies

All primary antibodies used for western blotting were diluted in TTBS containing 5 % (w/v) bovine serum albumin (BSA) or 5 % (w/v). Secondary antibodies used in this study were diluted in non-fat dry milk.

Table 20: Primary antibodies used in this study.

antibody	dilution	company	catalog number
DNMT3A	1:1000	R&D Systems	MAB63151
p-p65	1:1000	Cell Signaling	3031S
p65	1:1000	Cell Signaling	8242
p-IkB α	1:1000	Cell Signaling	2859
IkB α	1:1000	Cell Signaling	9242
β -Actin	1:1000	Sigma-Aldrich	A-5441
GAPDH	1:1000	Santa Cruz Biotechnology	sc-365062
Tubulin	1:2000	Abcam	ab6046
Draq5	1:4000	Cell Signaling	4084S
RhodaminePhalloidin	1:200	Molecular Probes	R415

Table 21: Secondary antibodies used in this study.

antibody	dilution	company	catalog number
mouse HRP	1:5000	Amersham Biosciences, Glattbrugg, Switzerland	NA931V
rabbit HRP	1:5000	Amersham Biosciences, Glattbrugg, Switzerland	NA934V
Alexa Fluor 555-goat α -mouse	1:400	Thermo Scientific, Bremen, Germany	A21424

9.9 Devices & Consumables

Table 22: Devices used in this study.

devices	company
7900 HT Fast Real-Time PCR System	Applied Biosystems/Life Technologies, Darmstadt, Germany
96-well thermocycler	Applied Biosystems/Life Technologies, Darmstadt, Germany
ABI PRISM [®] 3700 sequencer	Applied Biosystems/Life Technologies, Darmstadt, Germany
Analytic balance 870-15	Kern, Balingen, Germany
Assistant Mini-Centrifuge SPROUT	Heathrow Scientific, Nottingham, United Kingdom
Automated developer machine	Agfa, Mortsels, Belgium
Axio Imager.Z1	Zeiss, Jena, Germany
Cellometer Auto T4 Plus	PeqLab Biotechnologie GmbH, Erlangen, Germany
Centrifuge for 15/50 ml tubes: Megafuge 16R	Thermo Scientific, Bremen, Germany
Centrifuge for Eppendorf tubes: Fresco 21	Thermo Scientific, Bremen, Germany
Certomat MV, vortex mixer	B. Braun Biotech Internat., Melsungen, Germany
ChemiDoc XRS Imaging System	Bio-Rad, Munich, Germany
Confocal microscope: TCS SP5	Leica Microsystems, Wetzlar, Germany
Electronic pipet filler	Eppendorf, Hamburg, Germany
Eppendorf Research [®] , adjustable volume pipette	Eppendorf, Hamburg, Germany
FACSCalibur flow cytometer	BD Biosciences, Heidelberg, Germany
GeneAmp PCR System 9700	Applied Biosystems/Life Technologies, Darmstadt, Germany
Gentle-MACS [™] Dissociator	Miltenyi Biotec, Bergisch Gladbach, Germany

Incubator for cell lines	Binder, Tuttlingen, Germany
Incubator for <i>E. coli</i> in media: Orbital Incubator SI50	Stuart Equipment, Staffordshire, United Kingdom
Incubator for <i>E. coli</i> on agar plates: Incucell 111	MMM Group, Planegg, Germany
Laminar flow workbench HERASafe KS	Thermo Scientific, Bremen, Germany
Leica RM 2255 microtome	Leica Microsystems, Wetzlar, Germany
Magnetic stirrer C-MAG HS 7 IKAMAG	IKA, Staufen, Germany
Microwave R-239	SHARP, Hamburg, Germany
Mini-Sub Cell GT	Bio-Rad, Munich, Germany
Molecular Imager ChemiDoc XRS Imaging System	Bio-Rad, Munich, Germany
NanoDrop ND-1000 spectrophotometer	PeqLab Biotechnologie GmbH, Erlangen, Germany
Power Pac 300	Bio-Rad, Munich, Germany
SympHony Benchtop Meters	VWR, Darmstadt, Germany
Tecan Infinite F200 pro plate reader	Tecan, Männedorf, Switzerland
Thermomixer compact 5350	Eppendorf, Hamburg, Germany
Trans-Blot® Turbo™ Transfer System	Bio-Rad, Munich, Germany
Tube roller SRT6	Stuart Equipment, Staffordshire, United Kingdom
Vortex-Genie 2 Variable Speed	Sartorius, Göttingen, Germany
Water bath 1003	GFL, Burgwedel, Germany
Water purification system	TKA, Niederelbert, Germany
Wide Mini ReadySub-Cell GT	Bio-Rad, Munich, Germany
XCell SureLock® Mini-Cell	Life Technologies, Darmstadt, Germany

Table 23: List of consumables used in this study.

consumable	company
0.5 ml, 1.5 ml and 2 ml reaction tubes	Sarstedt, Nümbrecht, Germany
1 ml syringes	BD Biosciences, Heidelberg, Germany
100 ml culture flasks	Schott, Mainz, Germany
15 ml and 50 ml tubes	Sarstedt, Nümbrecht, Germany
26G needles	B. Braun, Melsungen, Germany
Blot paper	Bio-Rad, Munich, Germany
Chemiluminescence hyperfilm	Applied Biosystems/Life Technologies, Darmstadt, Germany
Culture-insert 4 well	IBIDI, cat nr. 80466
Glass beads	Carl Roth, Karlsruhe, Germany
HistoBond	Paul Marienfeld GmbH & Co. KG
MicroAmp Optical 384-Well Reaction Plates	Applied Biosystems
Microvette 500 (Potassium-EDTA)	Sarstedt, Nümbrecht, Germany
NuPAGE® Bis-Tris gel	Life Technologies, Darmstadt, Germany
Pipette tips and filter tips	Sarstedt, Nümbrecht, Germany
Pipette tips for electronic pipette	Biohit, Göttingen, Germany
Polyvinylidene difluoride (PVDF) membranes	Bio-Rad, Munich, Germany
Rotilabo 0.22 µm syringe filter	Carl Roth, Karlsruhe, Germany
Serological pipettes	Sarstedt, Nümbrecht, Germany
Surgical disposable scalpels	B. Braun, Melsungen, Germany
Tissue culture dishes 96-, 24- and 6well	Sarstedt, Nümbrecht, Germany

Table 24: List of top 100 upregulated genes rescued by DNMT3A1 and DNMT3A2.

	GeneSymbol	padj		GeneSymbol	padj
ENSG00000041982	TNC	0,00E+00	ENSG00000141068	KSR1	6,29E-25
ENSG00000203857	HSD3B1	0,00E+00	ENSG00000159445	THEM4	1,39E-23
ENSG00000092929	UNC13D	1,68E-275	ENSG00000110880	CORO1C	3,17E-23
ENSG00000197956	S100A6	7,11E-257	ENSG00000148834	GSTO1	4,87E-23
ENSG00000177469	CAVIN1	6,13E-206	ENSG00000123240	OPTN	8,39E-23
ENSG00000004139	SARM1	4,01E-186	ENSG00000131899	LLGL1	2,79E-22
ENSG00000162391	FAM151A	8,20E-148	ENSG00000053524	MCF2L2	1,51E-20
ENSG00000114378	HYAL1	1,61E-135	ENSG00000156675	RAB11FIP1	1,54E-20
ENSG00000162433	AK4	2,14E-135	ENSG00000130830	MPP1	2,04E-20
ENSG00000027697	IFNGR1	7,86E-123	ENSG00000112249	ASCC3	3,78E-20
ENSG00000164251	F2RL1	1,31E-115	ENSG00000110955	ATP5B	5,62E-20
ENSG00000186377	CYP4X1	1,04E-114	ENSG00000266714	MYO15B	7,88E-20
ENSG00000188643	S100A16	3,68E-98	ENSG00000151468	CCDC3	3,32E-19
ENSG00000104635	SLC39A14	5,14E-92	ENSG00000085415	SEH1L	7,80E-19
ENSG00000178772	CPN2	3,63E-92	ENSG00000233041	PHGR1	8,57E-19
ENSG00000100170	SLC5A1	3,07E-83	ENSG00000176014	TUBB6	1,42E-18
ENSG00000143153	ATP1B1	4,78E-83	ENSG00000159200	RCAN1	2,42E-18
ENSG00000165949	IFI27	1,68E-80	ENSG00000018408	WWTR1	3,88E-18
ENSG00000156510	HKDC1	5,25E-77	ENSG00000149090	PAMR1	7,56E-18
ENSG00000185442	FAM174B	1,34E-73	ENSG00000197728	RPS26	1,29E-17
ENSG00000040199	PHLPP2	2,07E-72	ENSG00000073921	PICALM	1,81E-17
ENSG00000255346	NOX5	4,38E-72	ENSG00000204386	NEU1	1,61E-15
ENSG00000142583	SLC2A5	5,14E-69	ENSG00000196154	S100A4	2,95E-16
ENSG00000050405	LIMA1	3,44E-67	ENSG00000134285	FKBP11	3,97E-15
ENSG00000115850	LCT	3,86E-67	ENSG00000111684	LPCAT3	5,86E-15
ENSG00000167588	GPD1	5,89E-64	ENSG00000071127	WDR1	1,12E-14
ENSG00000144820	ADGRG7	1,71E-59	ENSG00000106803	SEC61B	7,05E-14
ENSG00000184005	ST6GALNAC3	5,64E-57	ENSG00000119403	PHF19	7,45E-13
ENSG00000136717	BIN1	5,65E-52	ENSG00000159720	ATP6V0D1	9,15E-13
ENSG00000167080	B4GALNT2	9,02E-51	ENSG00000171877	FRMD5	1,16E-12
ENSG00000136881	BAAT	5,50E-49	ENSG00000183527	PSMG1	1,37E-12
ENSG00000121039	RDH10	2,42E-40	ENSG00000184076	UQCR10	1,80E-12
ENSG00000118515	SGK1	1,37E-38	ENSG00000144063	MALL	2,84E-12
ENSG00000173077	37226	4,61E-38	ENSG00000169991	IFFO2	3,35E-12
ENSG00000165376	CLDN2	3,57E-37	ENSG00000244509	APOBEC3C	3,79E-12
ENSG00000125872	LRRN4	3,59E-36	ENSG00000186198	SLC51B	6,66E-12
ENSG00000161714	PLCD3	8,78E-36	ENSG00000197181	PIWIL2	6,87E-12
ENSG00000111846	GCNT2	7,57E-35	ENSG00000105953	OGDH	2,19E-11
ENSG00000076351	SLC46A1	1,29E-31	ENSG00000113552	GNPDA1	3,08E-11
ENSG00000164211	STARD4	1,20E-30	ENSG00000150656	CNDP1	4,35E-11
ENSG00000103018	CYB5B	1,92E-30	ENSG00000116717	GADD45A	4,86E-11
ENSG00000170421	KRT8	2,53E-29	ENSG00000111490	TBC1D30	5,64E-11
ENSG00000175352	NRIP3	6,42E-28	ENSG00000164405	UQCRQ	1,05E-10
ENSG00000189159	JPT1	4,49E-27	ENSG00000110203	FOLR3	1,19E-10
ENSG00000197444	OGDHL	5,97E-27	ENSG00000117676	RPS6KA1	2,00E-10
ENSG00000240194	CYMP	1,31E-26	ENSG00000142227	EMP3	2,49E-10
ENSG00000164308	ERAP2	5,08E-26	ENSG00000142669	SH3BGRL3	2,75E-10
ENSG00000115762	PLEKHB2	6,47E-26	ENSG00000122121	XPNPEP2	2,98E-10
ENSG00000156587	UBE2L6	1,92E-24	ENSG00000134954	ETS1	1,25E-09
ENSG00000072210	ALDH3A2	5,08E-24	ENSG00000166825	ANPEP	1,52E-09

Table 25: List of top 100 downregulated genes rescued by DNMT3A1 and DNMT3A2.

	GeneSymbol	padj		GeneSymbol	padj
ENSG00000164266	SPINK1	1,52E-178	ENSG00000123636	BAZ2B	5,90E-17
ENSG00000170373	CST1	7,86E-109	ENSG00000162545	CAMK2N1	3,89E-17
ENSG00000158874	APOA2	2,86E-91	ENSG00000163453	IGFBP7	7,16E-16
ENSG00000070669	ASNS	3,47E-91	ENSG00000081026	MAGI3	5,04E-15
ENSG00000075223	SEMA3C	2,88E-83	ENSG00000178078	STAP2	5,05E-16
ENSG00000154277	UCHL1	5,69E-68	ENSG00000225210	DUXAP9	5,46E-15
ENSG00000114739	ACVR2B	5,80E-68	ENSG00000164125	FAM198B	3,27E-14
ENSG00000150893	FREM2	4,28E-67	ENSG00000170899	GSTA4	7,63E-14
ENSG00000177508	IRX3	3,01E-64	ENSG00000112715	VEGFA	1,07E-13
ENSG00000166575	TMEM135	2,01E-54	ENSG00000196557	CACNA1H	1,58E-13
ENSG00000115414	FN1	7,61E-54	ENSG00000011347	SYT7	2,46E-13
ENSG00000090530	P3H2	4,08E-52	ENSG00000147257	GPC3	2,09E-12
ENSG00000164379	FOXQ1	3,05E-48	ENSG00000064651	SLC12A2	2,40E-12
ENSG00000168672	FAM84B	6,59E-47	ENSG00000138468	SENP7	3,52E-12
ENSG00000075213	SEMA3A	8,39E-47	ENSG00000007062	PROM1	3,91E-13
ENSG00000084676	NCOA1	2,08E-46	ENSG00000136205	TNS3	1,30E-11
ENSG00000204335	SP5	7,28E-46	ENSG00000140564	FURIN	2,72E-12
ENSG00000047644	WWC3	5,09E-45	ENSG00000095059	DHPS	2,74E-12
ENSG00000127863	TNFRSF19	9,44E-44	ENSG00000165124	SVEP1	3,27E-11
ENSG00000124177	CHD6	5,36E-38	ENSG00000168916	ZNF608	6,90E-11
ENSG00000116117	PARD3B	6,32E-37	ENSG00000121064	SCPEP1	1,07E-10
ENSG00000150433	TMEM218	3,48E-36	ENSG00000168758	SEMA4C	1,92E-11
ENSG00000136010	ALDH1L2	2,43E-34	ENSG00000128923	MINDY2	2,38E-10
ENSG00000174804	FZD4	1,22E-33	ENSG00000196787	HIST1H2AG	2,57E-10
ENSG00000214796	AC098934.1	1,76E-33	ENSG00000168036	CTNNB1	3,15E-10
ENSG00000009765	IYD	4,21E-32	ENSG00000102760	RGCC	5,91E-10
ENSG00000162105	SHANK2	2,20E-29	ENSG00000136048	DRAM1	6,13E-10
ENSG00000177169	ULK1	4,48E-28	ENSG00000162367	TAL1	7,93E-11
ENSG00000237441	RGL2	6,63E-28	ENSG00000187837	HIST1H1C	8,05E-10
ENSG00000137648	TMPRSS4	1,21E-27	ENSG00000165219	GAPVD1	1,26E-09
ENSG00000109654	TRIM2	2,23E-26	ENSG00000134109	EDEM1	3,01E-09
ENSG00000165591	FAAH2	2,12E-25	ENSG00000163394	CCKAR	3,36E-09
ENSG00000115290	GRB14	2,69E-24	ENSG00000092758	COL9A3	1,39E-08
ENSG00000129353	SLC44A2	2,50E-23	ENSG00000105443	CYTH2	1,40E-08
ENSG00000124766	SOX4	8,16E-21	ENSG00000196747	HIST1H2AI	5,32E-08
ENSG00000137747	TMPRSS13	3,94E-20	ENSG00000165699	TSC1	2,39E-08
ENSG00000151726	ACSL1	5,49E-20	ENSG00000197122	SRC	4,80E-07
ENSG00000074181	NOTCH3	6,95E-20	ENSG00000149212	SESN3	6,72E-07
ENSG00000111058	ACSS3	8,91E-20	ENSG00000168994	PXDC1	1,85E-06
ENSG00000060656	PTPRU	5,05E-19	ENSG00000106799	TGFBR1	2,97E-06
ENSG00000105856	HBP1	6,96E-19	ENSG00000206557	TRIM71	3,13E-06
ENSG00000126217	MCF2L	1,94E-18	ENSG00000204054	LINC00963	5,99E-06
ENSG00000117724	CENPF	2,40E-18	ENSG00000178538	CA8	7,26E-06
ENSG00000130208	APOC1	2,46E-20	ENSG00000168159	RNF187	1,33E-05
ENSG00000141376	BCAS3	2,52E-19	ENSG00000143502	SUSD4	4,64E-05
ENSG00000122176	FMOD	2,73E-18	ENSG00000113369	ARRDC3	5,37E-05
ENSG00000049283	EPN3	4,16E-18	ENSG00000097096	SYDE2	6,00E-05
ENSG00000138439	FAM117B	7,32E-18	ENSG00000198756	COLGALT2	8,19E-05
ENSG00000157399	ARSE	8,54E-18	ENSG00000145555	MYO10	2,22E-04
ENSG00000203499	IQANK1	4,01E-17	ENSG00000069275	NUCKS1	2,56E-04

9.10 Acknowledgments

Firstly, I would like to sincere my gratitude to my supervisor Prof. Philip Rosenstiel for offering me the opportunity to start my scientific path working on this interesting topic for my PhD thesis. Your motivation, knowledge and experience in the field was extremely inspiring for me. Thank you for your support, your ideas and guidance through all my time as doctoral student.

Beside my supervisor, I would like to thank the other members of my PhD thesis committee Prof. Thomas Roeder and Prof. Andre Franke for their interest in evaluating my thesis and willing to be part of my evaluation committee.

I would like to thank the Research Training Group “Genes, Environment and Inflammation” (RTG1743), his spokesperson Prof. Andre Franke and the project coordinator Mrs. Eike Zell for financial support and for giving me the opportunity to work in an interdisciplinary network and to acquire relevant skills essential for my scientific career.

I own my deepest gratitude to Dr. Jan Kuiper, for being my mentor during my doctorate period. Thank you for your patience, your great knowledge, your constructive criticism and your willingness to teach me all qualities to be a good scientist. I would like to acknowledge Dr. Neha Mishra for her indispensable help in analysing the omics data, Dr. med. Go Ito for introducing me into the organoids field and helping with animal experiments and Dr. Philipp Arnold for his expertise in electron microscopy.

A special thanks go to Steffi, Dora, Berith, Anna, Helene and Anne. Thanks for your help, scientific discussion and the great time spent together in the lab/office and around Kiel.

I would like to especially thank the cell biology technicians: Sabine, Melanie, Dorina, Steffi, Maren, Karina, Tatjana, Katha and Tanja. Your unfailing support and assistance have been extremely helpful for my work.

I would also like to thank all the members of the Cell Biology group and colleagues at the IKMB for providing a nice working atmosphere.

Last but not the least, a special thanks go to Lele, my family and friends who supported me during these three and half years and gave me love, effort, advice and encouraged me along the way.

9.11 Curriculum Vitae

Personal data

First and last name	Antonella Fazio
Date of birth	06.12.1989
Place of birth	Lamezia Terme
Nationality	Italian
Contact	antonellafazio89@gmail.com

Education

Since 10/2015	Institute of Clinical Molecular Biology, Kiel University, Germany Principal Investigator: Prof. Dr. med. Philip Rosenstiel PhD candidate and member of the Research Training Group (RTG 1743) Thesis title: Role of DNA methyltransferase 3A (DNMT3A) in intestinal epithelial cells during homeostasis and inflammation
08/2012 - 08/2014	Messina University, Italy Master in Biology (MSc) Final grade: 110/110 <i>cum laude</i> Master Thesis: Acute Phase Response in Atlantic cod (<i>Gadus morhua L.</i>) after infection with <i>Aeromonas salmonicida a.</i>
08/2014 - 08/2014	Utrecht University, the Netherlands Summer school in Molecular Mechanisms in Cancer
08/2009 - 03/2012	Messina University, Italy Bachelor in Biological Sciences (BSc) Final grade: 103/110 Bachelor Thesis: Acute Phase proteins

Training

05/2018	Humanitas University, Milan Italy Principal Investigator: Prof. Gioacchino Natoli PhD visitor: ChromatinImmunoPrecipitation (ChIP) methodology
02/2015 - 07/2015	Physiology Institute, Tubingen University, Germany Principal Investigator: Prof. Dr. med. Florian Lang Internship: "On the physiological mechanisms underlying eryptosis process"
03/2013 - 09/2013	Institute of Experimental Pathology, Iceland University Principal Investigator :Prof. Sigridur Gudmundsdottir Master project: Acute phase response in Atlantic cod upon bacterial infection

Awards

11/2017 Kiel Life Science young scientist's conference - 3th prize (200€) best presentation
01/2015 Excellent academic grades, Messina University - 1000€ for my Master degree grade

Conferences contribution

06/2018 DACED conference, Mainz, Germany (Abstract and Talk)
11/2017 International Human Epigenome Consortium (IHEC), Berlin, Germany (Abstract and Poster)
10/2017 25th United European Gastroenterology (UEG) week, Barcelona, Spain (Abstract and Poster)

List of publications

Pan, W. H., F. Sommer, M. Falk-Paulsen, T. Ulas, P. Best, **Antonella Fazio**, P. Kachroo, A. Luzius, M. Jentsch, A. Rehman, F. Muller, T. Lengauer, J. Walter, S. Kunzel, J. F. Baines, S. Schreiber, A. Franke, J. L. Schultze, F. Backhed and P. Rosenstiel (2018). "Exposure to the gut microbiota drives distinct methylome and transcriptome changes in intestinal epithelial cells during postnatal development." Genome Med **10**(1): 27.

Fazio, Antonella, M. Briglia, C. Faggio, K. Alzoubi and F. Lang (2015). "Oxaliplatin Induced Suicidal Death of Human Erythrocytes." Cell Physiol Biochem **37**(6): 2393-2404.

Fazio, Antonella, M. Briglia, C. Faggio, K. Alzoubi and F. Lang (2015). "Stimulation of Suicidal Erythrocyte Death by Garcinol." Cell Physiol Biochem **37**(2): 805-815.

9.12 Eidesstattliche Erklärung

Hiermit erkläre ich, Antonella Fazio, an Eides statt, dass ich die vorliegende Arbeit unter der wissenschaftlichen Leitung von Prof. Dr. Philip Rosenstiel selbstständig und ohne fremde Hilfe verfasst habe. Die Abhandlung stellt nach Form und Inhalt meine eigene Arbeit dar und ich habe außer der Beratung meiner Betreuer, Prof. Dr. Philip Rosenstiel und Dr. Jan Kuiper, keine weitere Hilfe in Anspruch genommen.

Weiterhin habe ich keine anderen als die von mir angegebenen Quellen und Hilfsmittel benutzt und die den verwendeten Werken wörtlich und inhaltlich entnommenen Stellen als solche kenntlich gemacht. Die Arbeit wurde unter der Einhaltung der Regeln guter wissenschaftlicher Praxis der Deutschen Forschungsgemeinschaft erstellt. Auszüge der Dissertation wurden bereits in Posterbeiträgen veröffentlicht.

Ich versichere, dass ich weder an der Christian-Albrechts-Universität zu Kiel noch anderweitig versucht habe, eine Dissertation einzureichen oder mich einer Promotionsprüfung zu unterziehen.

Hiermit erkläre ich, dass mir kein akademischer Grad entzogen wurde.

Kiel, den